AD-A043 391 NATIONAL OCEANIC AND ATMOSPHERIC ADMINISTRATION BOUL--ETC F/G 4/2
WIND SHEAR CHARACTERIZATION.(U)
FEB 77 G E GREENE, H W FRANK, A J BEDARD DOT-FA76WAI-622
UNCLASSIFIED FAA-RD-77-33 NL

1 OF 2
AD
A043 391

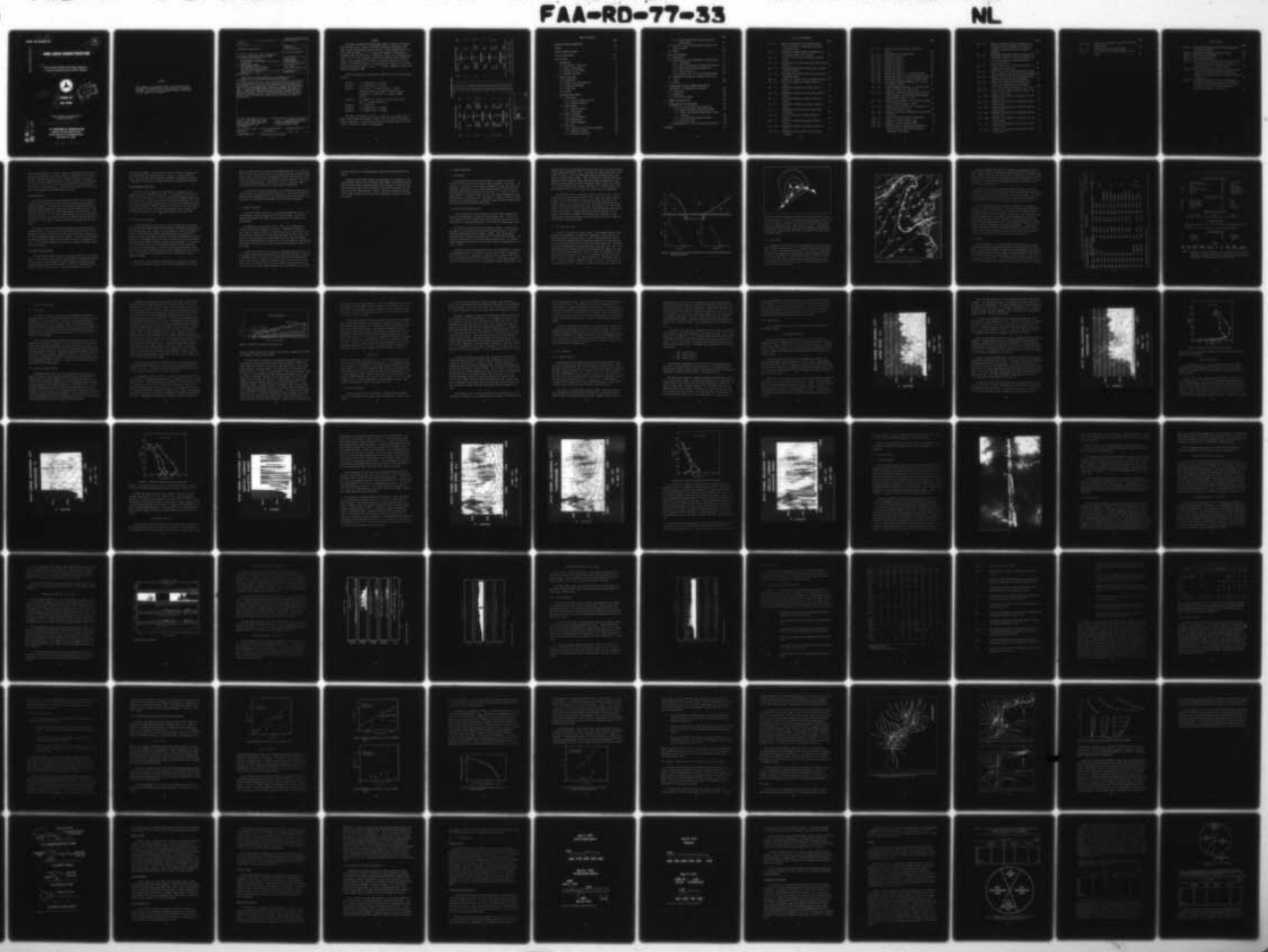

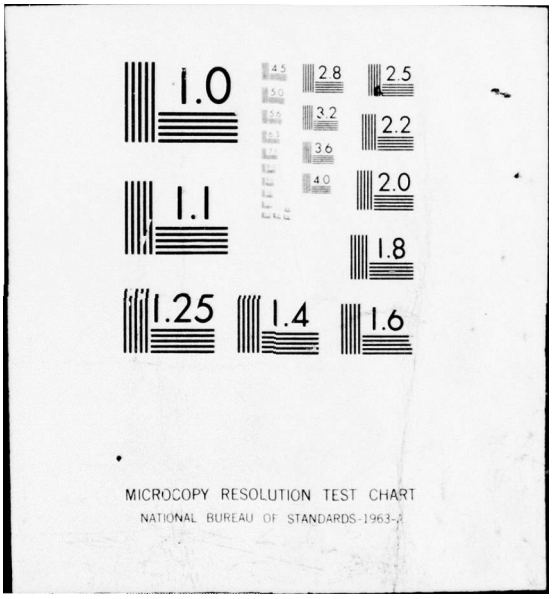
1.0
1.1
1.25
1.4
1.6
1.8
2.0
2.2
2.5
2.8
3.2
3.6
4.0
4.5
5.0
5.6
MICROCOPY RESOLUTION TEST CHART
NATIONAL BUREAU OF STANDARDS-1963-A

REPORT NO. FAA-RD-77-33

WIND SHEAR CHARACTERIZATION.

Gary E. Greene, Harold W. Frank, Alfred J. Bedard, Jr.,
J. Ann Korrell, Mary M. Cairns, and Peter A. Mandics

131 p.

FEBRUARY 1977

FINAL REPORT.
Apr 76 — Jan 77

DOT-FA76WAI-622

U.S. DEPARTMENT OF TRANSPORTATION
FEDERAL AVIATION ADMINISTRATION
Systems Research & Development Service
Washington, D.C. 20590

NOTICE

This document is disseminated under the sponsorship of the Department of Transportation in the interest of information exchange. The United States Government assumes no liability for its contents or use thereof.

Technical Report Documentation Page

1. Report No.	2. Government Accession No.	3. Recipient's Catalog No.
FAA-RD-77-33		

4. Title and Subtitle	5. Report Date
WIND SHEAR CHARACTERIZATION	February 1977
	6. Performing Organization Code
	8. Performing Organization Report No.

7. Author(s)	
G.E. Greene, H.W. Frank, A.J.Bedard, Jr., J.A. Korrell, M.M. Cairns, and P.A. Mandics	

9. Performing Organization Name and Address	10. Work Unit No. (TRAIS)
Wave Propagation Laboratory National Oceanic and Atmospheric Administration 325 Broadway Boulder, Colo. 80302	154-451-014B 11. Contract or Grant No. DOT-FA 76 WAI-622
	13. Type of Report and Period Covered Final Report April 1976 to January 1977
12. Sponsoring Agency Name and Address U.S. Department of Transportation Federal Aviation Administration Systems Research & Development Service, Airport Div. Washington, D.C. 20590	14. Sponsoring Agency Code FAA/ARD-450

15. Supplementary Notes

Prepared under Interagency Agreement No. DOT FA76WAI-622 TASK III, managed by the Aviation Weather Systems Branch, ARD-450.

16. Abstract

A brief review of the major causes of severe low-level wind shear indicates that the thunderstorm gust front is the most dangerous source of potential aircraft accidents. The study contains the analysis of several gust-front events in detail using meteorological tower, acoustic echo sounder, and pressure sensor data. The results have been compared with theoretical models and laboratory studies. Our analyses show that gust fronts can probably be detected reliably with a suitable array of different ground-based sensors. However, the determination of wind-shear severity is a more difficult problem. The results thus far show a promising relationship between the gust-front speed of motion and maximum shear.

17. Key Words	18. Distribution Statement
Wind Shear, Gust Front, Density Current, Atmospheric Pressure Jumps, Aircraft Safety, Anemometers, Surface Measurements, and Severe Weather	Document is available to the U.S. public through the National Technical Information Service, Springfield, Virginia 22151.

19. Security Classif. (of this report)	20. Security Classif. (of this page)	21. No. of Pages	22. Price
Unclassified	Unclassified	120	

Form DOT F 1700.7 (8-72) Reproduction of completed page authorized

PREFACE

This report represents the concentrated effort of numerous individuals during the past year. Several investigators generously provided us with data, advice, and guidance, however, they are in no way responsible for any errors that may remain. Mr. D. F. Sowa, Superintendent of Meteorology, Northwest Orient Airlines gave us insight into synoptic-front-generated wind shear. Mr. R. C. Goff, National Severe Storms Laboratory (NSSL), NOAA provided us with valuable data and counsel for analyzing the NSSL gust-front events. The streamline analysis at Stapleton Airport (Section 3.5) has been prepared and made available to us by Dr. F. Caracena, Atmospheric Physics and Chemistry Laboratory, NOAA.

In the following we list individuals responsible for writing the various sections.

Section 1:	G. E. Greene and J. A. Korrell
Section 2:	J. A. Korrell and G. E. Greene
Section 3:	H. W. Frank, J. A. Korrell, and G. E. Greene (The data analyses for Haswell and NSSL were performed by H. W. Frank and J. A. Korrell, respectively.)
Section 4:	A. J. Bedard, Jr., and M. M. Cairns (Section 4.2) and G. E. Greene (Section 4.3).
Section 5:	A. J. Bedard, Jr.
Section 6:	G. E. Greene and P. A. Mandics
Section 7:	P. A. Mandics and G. E. Greene

The authors are grateful to Drs. F. F. Hall, Jr., D. W. Beran, and W. H. Hooke, Wave Propagation Laboratory, NOAA for their assistance and numerous helpful suggestions. The meticulous typing and excellent cooperation of Mrs. Shirley J. Guiraud is gratefully acknowledged.

METRIC CONVERSION FACTORS

Approximate Conversions to Metric Measures

Symbol	When You Know	Multiply by	To Find	Symbol
	LENGTH			
in	inches	*2.5	centimeters	*cm*
ft	feet	30	centimeters	cm
yd	yards	0.9	meters	m
mi	miles	1.6	kilometers	km
	AREA			
in^2	*square inches*	6.5	square centimeters	cm^2
ft^2	square feet	0.09	square meters	m^2
yd^2	square yards	0.8	square meters	m^2
mi^2	square miles	2.6	square kilometers	km^2
	acres	*0.4*	*hectares*	*ha*
	MASS (weight)			
oz	ounces	28	grams	g
lb	pounds	0.45	kilograms	kg
	short tons (2000 lb)	0.9	tonnes	t
	VOLUME			
tsp	teaspoons	5	milliliters	ml
Tbsp	tablespoons	15	milliliters	ml
fl oz	fluid ounces	30	milliliters	ml
c	cups	0.24	liters	l
pt	pints	0.47	liters	l
qt	quarts	0.95	liters	l
gal	gallons	3.8	liters	l
ft^3	cubic feet	0.03	cubic meters	m^3
yd^3	cubic yards	0.76	cubic meters	m^3
	TEMPERATURE (exact)			
°F	Fahrenheit temperature	5/9 (after subtracting 32)	*Celsius* temperature	°C

*1 in = 2.54 (exactly). For other exact conversions and more detailed tables, see NBS Misc. Publ. 286, Units of Weights and Measures, Price $2.25, SD Catalog No. C13.10:286.

Approximate Conversions from Metric Measures

Symbol	When You Know	Multiply by	To Find	Symbol
	LENGTH			
mm	millimeters	0.04	inches	in
cm	centimeters	0.4	inches	in
m	meters	3.3	feet	ft
m	meters	1.1	yards	yd
km	kilometers	0.6	miles	mi
	AREA			
cm^2	square centimeters	0.16	square inches	in^2
m^2	square meters	1.2	square yards	yd^2
km^2	square kilometers	0.4	square miles	mi^2
ha	hectares (10,000 m^2)	2.5	acres	
	MASS (weight)			
g	grams	0.035	ounces	oz
kg	kilograms	2.2	pounds	*lb*
t	tonnes (1000 kg)	1.1	short tons	
	VOLUME			
ml	milliliters	0.03	fluid ounces	fl oz
l	*liters*	2.1	pints	pt
l	liters	1.06	quarts	qt
l	liters	0.26	gallons	gal
m^3	cubic meters	35	cubic feet	ft^3
m^3	*cubic meters*	1.3	cubic yards	yd^3
	TEMPERATURE (exact)			
°C	Celsius temperature	9/5 (then add 32)	Fahrenheit temperature	°F

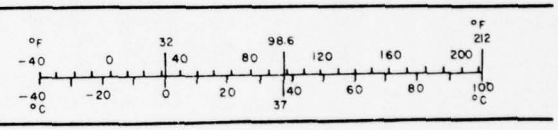

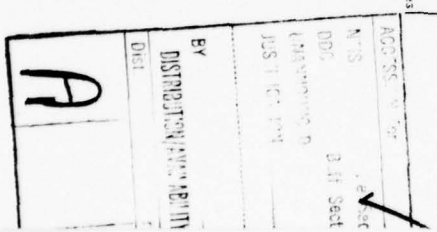

TABLE OF CONTENTS

LIST OF ILLUSTRATIONS

LIST OF TABLES

1. INTRODUCTION

Aircraft accidents resulting from severe wind shear during take-offs and landings have become a major source of concern in aircraft safety. Until recently, it was believed that shear generated by the synoptic-scale cold or warm front was the primary cause of hazardous shear. Two years ago, Grossman and Beran (1975) investigated the frequency of shear produced by synoptic-scale events. We have now concluded that a significant, if not major, portion of shear hazardous to aircraft is caused by the thunderstorm gust front on the small mesoscale, extending over distances of only a few kilometers.

In this report we consider the causes of low-level wind shear with a strong emphasis on the dynamics of the cold air outflow, or gust front associated with thunderstorms. From detailed case studies, we find general agreement with laboratory experiments and proposed density current models with some exceptions. Specific gust fronts, however, show considerable variations, as well as similarities, from one case to another. Our results suggest that the best single indicator of wind-shear severity that can be measured at the ground is the gust front speed of motion. We conclude that no one method for detecting gust fronts and estimating their severity is highly reliable but that an array of appropriate ground-based sensors can give adequate warning of potentially hazardous shear in most cases.

1.1 The Problem: Wind Shear

Wind shear is defined in the Glossary of Meteorology (1959) as the local variation of the wind vector, or any of its components, in a given direction. This variation can be a change in wind speed, direction, or both with the distance usually measured in the vertical or horizontal direction. Its effect on an aircraft is along the take-off and approach paths but in this report we will always consider the vertical and horizontal components, $\Delta\vec{v}/\Delta z$ and $\Delta\vec{v}/\Delta x$, where $\vec{v}$ is the vector wind velocity, and z and x are distances along the vertical and horizontal, respectively. Vertical wind shear is the variation in the vector wind velocity with changing height and horizontal

shear is the wind variation over some horizontal distance. The unit of shear is sec^{-1} since it is the quotient of velocity in m sec^{-1}, divided by distance in m.

Wind shear is important to the performance of an aircraft because the lift depends on the velocity of the airflow over its wings. That flow is the vector sum of the aircraft's speed relative to the ground and the wind velocity. Abrupt or large changes in wind speed can affect the lift quickly and drastically such that the pilot may not be able to respond in time to prevent a sudden drop or rise relative to the approach or take-off paths, either of which can result in a crash if it occurs sufficiently near to the ground. Therefore, pilots need to be forewarned of potentially hazardous wind shear so that they can be prepared to take corrective action.

Some degree of wind shear exists nearly all the time and usually poses no hazard. The magnitude of shear that becomes dangerous to aircraft is difficult to determine because it depends on a number of parameters such as the flight characteristics of the aircraft and its proximity to the ground. Various values of "significant" wind shear can be found in the literature; in this report we have adopted the significant shear value defined by Sowa (1974). He considers shear, defined from a pilot's point of view, to be significant when a change in airspeed greater than 8.4 m sec^{-1} occurs within 100 m which corresponds to a shear of 0.08 sec^{-1}. This is very close to the value derived by Snyder (1968) from a theoretical analysis of swept-wing aircraft dynamic response.

1.2 Causes of Wind Shear

Wind shear is caused by the motion of air masses relative to each other or to the earth's surface. In the lower boundary layer, for example, frictional forces at the earth's surface retard the mean wind aloft, resulting in vertical wind shear. Irregular terrain also alters the wind flow near the surface and produces horizontal shear. These kinds of shears are generally

small and not hazardous to aircraft. However, sub-synoptic discontinuities and meso-scale fronts, such as sea breezes or "coastal fronts," are often capable of producing hazardous shear. Orographic features, particularly strong airflow over mountainous terrain, can be important in the generation of such shear (Hill, 1976). There are three generally acknowledged major sources of significant wind shear. These are the low-level jet, the synoptic-scale frontal zone, and the thunderstorm gust front.

The Low-Level Jet

Low-level jets usually occur below 1500 m at night (and are sometimes referred to as nocturnal jets) under clear skies when a strong radiation inversion develops. The stability of the inversion suppresses mixing and momentum transfer between the large-scale flow aloft and the ground. With friction effectively cut off, a wind speed maximum, or low-level jet, forms above the inversion. At the surface, winds become light and variable because the stable inversion prevents the transfer of momentum from the high-speed winds aloft. Significant wind shear may then exist between the jet and the ground.

Much of the low-level jet wind-shear modelling work has been done by Blackadar (1957). He related the jet to the nocturnal inversion and later developed a method of predicting wind shear associated with a low-level jet at Tulsa, Oklahoma (Blackadar and Reiter, 1958). A low-level jet climatology was compiled by Bonner (1968) using two years of data at 47 rawinsonde stations. So far as we can determine, no aircraft accidents have been traced to low-level jet shear.

The Frontal Transition Zone

The front is the largest generator of severe wind shear on the synoptic scale. A front forms at the transition zone between two different air masses. This zone can be a sharp boundary or gradual change in the meteorological parameters across the air-mass interface. Wind shear is generated by the different winds existing in each air mass which meet with conflicting

directions and speeds. If the transition zone of the front is gradual, the shear generated can be relatively small. However, if the transition is abrupt, then the shear can be severe and potentially hazardous to aircraft. A more detailed discussion of frontal wind shear is presented in Section 2.

The Thunderstorm Gust Front

The gust front associated with thunderstorms is probably the most frequent source of significant wind shear. It originates as a cold, moist downdraft that spreads out as it hits the ground and propagates outward as a micro-cold front. The cold-air outflow creates strong wind gusts as far as 20 km away from the parent thunderstorm in a clear-air environment that makes the current difficult to detect, although it may show as a thin-line echo on a weather radar PPI scope. Much of the data analysis and discussion that will follow in Sections 3 and 4 will be concerned with the gust front.

1.3 Approach to the Problem

The primary concern of this report is the investigation of gust-front dynamics with the ultimate goal being the effective detection and forecast of the resultant wind shear. After a brief discussion of frontal wind shear in Section 2, we present in Section 3 thorough analyses of nine gust-front events for which a considerable amount of supporting meteorological data were available. Instrumented towers at Haswell, Colorado and the National Severe Storms Laboratory (NSSL), Oklahoma provided some measurements for increasing our understanding of the inter-relationships among gust-front parameters. The results of the data analysis should aid in predicting wind-shear magnitude from measureable quantities such as surface temperature drop or pressure jump. The case studies are compared with earlier experiments as well as theoretical models.

In addition, we have looked at the frequency of occurrence of significant vertical wind shear for several time intervals between April and June

1976 using the NSSL data. We have also developed statistics for a five-year period in the Chicago O'Hare airport area between barograph and other meteorological data. These studies are presented in Section 4 and provide a climatological overview of some of the important wind-shear features. One of the results from these analyses is amplified in Section 5, where we compare a source-driven gust-front model to a simple density current flow.

In Section 6 we summarize the results of our analyses and evaluate the current status of our understanding of wind shear. This leads into Section 7 where we make recommendations for future work which we view as necessary for providing a more complete understanding of the wind-shear phenomenon.

1.4 Summary Highlights

Frontal wind-shear generation is well enough understood to enable us to estimate shear severity and warn pilots of possible danger. Far less is known about the gust-front shear often occurring several kilometers from thunderstorms.

The detection of gust fronts is not as difficult as estimating the severity of wind shear produced by the event. Atmospheric conditions, particularly low-level stability, at the time of a gust-front arrival have a large bearing on the effects of measurable parameters near the ground. As a result, surface anemometers and thermometers may not provide an adequate measure of hazardous shears at higher levels. We find, however, that maximum shear within the density current may be related to the speed of motion of the gust front.

A statistical analysis of five years of barograph pressure data verifies that summer thunderstorms frequently produce large pressure jumps. Analyses of anemometer data in conjunction with these pressure jumps show that the surface gust surge, or change in horizontal wind in the direction of storm motion, can be related to the time rate of change of the pressure increase. This has led to a proposed model suggesting that the influence of the source

is quite important for thunderstorm gust fronts and can dominate their dynamics.

Statistics from the NSSL tower on the frequency of occurrence of vertical wind shear indicate that significant shear appears most often during the night-time hours and is probably caused by the low-level, or nocturnal jet. These events were generally not detected by the acoustic sounder or by the array of pressure-jump detectors. Usually, when the threshold of pressure rise rate was exceeded and the pressure jump detectors triggered, wind shear was present.

2. FRONTAL WIND SHEAR

2.1 Introduction

The recognition that low-level wind shear is a hazard to aircraft initially led to studies on the synoptic-scale generation of such shear. The passage of a cold or warm front frequently generates extreme wind gusts and turbulence, consequently aircraft safety concerns were at first directed at wind shear generated by the synoptic frontal zone. As a result, an operational method for forecasting shear severity from frontal parameters has been developed and is currently in use. This method is primarily the work of Sowa (1974) and is summarized below. An example of actual wind-shear measurements associated with a front concludes the section.

2.2 Frontal Shear Characteristics

A front is defined as the interface or transition zone between two air masses of different density (Glossary of Meteorology, 1959). In this section, however, we will be referring only to the synoptic-scale warm or cold fronts and not to the thunderstorm gust fronts that will be described later.

The frontal transition zone can be gradual or sharp. In either case, wind shear will be produced at the interface between the two air masses of different temperatures and wind regimes. However, only the more abrupt transition zones produce severe enough shear to be considered hazardous. The criteria given by Sowa for significant shear production are: 1) a surface frontal temperature difference of 5°C or more, and/or 2) frontal motion of 15 m sec^{-1} or more.

The vertical shape of the transition zone is also important in considering wind-shear effects. The denser air within a cold front is retarded by surface friction as it propagates so that the vertical profile of the interface is more abrupt than it is for a warm front. In the latter, the warm air flows over the top of the colder air, producing a smaller frontal slope. The

average slopes for cold and warm fronts range from 1/50 to 1/150 and 1/100 to 1/300, respectively (Byers, 1974). Their vertical cross sections are illustrated in Figure 2.1 with the associated temperature-height profiles that result from the differing slopes. When the effects of surface friction are neglected, frontal dynamics require that the slope be proportional to the vector wind shear across the front (Petterssen, 1956). Within the first km or so of the boundary layer, however, the behavior of frontal slopes is not well understood and as a result lower-level shears are less predictable.

The strongest shears are generated along the transition zone. Because of the differing directions of the two frontal slopes, the shear above the ground can occur either before or after the passage of the front at the surface. With a cold front the transition zone extends behind the surface front so that wind shear appears only after the passage of the front at the ground. For the warm front the transition zone extends ahead of the surface front and wind shear is present before the arrival of the front at the ground. The duration of potentially hazardous shear conditions is much longer with a warm front passage, not only because of its smaller slope, but also because it moves more slowly.

2.3 Forecasting the Shear

In order to be useful for airport safety, the knowledge that wind shear accompanies the passage of a front must be augmented by the capability to determine whether or not that shear is likely to be dangerous to aircraft. Sowa (1974) has attempted this by developing a method for finding the magnitude of wind shear from the surface wind and surface weather map. Figure 2.2 illustrates a hypothetical case involving both a cold and a warm front. From the surface winds at Airports A and B and the weather map isobars, the upper level winds have been determined. Airport A, under the influence of a cold front, has surface winds of 7.5 m sec^{-1} from the NW. Above the front the gradient wind is 10 m sec^{-1} from the SW resulting in a directional shear of 90°. A change in headwind component as large as 10 m sec^{-1} may occur if an aircraft lands to the SW. Airport B is under the influence of a warm front

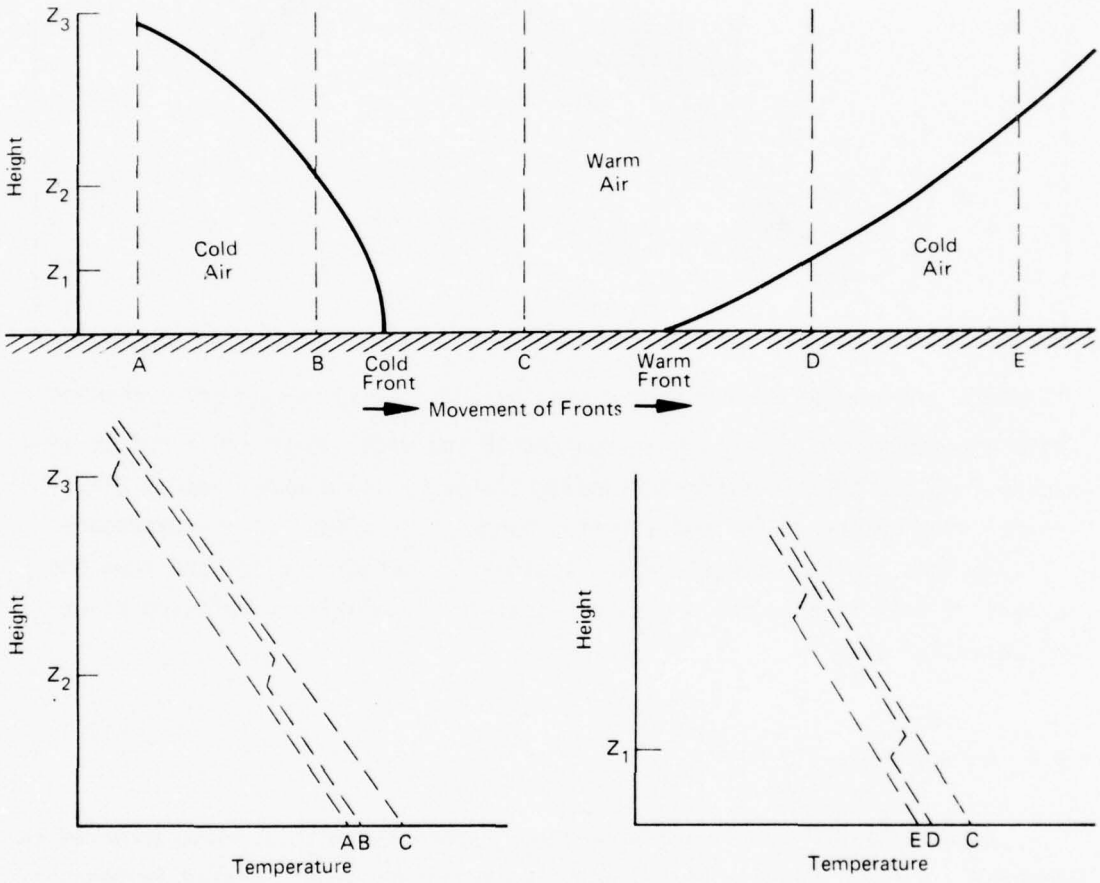

Figure 2.1 Vertical structure of cold and warm fronts. The cold front has a slope about twice that of the warm front.

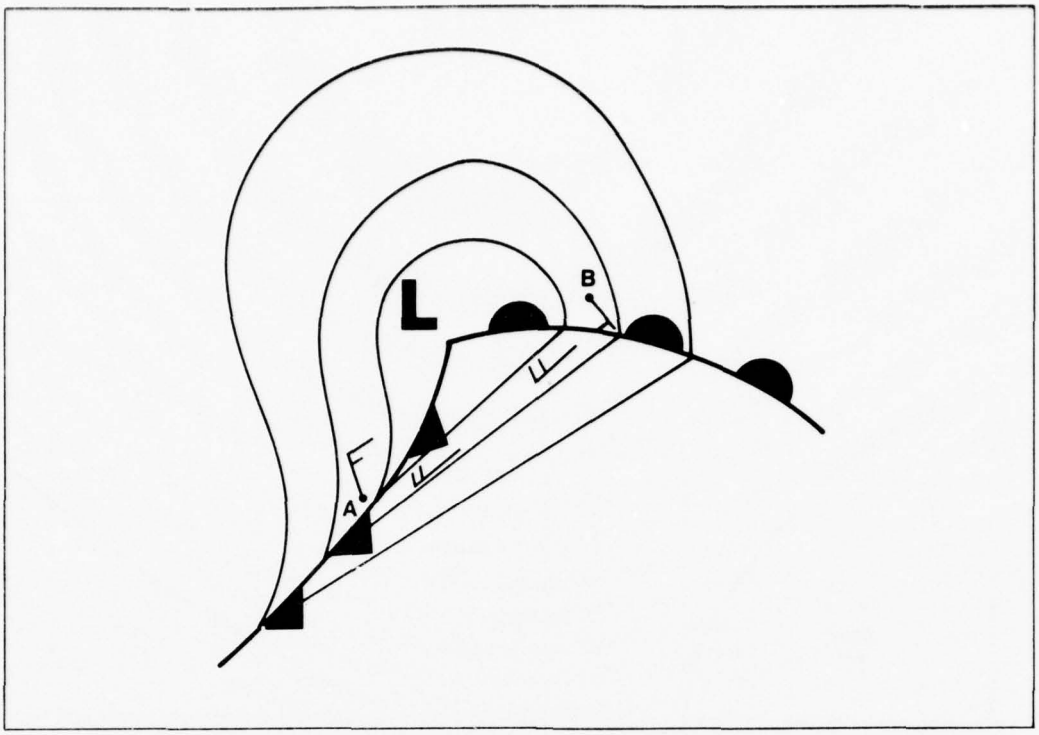

Figure 2.2 Hypothetical example showing the effects of a cold and warm front at an airport. with surface winds of 5 m sec^{-1} from the SE and winds above the front at 10 m sec^{-1} from the SW. An aircraft landing to the NE could experience a directional wind change of 90° and a speed change of 10 m sec^{-1}. The necessary calculations for this procedure are routine for meteorologists and thus the extent of both directional and speed shear are available to forewarn pilots of potential danger.

2.4 A Case Study

An example of significant wind shear associated with a front occurred on March 5, 1976 as shown in Figure 2.3. A stationary front located in Pennsylvania, Virginia, and Maryland fulfilled one of the criteria for significant wind shear: the temperature difference across the front exceeded 5°C along the entire frontal length. The surface winds across the front shifted by 90°, but the speeds were low and at some stations they were calm. Fog occurred in the cold air north of the front in Maryland and eastern Pennsylvania producing low visibilities.

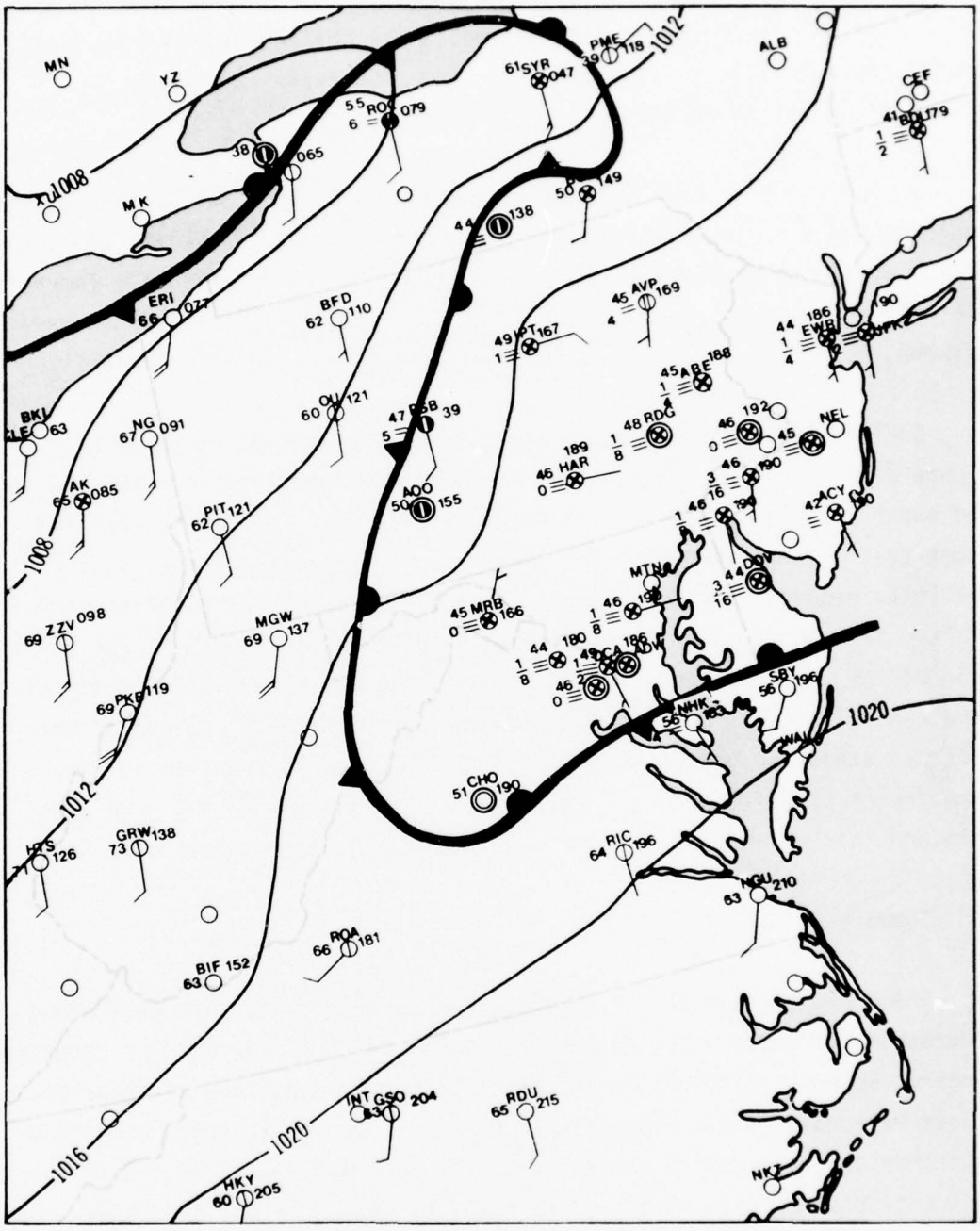

Figure 2.3 A frontal condition which produced significant shear.

The hourly weather observations at the Baltimore-Washington International Airport (Table 2.1) describe the weather conditions from 0200 to 1300 GMT. (Table 2.2 explains the notation used.) From 0700 to 1100 GMT the fog reduced visibility to 200 m with an indefinite ceiling of about 60 m vertical visibility. A light surface wind blew from the east. On Runway 10 the visual range was about 370 m.

During the four hour time period from 0700 to 1100 GMT, a specially instrumented U.S. Air Force C-141 aircraft made several takeoffs and landings on Runway 10 and measured 13 wind profiles up to 500 m altitude. The resulting data showed that shear exceeding .1 sec^{-1} was consistently observed between 150 and 400 m altitude, reaching a maximum value of .19 sec^{-1}.

One of these profiles, taken at 0813 GMT (0313 EST), is presented in Figure 2.4. The figure shows that in four 30 m layers between 200 and 400 m the shear exceeded .1 sec^{-1} or 3 m sec^{-1} per 30 m. The cross-track and along-track winds from which the shear is calculated are listed on the right and left, respectively. In Figure 2.5 the wind speed and direction are plotted as a function of height. The shear values indicated at the right side of the figure exceeded 0.1 sec^{-1} at altitudes where the wind direction remained relatively constant but the wind speed changed. In one of the profiles taken two hours later at 1001 GMT (0501 EST), plotted in Figure 2.6, a region of significant shear also occurred at 150 m when the wind speed remained fairly constant but the wind direction shifted by 65°.

2.5 Summary

The characteristics of frontal wind-shear generation are well enough understood to enable experienced forecasters to alert airports of potential danger. Sowa's (1974) method for determining the magnitude of shear severity allows meteorologists to forewarn pilots of probable hazardous conditions so that they can be prepared to take necessary corrective action should they in fact encounter serious shear. Thus with the use of synoptic weather maps and surface wind measurements, the capability for effectively coping with frontal

*Table 2.1 Hourly Weather Observations at Baltimore-Washington International Airport**

BALTIMORE-WASHINGTON INTERNATIONAL (Baltimore, MD) 4 to 5 March 1976

Time		Weather Observation							
GMT	EST	Ceiling	Vsby/Wx	P(msl)	T	Td	Wind	Alstg	RVR	Remarks
0200	2100	E3 OVC	2F	1022.0	48	46	1403	30.18		
0300	2200	E2 OVC	1 1/4F	1021.6	48	47	0000	30.17		607
0400	2300	W2X	1/8F	1021.2	48	47	1404	30.16	R10VR22V35	
0500	0000	W2X	1/8F	1020.3	48	47	1204	30.13	R10VR12V18	
0600	0100	W2X	1/8F	1020.0	47	46	0905	30.12	R10VR10V12	717
0700	0200	W2X	1/8F	1019.6	47	46	0903	30.11	R10VR12	
0800	0300	W2X	1/8F	1019.0	46	45	1103	30.09	R10VR10	
0900	0400	W2X	1/8F	1018.4	46	45	1205	30.08	R10VR10	715
1000	0500	W2X	1/8F	1018.3	45	44	1103	30.07	R10VR12V14	
1100	0600	W2X	1/8F	1018.2	45	44	1304	30.07	R10VR10V12	
1130	0630	-X E250 BKN	1/8F				1003	30.06	R10VR12	F6
1200	0700	-X E250 BKN	1/8F	1018.0	45	44	0000	30.06	R10VR6	F5 705
1300	0800	-X E250 BKN	1/8GF	1017.8	46	45	2403	30.06	R10VR10	F4

* See Table 2.2 for explanation of symbols.

Table 2.2. Explanation of Weather Observation Symbols

Weather Observation Symbols

T	Thunderstorm	RW	Rain Showers
T^+	Severe Thunderstorm	S	Snow
A	Hail	SG	Snow Grains
IC	Ice Crystals	SP	Snow Pellets
IP(W)	Ice Pellets (Showers)	SW	Snow Showers
L	Drizzle	ZL	Freezing Drizzle
R	Rain	ZR	Freezing Rain

Obstructions to Vision

BD	Blowing Dust	H	Haze
BN	Blowing Sand	D	Dust
BS	Blowing Snow	F	Fog
BY	Blowing Spray	GF	Ground Fog
K	Smoke	IF	Ice Fog

Weather Intensity Symbols

-- Very Light - Light + Heavy

Absence of symbol indicates moderate except for T, A, and IC

Sky Cover Symbols

- X Partly obscured sky (0.1 to 0.9 sky hidden by surface-based obscuration.)

X Obscuration (1.0 sky hidden by surface-based obscuration.)

Ceiling Designators

M	Measured	B	Balloon
A	Aircraft	E	Estimated
W	Indefinite	R	Radar

Sample

GMT	EST	CEILING	VSBY/Wx	P(msl)	T	Td	WIND	ALSTG	RVR
0400	2300	W2X	1/8F	1021.2	48	47	1404	30.16	R10VR22V35

CEILING - Indefinite ceiling with 200 ft vertical visibility. Sky totally obscured. The number preceding X is vertical visibility into phenomenon. Symbol after height is amount of sky cover and letter before height is method used to determine height.

Table 2.2. - Continued

VSBY/Wx	- Visibility 1/8 mile with fog.
P(msl)	- Mean sea level pressure = 1021.2 mb.
T	- Temperature = 48° F
Td	- Dew point temperature = 47° F.
WIND	- 140° at 4 kts. First two digits x 10 are the direction, last two digits are speed in knots.
ALSTG	- Altimeter setting = 30.16 inches.
RVR	- Runway Visual Range. Runway 10 has visual range variable between 2200 and 3500 ft in past 10 min. When visual range constant for past 10 min, only the constant value is reported.

shear exists and is far more advanced than shear prediction for the thunderstorm gust front about which much less is known. We will try to narrow that gap in the following sections.

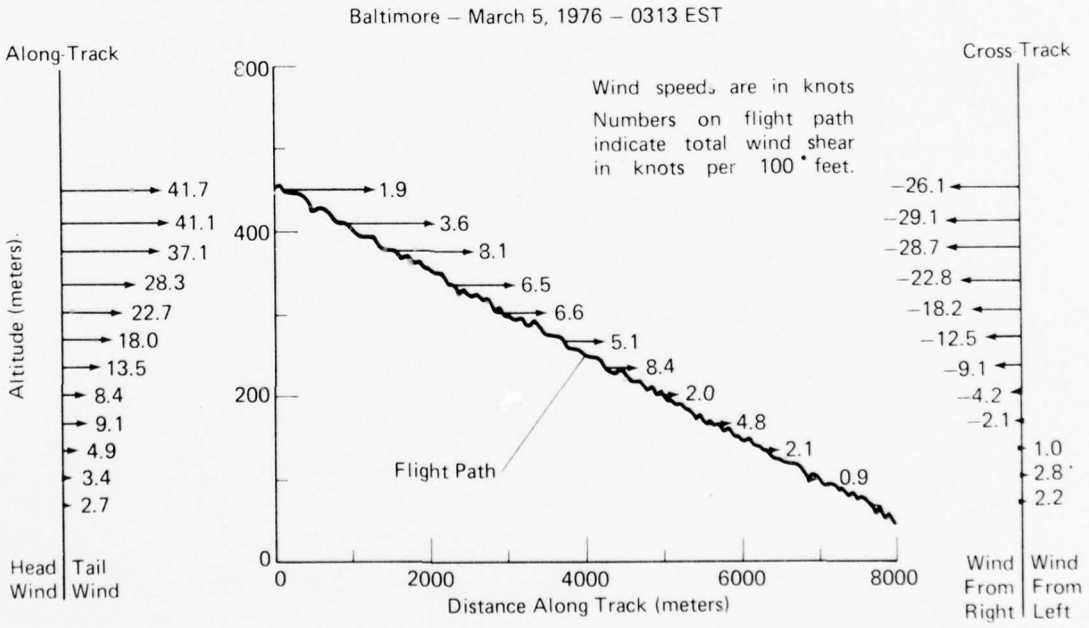

Figure 2.4 Wind profile at Baltimore-Washington International Airport.

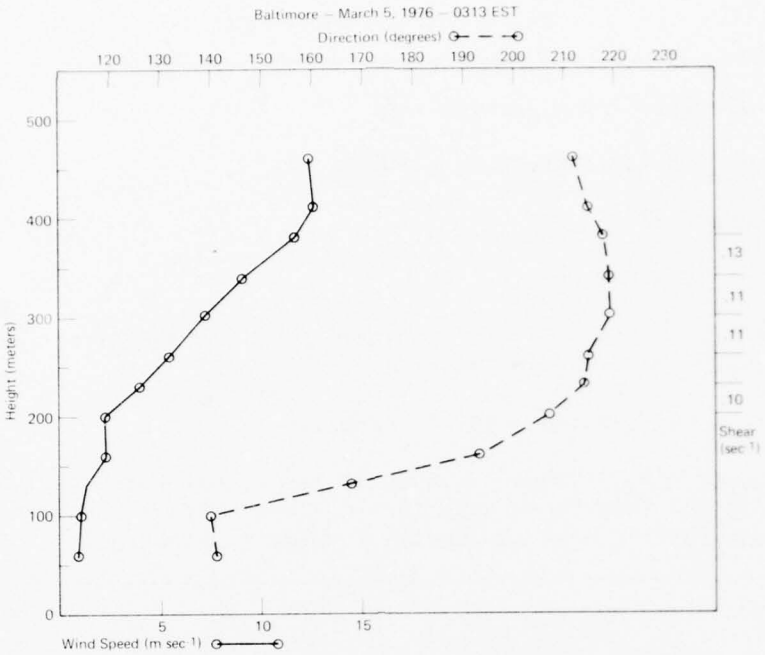

Figure 2.5 Wind speed and direction profiles with resultant significant shear.

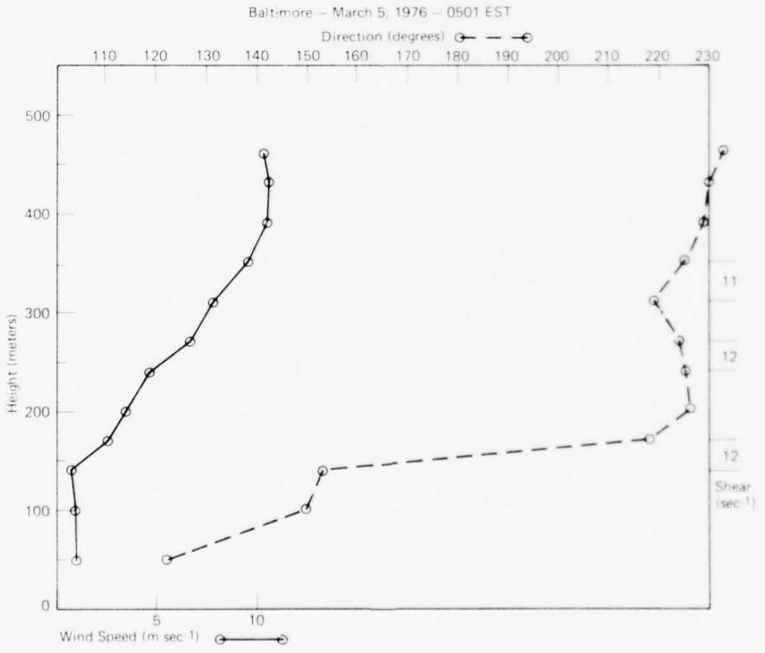

Figure 2.6 Wind speed and direction profiles with resultant significant shear.

3. GUST-FRONT CASE STUDIES

3.1 Introduction

In contrast to synoptic-scale sources of wind shear, thunderstorm outflows (gust fronts) are local and relatively short lived, and do not lend themselves to routine forecasting. They are in fact seldom detected by existing observing facilities. Weather radars can monitor thunderstorm activity, thereby alerting us when gust fronts are likely to be present in a general area, but at present the means for providing specific gust front warnings (other than the present pressure arrays at Dulles and O'Hare airports) are not available.

In this section we examine detailed observations of nine gust-front events and review previous studies. Our aim is to establish what criteria can be used to estimate the hazards associated with particular events. We discuss the models upon which the case-study analyses are based and the way the analyses were carried out. Individual events are described in Sections 3.2 and 3.3 and are discussed together in Section 3.4. In Section 3.5 we review the circumstances of a gust-front related airplane accident at Stapleton International Airport at Denver. Section 3.6 gives a brief summary of our observations and evaluations.

3.1.1 Gravity Current Structure

Thunderstorm gust fronts result from downdrafts of relatively cold, dense air produced in the storms by evaporative cooling and the weight of precipitation. When dense downdraft air collides with the ground it is forced to spread outward, flowing away from the downdraft center and undercutting the warmer (and therefore lighter) air outside the storm. As the outflow proceeds away from its source it can be described as a "density current" or "gravity current", so called because the primary motive force is provided by gravity and the density gradient. This description is generally valid for thunderstorm outflows, although non-gravitational forcing may occur when the downdraft contains substantial horizontal momentum.

Laboratory studies performed by Keulegan (1957, 1958), Simpson (1969, 1972) and Middleton (1966) have revealed a great deal about the nature of density currents in water, and have established non-dimensional descriptive parameters that apply to currents of widely different dimensions and intensity. Unfortunately the rules governing laboratory density flows cannot be transferred directly to their atmospheric counterparts with substantially different Reynolds numbers, ambient stabilities and generating mechanisms. Limited observations of density currents in the atmosphere show encouraging similarities, but the great difficulty of obtaining needed measurements has precluded a thorough description of atmospheric density currents. Simpson (1972) found similarities between density current models and atmospheric density flows, including thunderstorm gust fronts. Using data from the National Severe Storms Laboratory's (NSSL) surface observation network and an instrumented 481 m tower, Charba (1972) analyzed one gust front and compared it to the density current model. Goff (1975) analyzed 20 gust fronts of varying intensities observed at NSSL. A two-dimensional numerical model of the thunderstorm gust front, developed by Mitchell (1975), investigates regions of wind shear and the effects of the temperature drop and ambient stability upon the gust-front structure with the model. Other gust-front studies have been conducted by Colmer (1971), Goldman and Sloss (1969), Idso et al. (1972), and Hall et al. (1976).

Research on gravity flows in the laboratory and in the atmosphere has produced accepted terminology for certain features which are observed in virtually all cases. These terms will be quickly reviewed here with reference to Figure 3.1, which shows a "typical" structure.

The atmospheric gravity current is a dynamically-produced mass of relatively dense air propagating along the ground. The layer is usually no more than 2 km deep. At the leading edge of the dense mass a sharp density gradient defines the current front, or gust front; the passage of the front is marked at the surface by a sharp pressure rise. An elevated head of dense air is maintained behind the front, followed by a wake region, characterized by turbulence and mixing, expanding in depth with increasing distance behind the front. Photographs of laboratory and atmospheric density flows, and

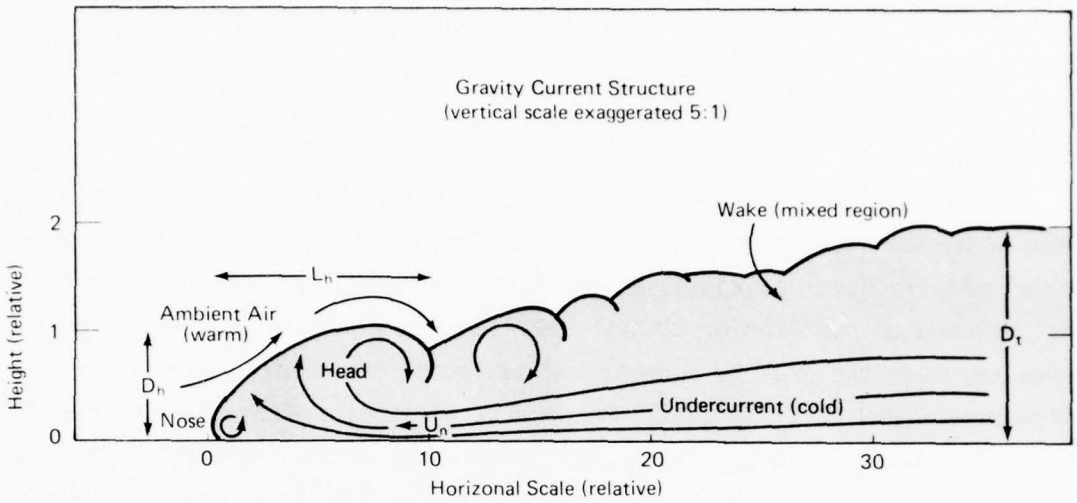

Figure 3.1 Depiction of "typical" gravity current structure.

acoustic sounder observations presented in this report, suggest that the wake may extend well above the head height.

Friction retards the current at the ground so the leading edge, or nose, of the current may be found some distance above the surface. Dense fluid moves forward with respect to the front in the lower portion of the current (under the wake), diverging upward in the forward part of the head close behind the front. A large roll may be formed in the top of the head as shown in Figure 3.1, with downward flow behind the head and upward motion in the front part of the head. Updrafts are also found ahead of the front where ambient fluid is lifted over the head. The roll feature was observed in laboratory flows by Simpson (1972) and is predicted by Mitchell's (1975) atmospheric model. The maximum speed of the forward flow, or undercurrent, occurs beneath the downflow at the rear of the head, where the forward current is compressed and pushed toward the ground. This location of the high-speed wind "core" is verified by Middleton's (1966) experiments and by Mitchell, who also finds that peak surface wind is found below the core. Because of surface friction, the maximum wind is always some distance above the

ground (up to several hundred meters), reaching its lowest height in the core region where the wind speed is about 1.5 times the front speed. Mean velocity within the steady dense current following the front is generally somewhat greater than the front speed, providing an excess of dense fluid which must be entrained into the wake.

In the initial stage of outflow from a dense fluid source (for example, when a thunderstorm downdraft first reaches the ground) the gravity current model clearly does not apply, as the head and horizontal flow pattern have not reached an equilibrium state. The laboratory experiments indicate, however, that the gravity current configuration is attained soon after the flow begins and persists until the current dissipates after the source of dense fluid is depleted. As the supply of dense fluid diminishes, the depth and velocity of the current decrease, but the current maintains a similar structure in that its shape is preserved and key parameters of the flow do not change appreciably. "Similarity" for gravity currents is generally expressed in terms of the non-dimensional Froude number, F, given by

$$F = \frac{c}{(g\ D\ \Delta\rho/\rho_0)^{\frac{1}{2}}}$$

where c is the speed, D the depth, and $\Delta\rho/\rho_0$ the relative density of the current, and g is the gravitational acceleration. In the following analyses our discussion will be confined to the Froude number of the density current head, using C_p for the front propagation speed, and D_h for the head depth. The theoretical value of F for the head region of an idealized flow is near unity (see Benjamin, 1968). However, observations in the laboratory (e.g., Keulegan, 1958; Middleton, 1966) indicate smaller values for F, in the neighborhood of 0.75. Limited observations in the atmosphere (Simpson, 1969; Charba, 1972) suggest F values ranging from 0.4 to 1.1.

3.1.2 Analysis Approach

In this section we discuss our analysis in general terms; comments specific to individual case studies or data sets appear later where appropriate.

For the nine events observed at NSSL and Haswell, the primary data sources were tower-mounted wind and temperature instruments, and ground-based acoustic sounders. Most of the events were first identified by their acoustic sounder signatures and later verified by wind and temperature analyses.

At Haswell, propagation speeds and directions were measured by means of a ground-based array of microbarographs. This allowed us to separate the wind components along and across the direction of gust-front motion. Since propagation data were not available at NSSL, wind direction was ignored in those cases and the wind fields are represented by speed only. Temperature and wind measurements were plotted in time vs. height coordinates, and contour lines were drawn to display two-dimensional cross-sections of the temperature and wind fields. These plots were scaled to match the appropriate acoustic sounder records. Important parameters for the various gravity current events were determined from the plots and tabulated (Section 3.4) so that we could conveniently evaluate possible indicators of gust-front intensity. For convenience the case studies are numbered in the order they are presented; NSSL cases are numbers 1, 2 and 3, and Haswell cases are 4 through 9.

The acoustic sounders were located near the bases of the respective towers, and measured vertical profiles of the atmosphere's acoustic backscattering cross-section as a function of time. Acoustic backscatter is produced by index of refraction inhomogeneities, resulting from temperature and humidity fluctuations (see Neff, 1975). The cool, moist air within the observed gravity currents produced large backscatter, which is represented by the dark portions of the sounder records shown in Sections 3.2 and 3.3. Excellent agreement between the tower data and acoustic sounder records verifies the sounders' ability to define the dense air mass. We were thus able to determine current depths quite accurately when acoustic sounder data were available, even when the depths were greater than the height of the tower.

Two-dimensional cross-sections displayed in the following analysis are convenient for comparison to laboratory experiments which, for the most part,

treat two-dimensional flows. Care must be exercised in the interpretation of these displays, since it is tempting to view them as "snapshots" of gust front structure. Because the structure is not necessarily steady over the time periods represented, the snapshot interpretation is not valid except for short time intervals. Therefore we focus attention in the following discussion on the immediate vicinity of the head, where we expect to find the most intense wind and wind shear (and, as a result, greatest potential aircraft hazard).

The aim of the analysis in Section 3.5 is to reconstruct as accurately as possible the conditions which led to an airplane accident. After a preliminary examination suggested that the accident occurred very close to a thunderstorm downdraft, an attempt was made to locate the downdraft position by careful analysis of the available surface wind data, and to define the exact meteorological situation at the time of the accident. Details of this analysis are given by Caracena (1976).

3.2 NSSL, Oklahoma

3.2.1 Data and Analysis

The data base for the National Severe Storms Laboratory (NSSL) study consists of meteorological tower data and acoustic sounder records. Tower data were taken from April 15 to June 24, 1976 at the NSSL tower, located 10 km N-NE of downtown Oklahoma City. Owned by KTVY-TV for their TV transmitter, NSSL instrumented it at six levels; 25, 45, 90, 177, 266, and 444 m. The date, time, and eight meteorological parameters were recorded on magnetic tape using sampling intervals of 10, 1.7, or 1.3 sec. These parameters included the wind speed and direction, temperature at the six tower levels and the surface, and the vertical velocity at each tower level.

The sensors on the tower were mounted on booms. Temperature measurements were made with Yellow Springs Instrument Co. linearized thermistor sensors housed in aspirated radiation shields. Ambient temperatures were

measured directly at each level, as opposed to a previous method that measured the difference in temperature between the thermistor at each level and a reference thermistor at the 444 m tower level. Bendix Model 120 aerovanes measured the wind speed and direction with an accuracy of ± 0.26 m sec^{-1} and $\pm 3°$, respectively. The vertical velocity was sensed with R. M. Young Model 1200 propeller anemometers. Goff and Zittel (1974) give a more complete description of the tower, calibration procedures, and other instruments for the 1972 data collection program. Only a few changes have been made since then.

From 20 May to 23 June, 1976 a monostatic acoustic sounder was operated near the tower. During the operation of the acoustic sounder, 14 gust fronts passed over the tower site. Five of these occurred while the sounder was not in operation and in four cases wind-generated noise obscured the facsimile record. Three of the 14 gust-front events were analyzed in detail and compared with the sounder record. The analysis was completed for the following three events:

1. 0118 - 0242 CST May 24
2. 1830 - 1920 CST May 30
3. 0330 - 0500 CST May 31

The wind speed, temperature, and vertical velocity were plotted as a function of time and height using 30 sec averaging. To compare the tower data with the acoustic sounder facsimile, the plots were scaled to match the height and time scales of the facsimile, then overlaid on it.

The three events chosen for analysis represent three different intensities of gust-front strength. The first case on May 24, was a very weak gust front and the only one to pass entirely within the acoustic sounder and tower's height range. The upper boundary of all the other gust fronts exceeded the range of the sensors. The second case, May 30 at 1830, was the most vigorous gust front analyzed. Its associated winds initially obscured the facsimile record with noise. This was the first in a series of gust

fronts and thunderstorm activity that started at 1830 May 30 and continued until 0745 May 31. In all, four gust fronts could be clearly distinguished on the acoustic sounder record during that night. The third case, May 31 at 0330, was one of these gust fronts, but unlike the 1830 event, this one was of moderate strength and produced an acoustic record free of wind noise, revealing detailed turbulence echoes within the gust front.

3.2.2 Observations

In this section the NSSL gust-front observations and data analyses are described in detail.

24 May 1976 (Event 1)

The distinctive feature of this gust front is that it was weak and shallow enough to be probed through its entire depth by the tower instruments and acoustic sounder (Figure 3.2). Since it was a weak outflow, its vertical velocity field, showing only a very few weak updrafts and downdrafts, was not plotted. However, the temperature and wind speed plots exhibit some interesting features.

At 0130 the gust front made its first appearance at the 200 m level where the wind speed started increasing. A nose or bulge, a common feature of gust fronts (Goff, 1975), is apparent in the wind field. Below 150 m and above 250 m the increase in wind speed lagged behind the initial surge at 200 m. At the surface the wind did not start increasing until 0140, 10 minutes after its arrival aloft.

During the first 40 minutes of the gust front passage the wind speed did not exceed 4 m sec^{-1} for any significant length of time. The cyclic appearance of wind speed maxima agrees with Hall et al. (1976). At 0204, 34 minutes after the gust front arrival, the winds suddenly increased. The core of maximum winds occurred at 176 m with speeds of 7 m sec^{-1}. The late arrival of the wind maximum suggests that a second gust front merged with the first outflow.

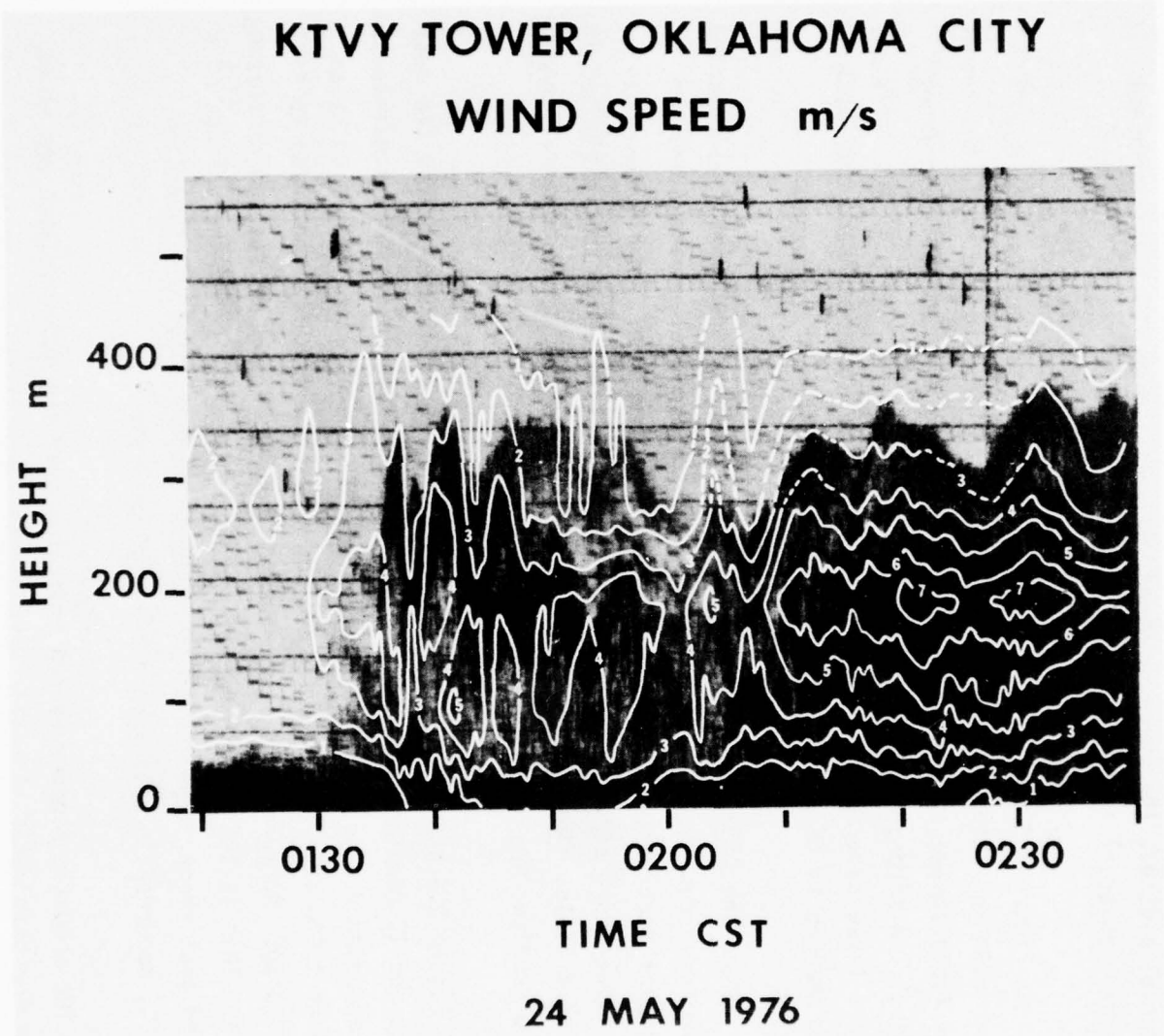

Figure 3.2 Wind field isotachs and sounder record for event 1.

Within this second outflow, the wind speed shear reached a magnitude of .04 sec^{-1}. This estimate of shear is conservative since wind direction was not taken into consideration. The shear extended through a layer between the surface and 175 m and lasted for 15 minutes, from 0220 to 0235. During the interval plotted, the shear exceeded .04 sec^{-1} below 100 m only once when it reached .05 sec^{-1} for one minute at 0143.

In Figure 3.3 the temperature field has been plotted for the May 24 event with an isotherm interval of 0.5°C. Similarly to the wind, the temperature field showed little variation or turbulence prior to the gust front arrival. A strong nocturnal inversion 50 m deep had formed at the surface with a lapse rate of -40°C/km (-2°C/50 m). Above the inversion the lapse rate changed to the normal dry adiabatic lapse rate of 9.8°C/km.

After the 0130 passage of the gust front, the temperature field started changing. From the stratified layers, the temperature decreased and the isotherms started peeling off the top of the inversion. An elevated nose in the temperature structure is apparent at 200 m, similar to that exhibited in the wind field. The temperature drop was retarded and the horizontal temperature gradient was weakened near the surface.

Figure 3.4 shows the temperature profiles for 5 minutes before the gust front and 10 minutes after its arrival. The surface inversion was maintained and deepened during the 15 minute period. The temperature decreased by as much as 1.5°C at 175 m, 100 m above the inversion top, and continued to fall until 0150. No further change occurred until 0205 when it started decreasing again. This is the same time that the wind field indicated the passage of a second gust front. The lowest thermometer reading above the inversion, 17.5°C, occurred in this second blast of cold air.

The acoustic sounder record indicates that the outflow depth was about 375 m for this case. Acoustic echo patterns are strikingly correlated with the temperature and wind fields. In particular, the 3 m sec^{-1} isotach (Figure 3.2) roughly traces the upper boundary of the echos produced by the

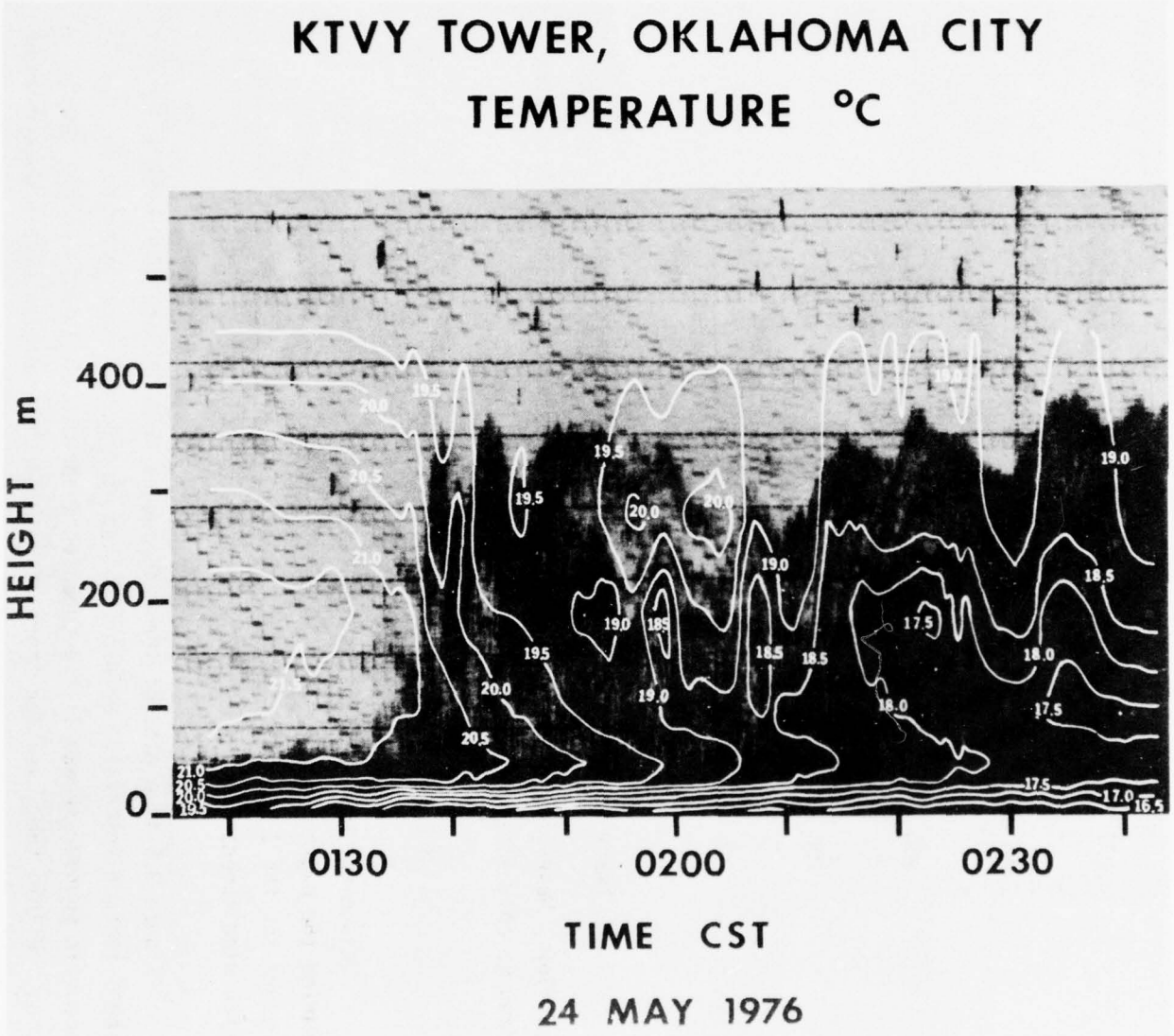

Figure 3.3 Temperature isotherms and sounder record for event 1.

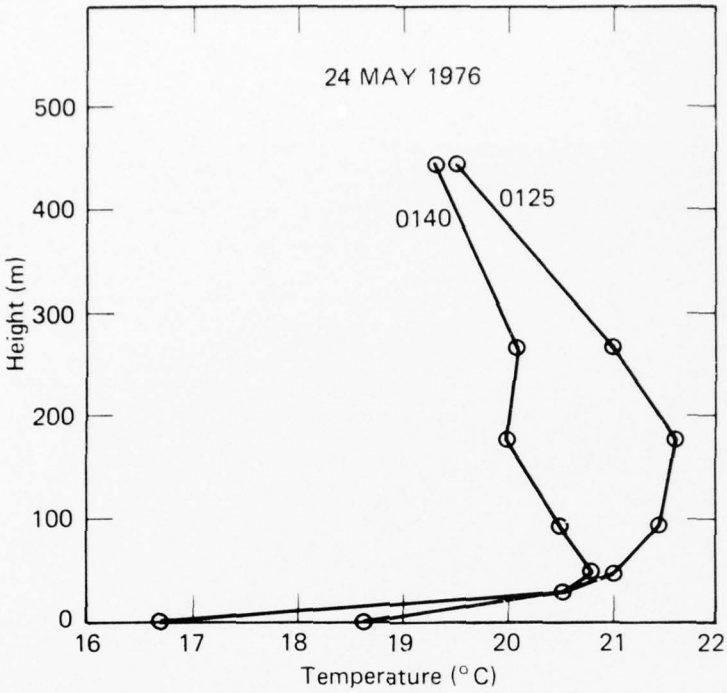

Figure 3.4 Temperature profiles before and after onset of event 1.

outflow. Wave-like patterns are apparent at scales ranging from 30 minutes down to only a few minutes.

30 May 1976 (Event 2)

This event was the first of at least four gust fronts that occurred during the night from 1830 May 30 to 0745 May 31. The acoustic sounder record for the 1830 gust front was obscured by wind noise generated by the high wind speeds.

Figure 3.5 is a plot of the wind speeds from 1820 to 1920 with a 3 m sec^{-1} isotach interval. Before 1830 the wind speeds were moderate and the acoustic sounder showed little turbulence above a 50 m deep surface inversion. Within the inversion there was a wind shear region with a magnitude of .07 sec^{-1}. Large values of shear can be generated within low-level inversions due to their stability which suppresses mixing in the vertical. The gust front arrived at 1830 with a sudden increase in wind speed at all levels.

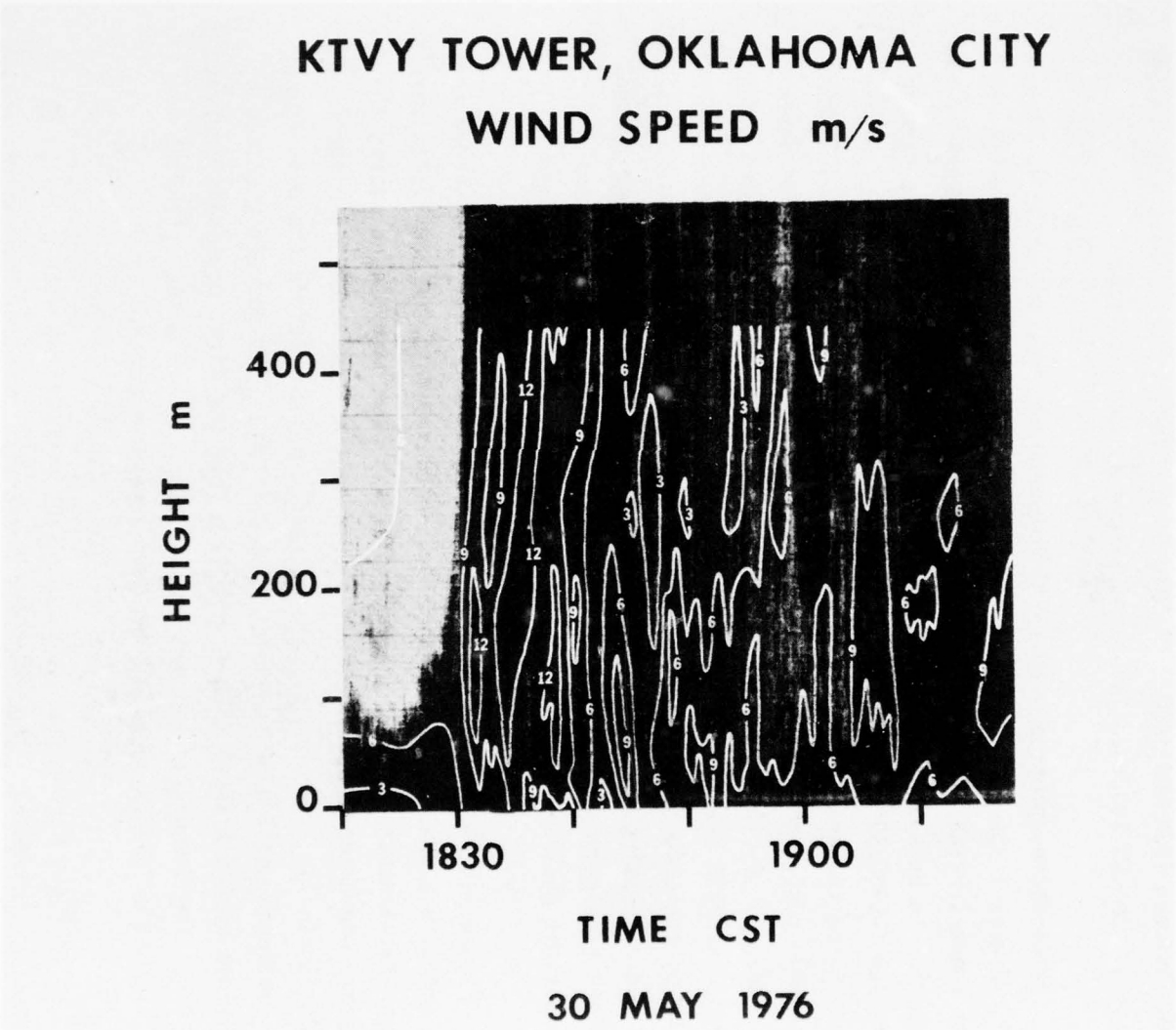

Figure 3.5 Wind field isotachs and sounder record for event 2.

At 90 m the wind speed reached a maximum of 12 m sec^{-1} within 3 minutes. At the ground, the first gust did not occur until 1834 and the gust strength was much less than at higher altitudes. Wind shears were consistently large throughout the entire event. Shears exceeding .08 sec^{-1} occurred several times between 1830 and 1850. In this 20 minute interval shears with values ranging from .09 sec^{-1} to .22 sec^{-1} lasted up to one minute.

Temperatures plotted with a 1°C isotherm interval are shown in Figure 3.6. A weak temperature inversion had formed at the surface prior to the gust front arrival. The acoustic sounder record indicated the depth of the inversion to be approximately 50 m and the tower measured a lapse rate of -14°C/km (-.7°C/50 m). At 1830 the temperature dropped suddenly. Figure 3.7 shows three temperature profiles taken 5 minutes before, and 5 and 10 minutes after the gust-front arrival. The surface inversion persisted but became much weaker. By 1835 the temperature had decreased 2.5°C at the 90 m tower level. At 1838 a brief temperature rise occurred as seen in Figure 3.6 and shown by the 1840 temperature profile in Figure 3.7. After 1840 temperatures started decreasing again and continued to decrease through the end of the plotted time period. The maximum temperature drop was greater than 4°C at the highest observed level.

Figure 3.8 shows the vertical currents with the downdrafts shaded and the updrafts unshaded. The vertical velocities within the downdrafts were so large that isotachs were omitted for clarity. The dashed line marks the boundary where the updrafts became significant and exceeded ±.5 m sec^{-1} (±100 ft min^{-1}). A strong updraft started 3 minutes before the gust front and continued until 1837, well into the outflow. This updraft attained a magnitude of 2.5 m sec^{-1} (500 ft min^{-1}) before the first downdraft arrived. The first few downdrafts had magnitudes less than -.8 m sec^{-1} (160 ft min^{-1}) and did not extend through much of the gust-front depth.

At 1837 the strong downdrafts started, alternating with updrafts of substantial intensity. These up- and downdrafts extended through the entire tower depth between 444 m and 25 m. The cores of these currents where the vertical velocities achieved their largest values were found at the altitude

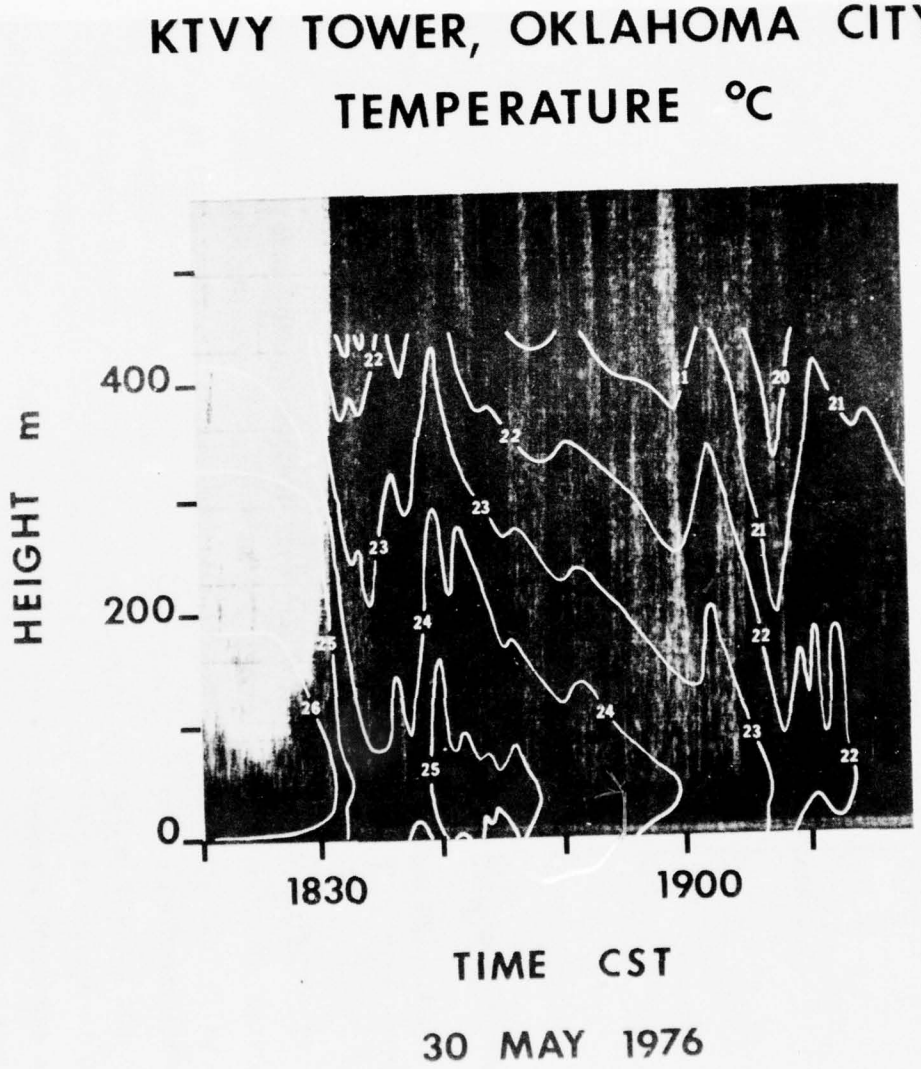

Figure 3.6 Temperature isotherms and sounder record for event 2.

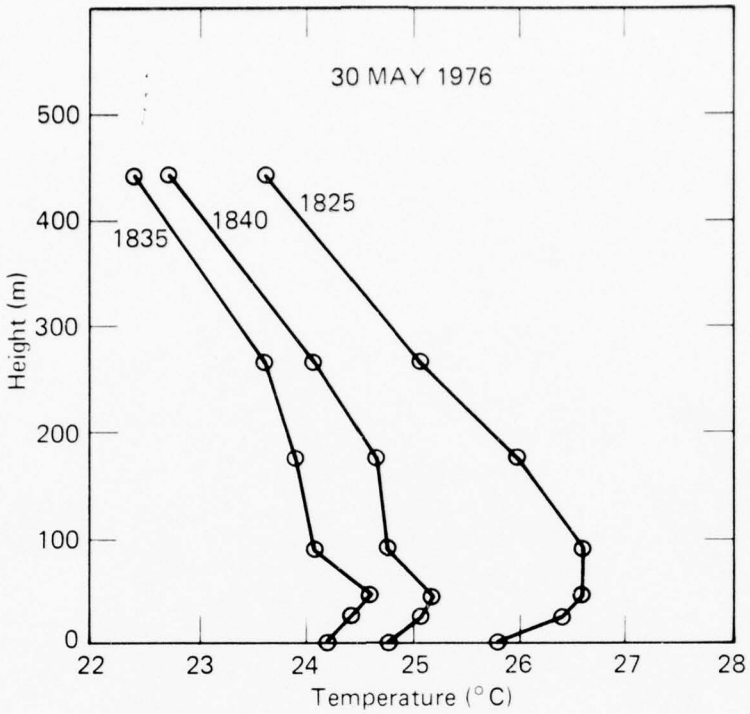

Figure 3.7 Temperature profiles before and after onset of event 2.

of 220 m. The updrafts had core vertical velocities averaging +1.5 m sec^{-1} (300 ft min^{-1}) while the downdrafts averaged -3.4 m sec^{-1} (680 ft min^{-1}).

At 1855 the strong vertical currents stopped. After this time the updrafts were less than +.5 m sec^{-1} (100 ft min^{-1}) and the downdrafts gradually lost strength with magnitudes less than -.8 m sec^{-1} (160 ft min^{-1}). The maximum vertical velocity cores in these weaker currents changed from 220 m to the highest measurable level, 444 m. In general, strong downdrafts are seen in regions where temperature is increasing with time, suggesting that they represent downward intrusions of warmer ambient air into the cold air current.

31 May 1976 (Event 3)

This gust front, arriving at 0343, was the third recognizable event on the acoustic sounder record for the night of 30-31 May. The disturbance of the atmosphere caused by the passage of the earlier gust fronts may have been

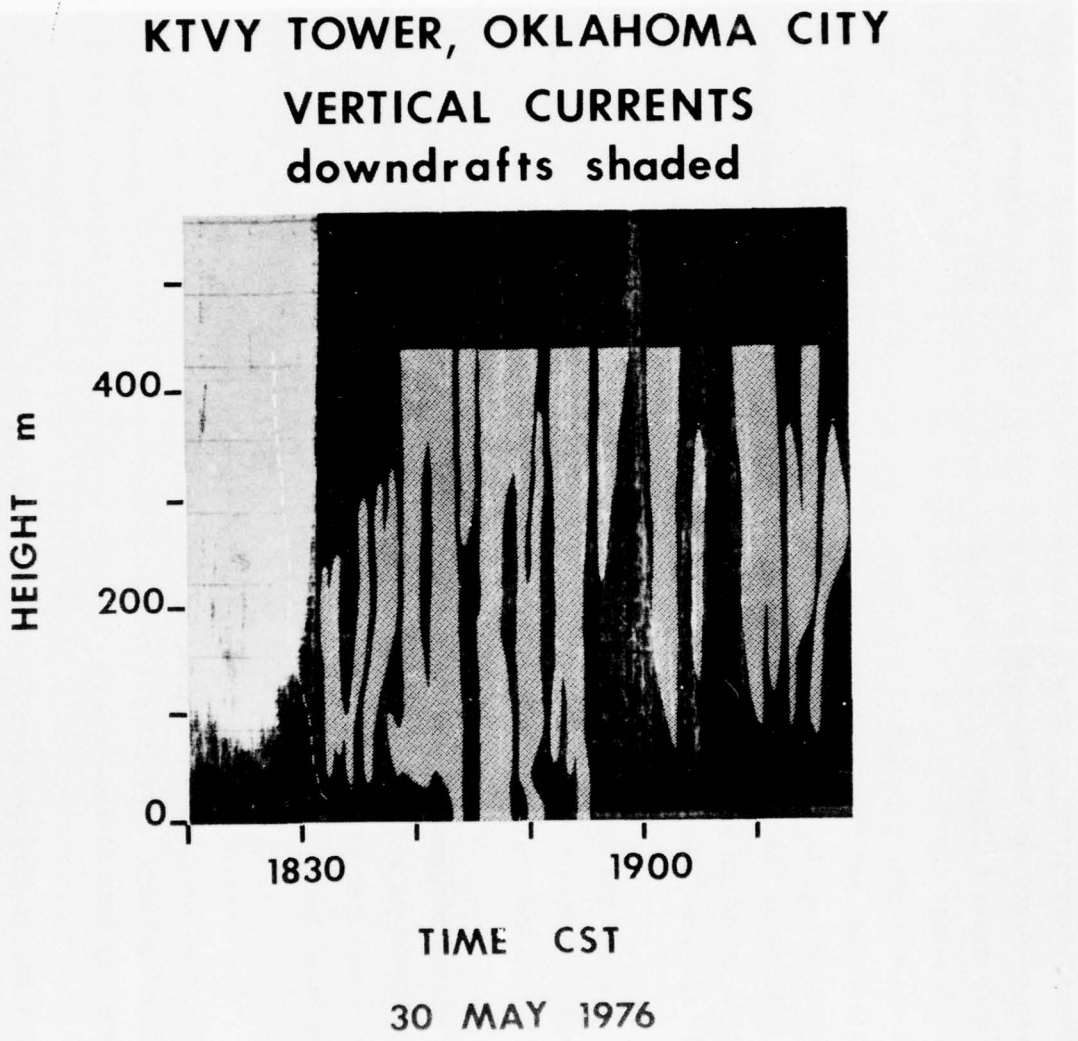

Figure 3.8 Vertical currents and sounder record for event 2.

responsible for the anomalous temperature conditions discussed later. The wind field for this event is shown in Figure 3.9. Data from 0330 to 0500 were plotted using an isotach interval of 2 m sec^{-1}. Before 0343 the winds were moderate and increased with height. They oscillated somewhat with time but no drastic change in the wind field occurred until 0343 when the gust front passed the tower. At this time the winds at 175 m increased from 4 to 11 m sec^{-1} over a period of 5 minutes. The gusts at other levels were not this large, but they were stronger below 175 m than above. During the gust-front passage the 8 m sec^{-1} isotach dropped from a height of 400 m to 50 m in 5 minutes as the high-speed winds moved in. Near the ground, the isotachs again exhibited a backward slope into the gust front as friction slowed the air and prevented the higher wind speeds from reaching the ground.

After the passage of the initial gust surge (around 0430), the winds gradually returned to the same configuration as before. They increased with altitude and the isotachs oscillated around a constant height. The shear was only .03 sec^{-1} between 100 m and the ground before 0340 but from 0430 to 0500 it ranged between .07 and .08 sec^{-1}, approaching the .08 sec^{-1} limit that is considered hazardous to aircraft. The largest shear of the event was .14 sec^{-1} measured at 0344 between the 25 and 45 m levels of the tower. Overall, the largest shears were found below 100 m.

The temperature structure exhibited by this event is more complicated than those previously discussed in that it initially increased with the frontal passage. The coldest temperatures in the current were above the tower, as seen in Figure 3.10 where the temperature field has been plotted using an isotherm interval of 0.5°C. Figure 3.11 shows two temperature profiles, at 0338 and 0348, five minutes before and after the gust front onset. Ahead of the front a 50 m deep inversion with a lapse rate of -20°C/km was topped by a nearly isothermal layer extending to 250 m where the temperature started decreasing with height. At the inversion top, the maximum temperature rise of 1.1°C occurred but there was some increase during the first five minutes throughout the entire height.

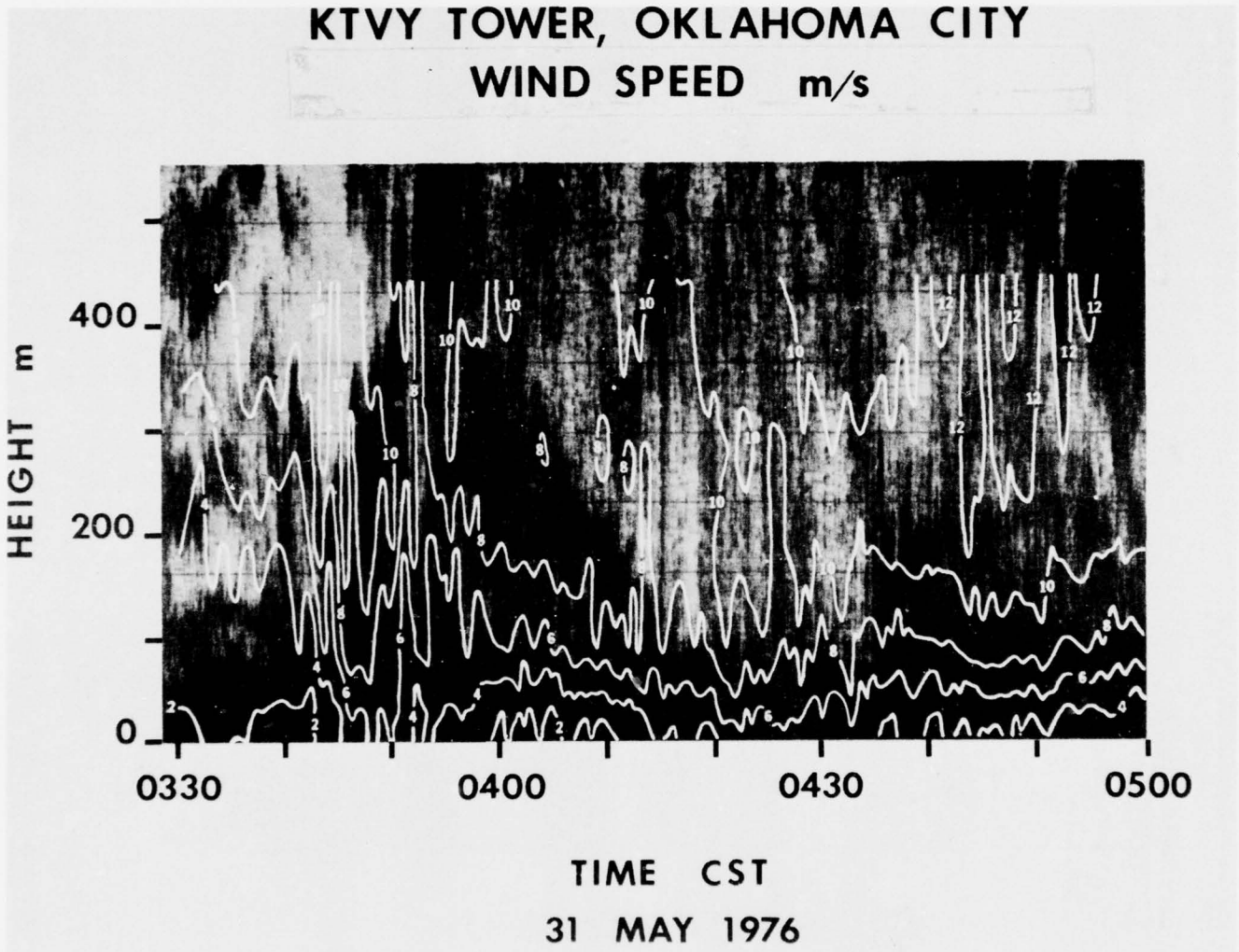

Figure 3.9 Wind field isotachs and sounder record for event 3.

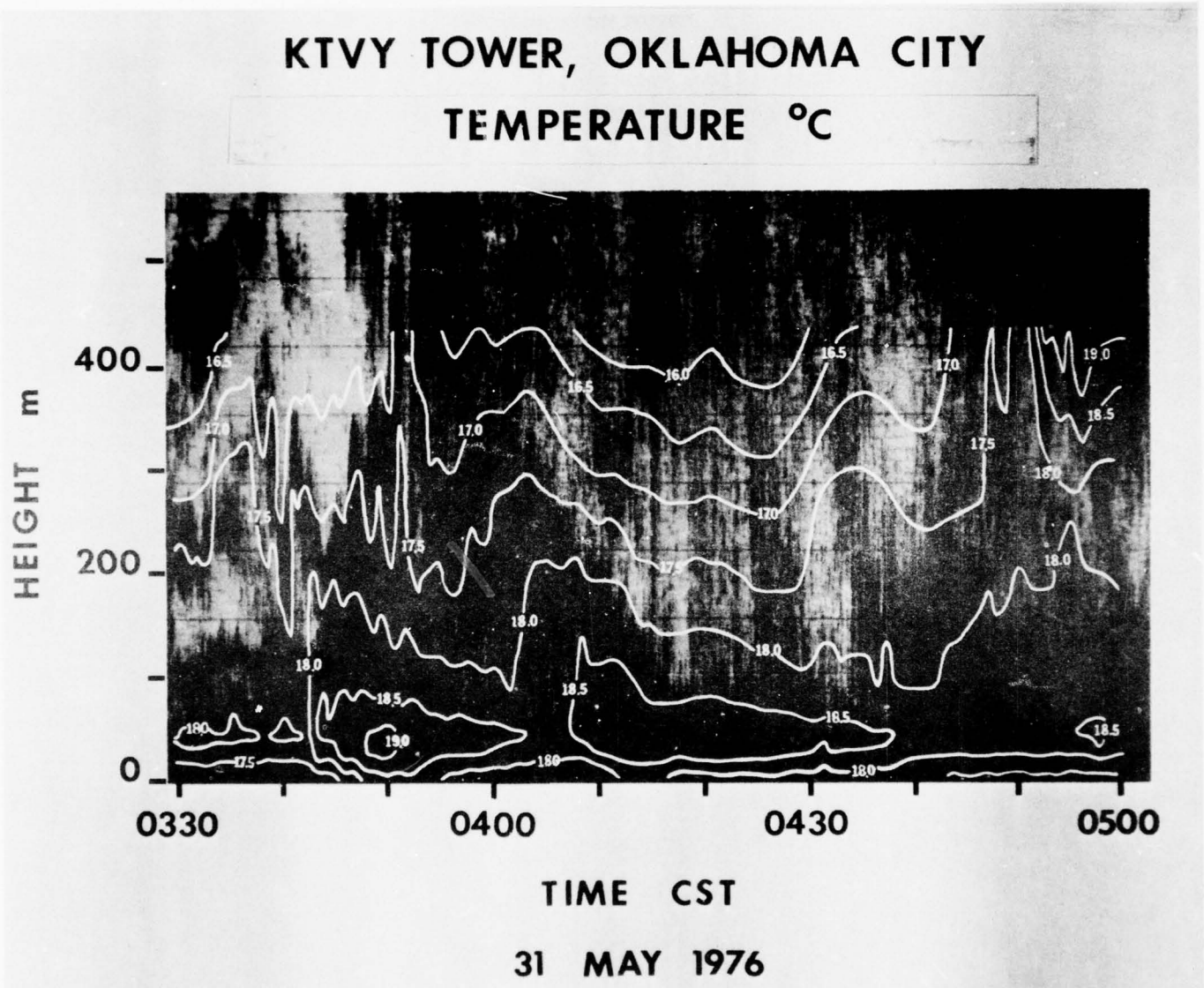

Figure 3.10 Temperature isotherms and sounder record for event 3.

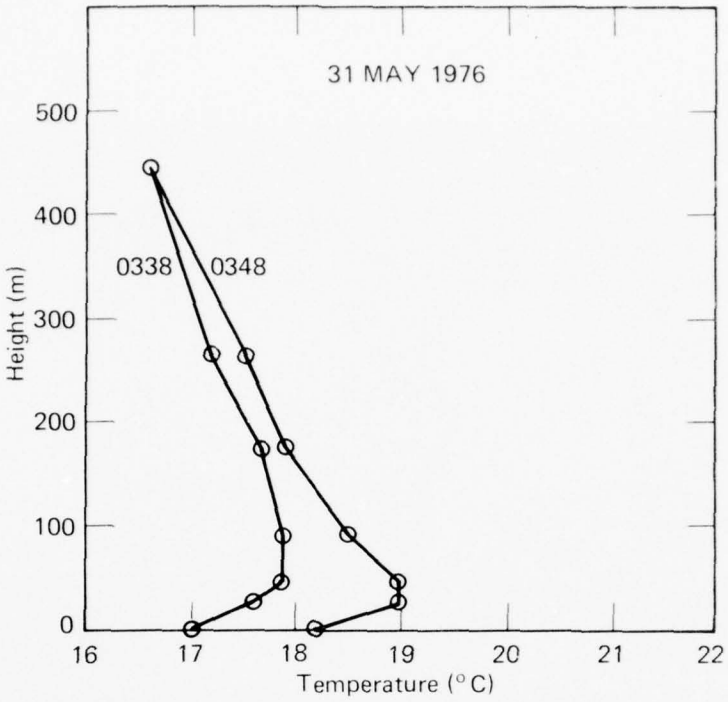

Figure 3.11 Temperature profiles before and after onset of event 3.

It is difficult to invoke a mechanism whereby a "cold-air" density current can result in a temperature increase, particularly at the surface. The situation was complicated since the ambient air had been considerably cooled by the passage of the earlier gust fronts (compare Figures 3.6 and 3.10) and may have been cooler than the outflow of this event. However, we would then expect the warmer current to ride over the cooler air ahead of it, similarly to the passage of a warm front. If the downflow had been near the tower, there may have been enough horizontal momentum for the current to initially penetrate under the cooler air before mixing began. The vertical velocity field of Figure 3.12 shows a maximum updraft of 1 m sec^{-1} (200 ft min^{-1}) beginning at 0344, followed by a stronger downdraft. The vertical velocities were large for only about 15 minutes after which they rapidly died out.

On the other hand, warm temperatures near the ground may simply represent pockets of warm air trapped beneath the nose of an overriding cold current and carried along with it. Note that a cold air mass, centered above

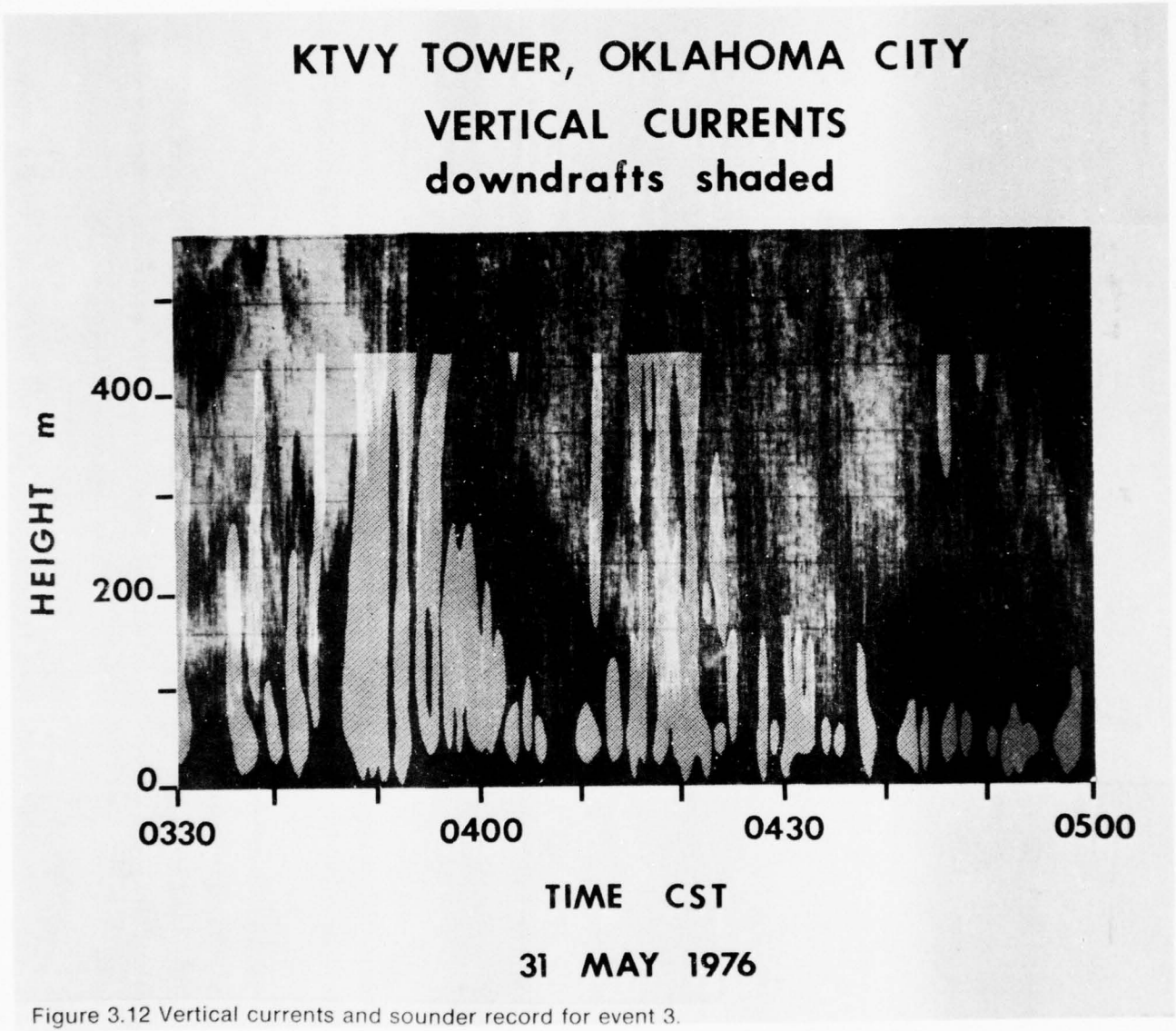

Figure 3.12 Vertical currents and sounder record for event 3.

the tower summit, is evident between 0350 and 0440 in Figure 3.10, suggesting a cold air current considerably deeper than the observed layer.

Whatever the mechanism was, significant shears were produced and this event helps to illustrate the complexities of gust front dynamics in a real atmosphere.

3.3 Haswell, Colorado

3.3.1 Data and Analysis

The 152 m Haswell tower (Figure 3.13) was instrumented with bivanes and temperature sensors at 30 m intervals beginning at 30 m, except that temperature was measured at the surface and not at 120 m for events 6 through 9. Calibration of these instruments was performed daily, but offsets in the vertical velocity were not recorded and these data were adjusted by assuming zero mean vertical motion in the ambient air outside gravity flows. Occasional uncertainties in the offset of temperature instruments were resolved by hygrothermograph recordings at 0, 30, 100 and 152 m. Wind and temperature data were recorded at one-second intervals on magnetic tape, and one minute averages were later computed to construct time-height plots. Twelve-second averages were used for a portion of event 9 as discussed below.

Gust-front propagation speeds and directions were determined from pressure disturbances at three surface microbarographs near the tower. The local frontal motions determined this way may not represent the average motions because of possible irregularities and unsteadiness at the fronts such as those described by Simpson (1969, 1972). Horizontal wind components normal to the fronts (along the propagation direction) and parallel to the fronts were computed using these estimates of frontal motion. Horizontal distance scales are given on the top border of each plot assuming that the fields are steady-state and propagating with the front. This assumption is of course invalid in many cases and the time-height representations cannot be treated as instantaneous vertical cross sections except over short time intervals. Contours are drawn by hand from the averaged data, smoothing out

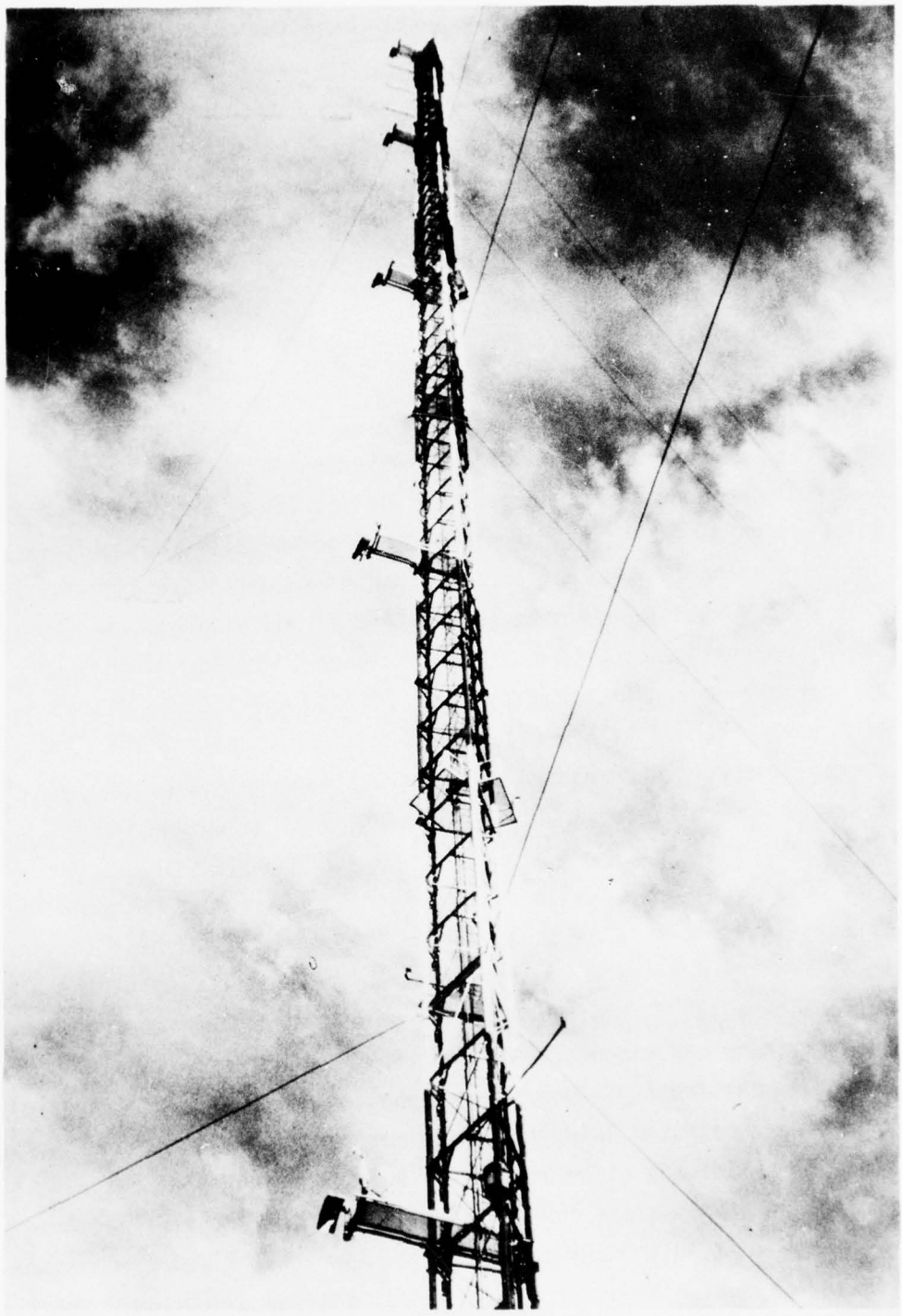

Figure 3.13 Instrumented 152 m Haswell Tower.

scales smaller than one or two grid intervals. Vertical velocity at the 152 m level is included for the first four events, and is similarly hand smoothed from averaged data.

Radar echo maps from the National Weather Service WSR-57 radar at Limon, Colorado were used to determine the proximity and motion of thunderstorms in the area where appropriate.

On 8 August 1972 additional measurements were obtained from a rawinsonde released close behind the front, and for a short time (from 0541 to 0554 MDT) a Doppler radar was operated in the VAD mode (see Lhermitte, 1966) 10.5 km WNW of the tower. The Doppler data covered the height interval from 74 to 356 m with about 50 m height resolution, and provided a profile of horizontal wind as well as a measure of local horizontal divergence which will be discussed later.

Two events observed at Haswell are not attributed to thunderstorm activity. They occurred on 8 August 1972 (a cold front passage) and 22 March 1974 (a sub-freezing current of unknown origin). Because these cases exhibited gravity current structure and potentially hazardous wind shears, they were analyzed in the same way as the others and are considered pertinent to this study.

3.3.2 Observations

The six events described here (Figures 3.14 through 3.19) vary widely in dimension and intensity. Events 4, 5, 7 and 9 are attributed to cold air outflow from thunderstorms, although for event 9 no radar data is available to verify storm location. A few small thundershowers were present in the area at the time of event 6, but the much longer time scale and absence of large storms suggests that a synoptic-scale cold front was observed in this case. Synoptic surface maps show a cold front, oriented west-east and moving southward, in the Haswell area at the time. Subfreezing temperatures in case 8 suggest that it was not related to convective activity; perhaps this current resulted from cold air drainage into the shallow depression around the

tower site. This current propagated very slowly and differs in Froude number from the other flows, as indicated in the plots and in later discussion. No discernible pressure signature accompanied the event, so in this case front propagation is assumed to be in the direction of the core wind.

Most of the important descriptors for these flows are summarized in Table 3.1 and comments on the individual cases are presented below.

2 August 1972 (Event 4, Figure 3.14)

After an initial rapid temperature drop of about 5°C at 1827, the temperature continued to decrease throughout the observed time. Although the coldest area was apparently above the tower top, a well-defined wind maximum was located near 60 m height and ahead of the temperature minimum. Contoured fields show evidence of retardation (elevated nose) in the temperature field, and clearly indicate that the wind profile nose is about 150 m high. Large eddies (i.e., large with respect to the data intervals) are indicated by flow reversal below the wind nose. Data collection was stopped around 1910 as a number of the instruments were destroyed by high winds. Acoustic signals were masked by wind noise, therefore, the depth was estimated at 450 m on the basis of temperature drop, ΔT_{max}, and propagation speed, C_p, assuming that the Froude number was 0.76 (see the discussion in Section 3.1.1).

5 August 1972 (Event 5, Figure 3.15)

With the arrival of the gust front at 1931, temperatures dropped very rapidly at all tower levels by about 10°C. All temperature recorders were off scale for approximately 7 min, preventing us from plotting temperatures in the front vicinity. Since the initial drop occurred almost simultaneously at all levels, the front must have had a nearly vertical slope in the tower layer. The wind maximum was apparently just above the tower at about 200 m, but the earliest evidence of wind increase in the lowest 150 m occurred near the ground, 10 min ahead of the temperature transition. A well-defined cold-air mass and wind core persisted for about 30 min after the frontal passage, followed by relatively constant temperatures and winds.

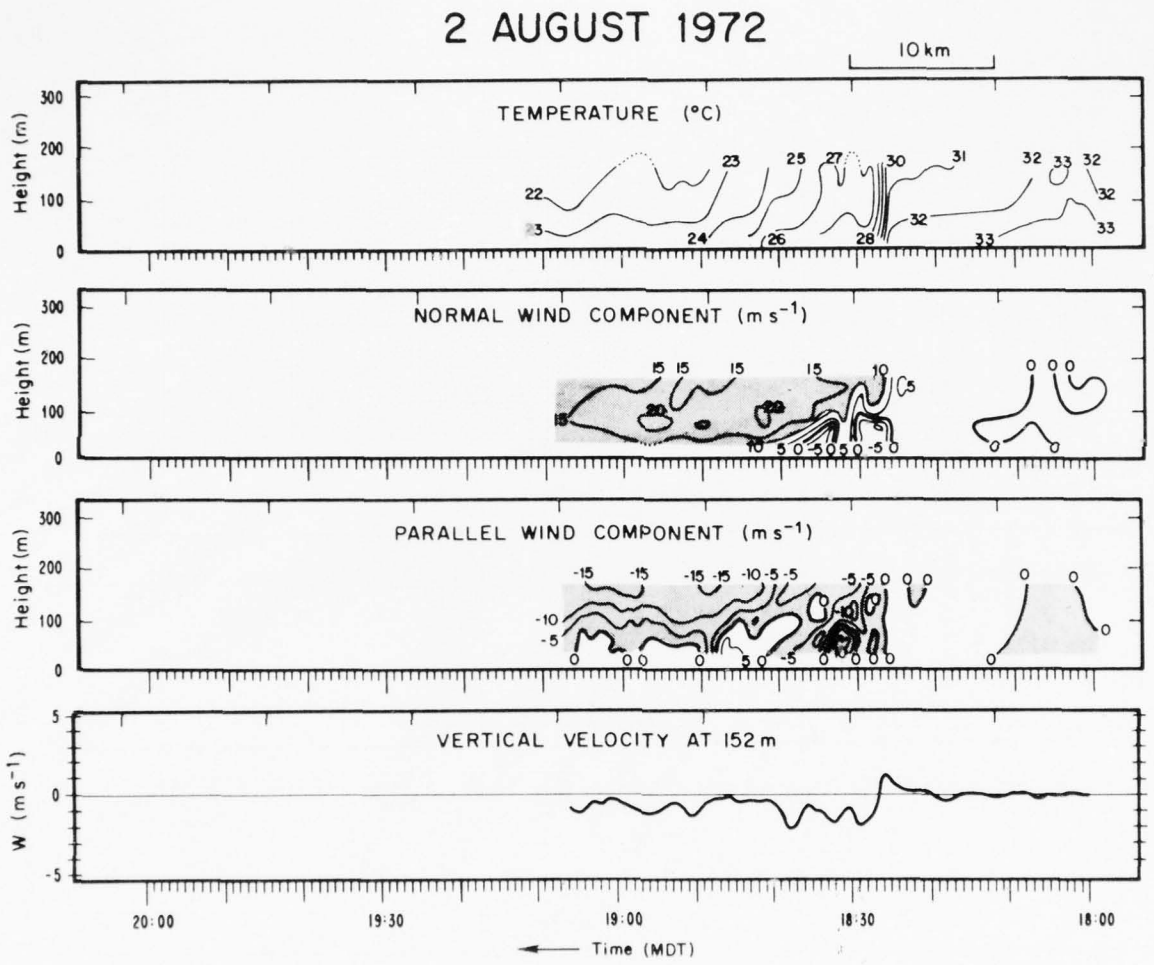

Figure 3.14 Profiles for event 4.

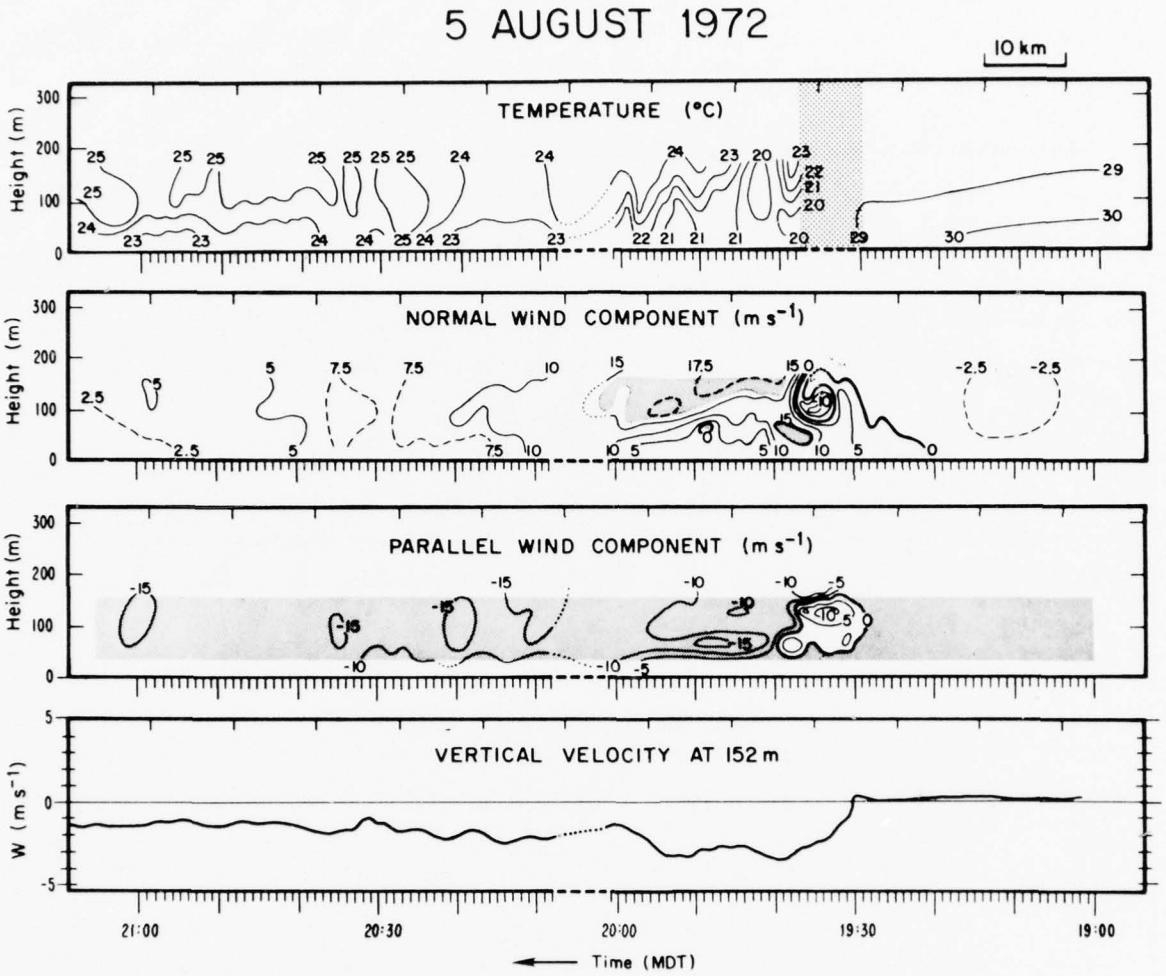

Figure 3.15 Profiles for event 5.

As in the preceding case, intense eddies appeared near the leading edge of the maximum wind core, and again there was no useable acoustic sounder record. Outflow depth was estimated at about 1400 m by the same method as mentioned above. A brief period after 2000 when no data were recorded is indicated in the plots by a dashed section of the time axis.

This event was the most intense one observed at Haswell, perhaps owing to the relatively close proximity (less than 10 km) of the thunderstorm which produced it.

8 August 1972 (Event 6, Figure 3.16)

As was mentioned earlier, this case is attributed to a synoptic front. It is not surprising, therefore, that the scales (particularly time) associated with it are notably different from the other cases. The wind disturbance preceded the temperature change by about one hour, and similarly to the two previous cases, strong fluctuations preceded the wind core. With the arrival of the temperature drop and wind maximum, wind noise obscured the sounder record. The depth of this current was estimated at 1327 m, assuming a Froude number of 0.76. An 0456 temperature sounding, probably taken ahead of the deepest part of the current, verified that the depth was at least 800 m.

Tower measurements indicate that the maximum normal wind (>20 m sec^{-1}) occurred around 0510 above the tower. Doppler radar results at 0547 showed the wind increasing with height to about 17 m sec^{-1} at 350 m, indicating the wind maximum was weaker and higher after the peak wind core had passed. Also, local horizontal divergence measured by the radar was positive below 150 m and negative above. This suggests that maximum downward velocity at the time was located near 150 m, where the tower instrument recorded a 2 m sec^{-1} downdraft.

It is interesting to note that the acoustic sounder record showed no evidence of the strong winds ahead of the temperature transition, except for disturbances on the surface inversion which was present before the front arrived.

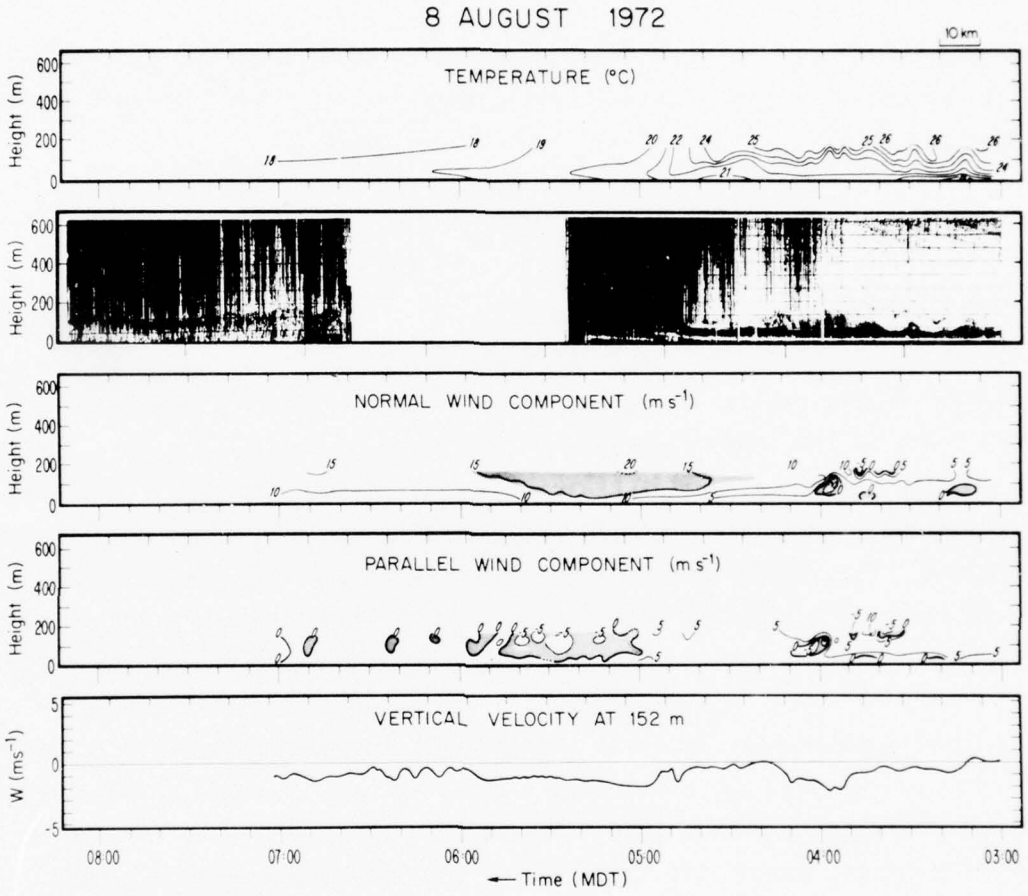

Figure 3.16 Profiles for event 6.

11 August 1972 (Event 7, Figure 3.17)

This was the first of three relatively mild gravity currents that nevertheless provided exceptionally good descriptions of atmospheric gravity flow structure. A number of features described in Section 3.1.1 are illustrated in Figure 3.17; the current head, 375 m deep, is clearly outlined on the acoustic sounder display between 2317 and 2323. Minimum temperature and a well-defined wind core appear in the head region. Vertical velocity at 152 m is upward ahead of the front and downward in the rear portion of the head, suggestive of the expected roll within the head.

The maximum normal wind in this case, 4.3 m sec^{-1}, is less than the 6.7 m sec^{-1} propagation speed of the front, a surprising observation that may result from the irregular local motion of the front (which might cause a poor estimate of propagation speed). Middleton (1966) observed similar cases in dissipating currents and suggests that the front may temporarily move faster than the following flow if the head depth is decreasing. It appears possible, therefore, that at the time of these observations the current was approaching dissipation, and the head was beginning to collapse.

A surface-based temperature inversion observed before this event was disrupted only temporarily near the ground, and was re-established soon after passage of the head. The stability of the ambient atmosphere may have had a suppressing effect, contributing to the shallowness of the flow.

22 March 1974 (Event 8, Figure 3.18)

Low wind speeds and little evidence of turbulent fluctuations distinguish this event from the others presented in this study. The Froude number was approximately 0.23, much smaller than for the other cases, and the current's appearance is that of a slow-moving mass of cold air sliding beneath the very stable ambient air (again a surface-based inversion preceded the flow). Substantial wind shear (0.11 sec^{-1}) occurs as the ambient flow is forced over the cold current.

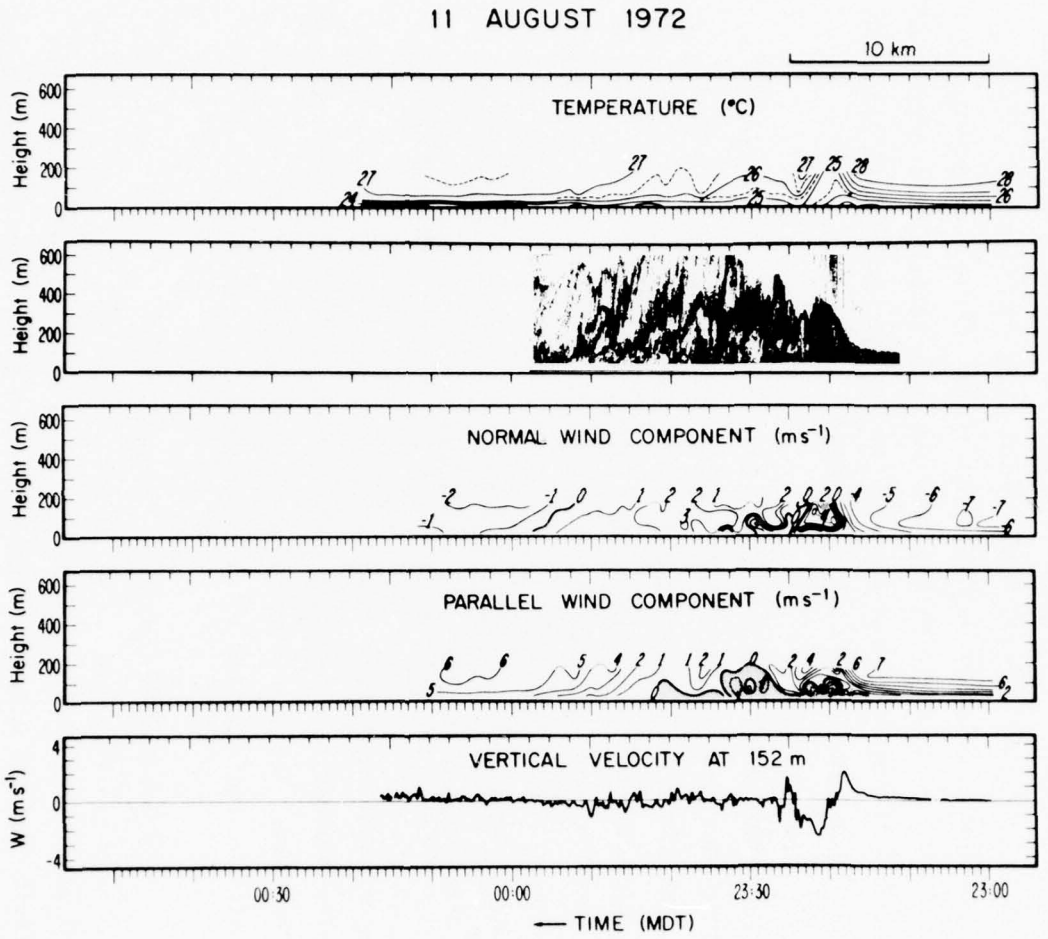

Figure 3.17 Profiles for event 7.

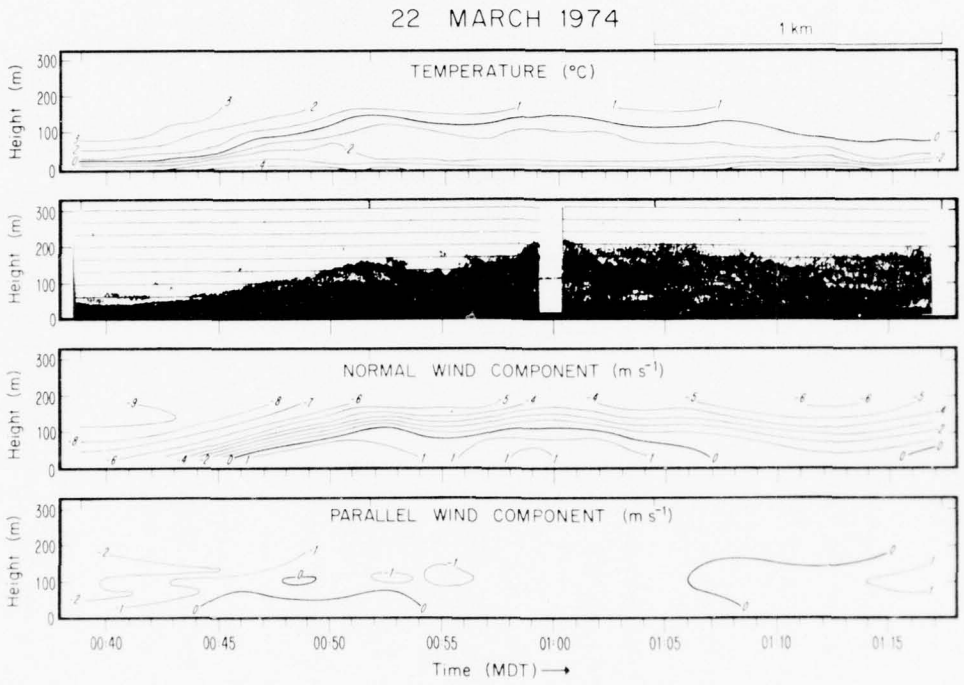

Figure 3.18 Profiles for event 8.

27 March 1974 (Event 9, Figure 3.19)

While similar to the preceding case in some respects (temperature drop and ambient stability) this current moved faster and displayed a head and turbulent wake. The wind maximum was close to the ground, below the lowest tower instrument level at 30 m, and near the center of the head.

From 0005 to 0025, tower data were plotted at 12 sec rather than 1 min intervals to emphasize the turbulent wake and the detailed correspondence of the acoustic sounder record.

3.3.3 General Comments

For most of the Haswell gravity currents, the forward flow with respect to frontal motion persists for fairly short periods. There are two likely explanations for this: (1) the currents may be separated from their source when they reach the tower site and are thus not sustained by a steady flow of new dense air, and (2) the currents might dissipate significantly during the observation period.

In the first four cases, for which vertical velocity is recorded, there is a clear indication of downflow behind the fronts. Significant updrafts ahead of the fronts are apparent only in the shallower cases 4 and 7; presumably, similar updrafts would have been recorded for the deeper currents if the measurement had been taken at a higher level (i.e., above the wind core). Maximum vertical velocity is on the order of 2 m sec^{-1} (400 ft min^{-1}) in each case.

An interesting feature common to the Haswell events is that the core wind is directed from 5° to 35° to the right of frontal motion. While it is tempting to attribute this to Coriolis effects, there is no clear dependence on age; the largest deviations occur in the weaker and shallower currents, however.

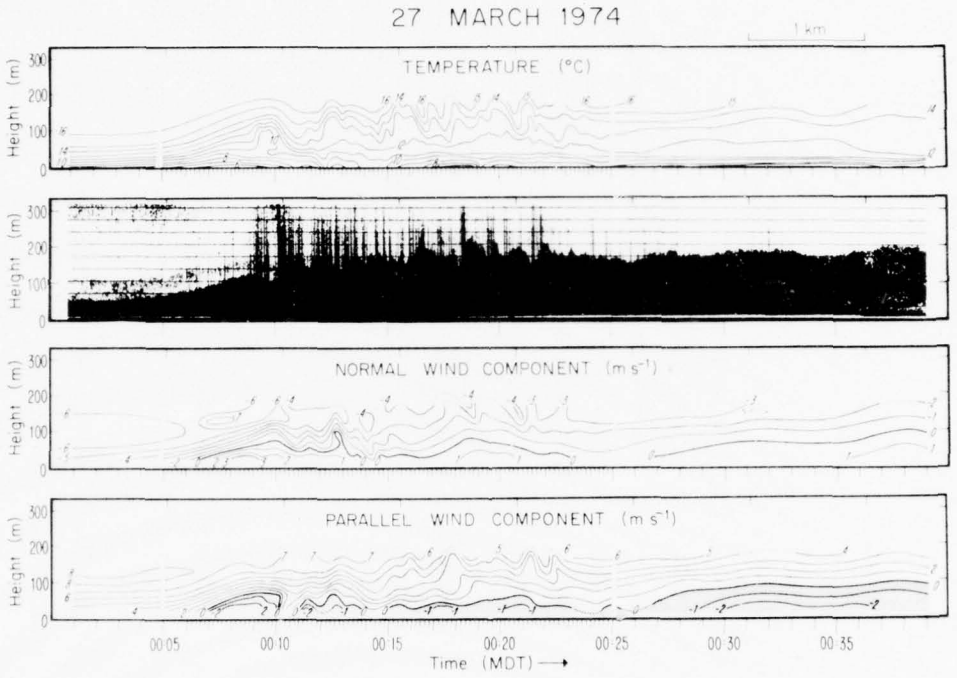

Figure 3.19 Profiles for event 9.

3.4 Discussion

In this section we summarize and discuss observations presented in Sections 3.2 and 3.3, making frequent reference to the models and observations described in Section 3.1.1. We then turn to the specific problem of choosing practical indicators of wind-shear intensity.

3.4.1 Observed Gravity Current Structure

Table 3.1 lists the parameters which were chosen to represent vital features observed in the various case studies. For the most part these descriptors are derived from the time-height plots, and therefore represent time scales generally greater than one minute. Instantaneous peak values of some parameters are likely to exceed the listed values. The symbols used in Table 3.1, and the methods used to determine parameter values are defined as follows (exceptions are marked with (*) in the table and are discussed later):

C_e : thunderstorm echo propagation speed where appropriate; determined from serial radar maps.

C_p : front propagation speed; determined from microbarograph array.

d : distance travelled from apparent source thunderstorm where appropriate; determined from serial radar maps.

D_h : depth of current head; determined from acoustic sounder record.

D_t : total depth of current (includes mixed layer); determined from acoustic sounder record.

$H(S_n)$: height at which S_n occurs; determined from contoured u_n field.

Table 3.1 Gravity Current Parameters (symbols defined in text)

Event No.	1	2	3	4	5	6	7	8	9
Date	5/24/76	5/30/76	5/31/76	8/2/72	8/5/72	8/8/72	8/11/72	3/22/74	3/27/74
Time (Local)	0130	1830	0340	1821	1931	0443	2316	0045	0005
ΔT_{30} (°C)	3.0	4.0	-1.0**	9.7	9.8	4.1	1.6	4.1	4.2
ΔT_{max} (°C)	4.0	4.0	0.0**	(≥9.7)	(≥9.8)	(≥7.7)	4.0	5.5	5.5
$H(\Delta T_{max})$ (m)	175	190	40	(≥152)	30	(≥152)	152	91	61
T_a (°C)	20.5	25.5	17.5	32	29	24	28	01	13
D_h (m)	370	770*		450*	1394*	1327*	375	170	100
D_t (m)							700	240	220
L_{ts} (km)				7.0*	8.6*	25.0*	3.2	0.78	1.0
S_n (sec^{-1})	0.4	.22	.09	0.7	1.1	0.7	0.23	0.11	0.16
$\hat{S}_n$ (sec^{-1})				0.32	0.26	0.25	0.14	0.11	0.16
$H(S_n)$ (m)				76	76	137	46	76	76
U_n (m sec^{-1})	7*	15*	11*	20.4	(>19.5)	(>19.8)	4.2	1.9	4.0
$H(U_n)$ (m)	90*	120*	200*	60	200*	250*	60	20*	15*
t_s (min)				45	35	80	16	10	8
t_{ws} (min)	7	1	0	0	3	60	0	2.5	0
α							0.2	0.16	0.11
C_p (m sec^{-1})	4.7*	10*	7.4*	9	16	14	6.7	1.3*	3
Θ_p (deg)				000	335	025	305	000*	250
V_c (m sec^{-1})	7	15	11	20.5	(>20.2)	(≥20.0)	4.9	1.9	4.8
Θ_c (deg)				005	(352)	(030)	330	000	285
C_e (m sec^{-1})				13	9	(Little motion)	(Little motion)		
Θ_e (deg)				290	320				
d (km)				35	9		65		
λ (°C/120 m)	+1.0	0	-0.5	-1.7	-1.3	+3.2	+3.3	+2.2	+3.9

** See text for explanation.
* Estimated (see text).
( ) Approximate or limiting measured value.

$H(\Delta T_{max})$: height at which ΔT_{max} occurs.

$H(U_n)$: height at which U_n occurs; estimated from contoured u_n field.

L_h : horizontal length of head estimated using time-distance conversion; determined from acoustic sounder record.

S_n : maximum value of vertical shear of the normal wind, du_n/dz; determined from contoured u_n field.

$\hat{S}_n$: time-average of maximum shear observed under the wind core; estimated from contoured u_n field.

t_s : time duration of $du_n/dz > 0.08$ sec^{-1}; determined from contoured u_n field.

t_{ws} : length of time between initial wind shift and temperature drop; determined from contoured fields.

T_a : mean ambient temperature in the tower layer; estimated from contoured temperature field.

ΔT_{max} : difference between ambient temperature and minimum temperature within current as measured at the level of maximum temperature difference.

ΔT_{30} : difference between ambient temperature and minimum temperature within current as measured at the 30 m level.

U_n : maximum value of normal wind component, u_n; the largest measured u_n value is used.

V_c : speed of wind at the "core" of the current (near the location of U_n); determined from maximum recorded wind speed.

α : slope, $\Delta Z/\Delta X$, of temperature contours at the leading edge of the head (frontal slope); determined from contoured temperature field using time-distance conversion.

λ : ambient temperature gradient in tower height interval, T(152 m) - T(30 m); determined from contoured temperature field.

θ_c : wind direction at core; determined from recorded direction corresponding to V_c.

θ_e : thunderstorm echo propagation direction (direction from which echos move); determined from serial radar maps.

θ_p : front propagation direction (direction of arrival); determined from microbarograph array.

In Table 3.2 we have listed a few non-dimensional parameters, computed from the data in Table 3.1, which represent similarity between the different cases. Asterisks appear next to values that were not actually measured; these were determined as follows. Head depth, D_h, was estimated from temperature drop, ΔT_{max}, and propagation speed, C_p, assuming the Froude number to be 0.76 (determined by Keulegan (1958) from laboratory currents in relatively large tanks). The estimated values appear to be valid in that other parameters involving the estimates of D_h (Table 3.2) compare well with each other. Where sounder data were lacking, the head length, L_h, was assigned subjectively, primarily on the basis of the wind core location. Maximum normal wind, U_n, for the NSSL cases was set equal to the wind speed maximum. Where the normal wind maxima occurred above or below the instrumented levels, their locations were estimated subjectively from the appearance of the contoured U_n field. Based on observations discussed in Section 3.1.1, the ΔT values for

Table 3.2. Parameter Relationships

Parameter	Event Number								
	1	2	3	4	5	6	7	8	9
$F = C_p\left[g\ D_h \frac{\Delta T_{max}}{T_a}\right]^{\frac{1}{2}}$	.67*	-	-	-	-	(<.98)	.96	.23	.69
C_p/U_n	-	-	-	.44	(<.82)	(<.71)	1.6	-	.75
$H(U_n)/D_h$	.24	.16	-	.13	.14	.19	.16	(<.18)	(<.3)
D_h/L_h	-	-	-	.06*	.16*	.05*	.12	.22	.10
$R_e = \frac{C_p D_h}{\nu}$ $(\times 10^{-8})$	1.2*	5.3*	-	2.6	15	7.8	1.7	.18	.21

event 3 (double asterisks) are not considered to be representative because the "ambient" air was strongly influenced by previous gust-front passages. When propagation speeds were not measured directly, they were assigned a value of 0.67 times the maximum normal wind.

3.4.2 Geometric features

Many of the gravity current features described in Section 3.1.1 are apparent in our case studies. We find clear evidence of the head feature and of forward flow beneath the head with respect to the front. Middleton (1966) observed in laboratory flows that the ratio of front propagation speed to that of the steady upstream flow increased with distance travelled, and a similar observation was made by Simpson (1964) for sea-breeze currents. The ratios observed ranged from about 0.5 to 1.0. Charba (1972) found the ratio C_p/U_n to be 0.63 for one thunderstorm outflow current, and Goff (1975) observed an average $C_p/U_n = 0.67$ for thunderstorm gust fronts. Our data show no trend in this ratio as a function of distance travelled, but are fairly consistent with the results of Goff and Charba. The anomalous behavior of event 7 was discussed earlier.

It was mentioned earlier that surface drag might cause an elevated nose at the leading edge of a density current. Simpson (1969) argues that in the atmosphere an elevated nose in the temperature profile can exist only temporarily before collapsing due to instability, and Mitchell's (1975) model indicates that production of circulation in the head is sufficient to prevent formation of such a feature. Laboratory flows exhibit the nose feature, and Simpson (1972) determined that the ratio of nose height, h, to the head depth depends on Reynolds number, Re, according to

$$h/D_h = .61\ Re^{-.23}$$

for Re between 10^2 and 10^4. Extrapolating this relation to the larger Reynolds numbers of atmospheric flows results in nose heights of at most a few meters. Events 1, 2 and 4 (and perhaps 3) show elevated noses in the temperature profiles, but the feature is not apparent in most of the shallower cases. However, elevated noses are apparent in all of our observed wind profiles (except where the wind maximum occurred below the instrumented interval in cases 8 and 9). We find a strong relationship between the heights of wind maxima and depths of the heads (see Table 3.2) with an average observed ratio $H(U_n)/D_h = 0.17$.

The shapes of the Haswell currents are consistently longer and shallower than their laboratory counterparts. For example Keulegan (1958) and Middleton (1966) found that current heads had depth-to-length ratios, D_h/L_h, of about 0.4, but in all the Haswell currents this ratio is much smaller, averaging about 0.12.

The relative elongation of the atmospheric currents is further evidenced by the shallow frontal slopes observed in events 7, 8 and 9. These currents propagated on top of fairly strong surface temperature inversions which served to minimize surface friction. Simpson (1972) found that as surface drag was diminished in laboratory flows (by moving the lower boundary with the flow or by providing a thin layer of dense fluid ahead of the flow), the frontal slope became smaller approaching a minimum of $\pi/8$ or 0.39. Referring

to Table 3.1 we see that frontal slopes are no greater than 0.2 in the above-mentioned cases. However we also observe that the more intense gust fronts all have steep slopes, even though strong and persistent stable surface layers were present preceding some of these events. This suggests that in atmospheric gust fronts, the slope is more sensitive to age and intensity than to surface drag.

On the other hand, the presence of inversion layers appears to inhibit strong winds and large temperature changes at the surface, as in cases 1, 2, 3 and 7 (and possibly cases 8 and 9). (The relevance of this observation to gust front detection is discussed later.) Evidence of mixing and turbulent wakes behind the heads is seen in events 5, 7 and 9 as average temperature increases and temperature gradients weaken with time. Well behind these gust fronts the mixed layer extends down to the ground or to the tops of thin surface inversion layers. Acoustic sounder data show that the mixing also extends upward above the heads and turbulence in the wake region is evidenced by fine-scale fluctuations in all the measured quantities. There is little sign of mixing in event 8, as mentioned earlier, but wakes probably would have been seen in cases 4 and 6 had the observations extended over a longer time.

Wave-like patterns behind the heads in events 1, 7, and 9 suggest gravity waves or large turbulent eddies. Since the patterns break down into smaller and smaller scales with time, the latter seems more likely. As mentioned in Section 3.3.2, measured vertical velocity patterns are consistent with the presence of large rolls in the head region which would produce a deep intrusion of warm air downward into the cold current, thereby initiating the mixing process in a fairly deep layer immediately behind the head.

Our observations indicate that mixing in atmospheric gravity currents is considerably greater than in laboratory experiments, and this might significantly affect the behavior of thunderstorm gust fronts. If an outflow current is disrupted by mixing close behind the initial front, a new front must form provided that the outflow supplying the cold air persists. In the absence of a steady supporting current, the initial front must eventually

dissipate. This mechanism might explain some cases in which multiple surges have been observed in storm outflows (see our event 1, and Goff, 1975). These events have heretofore been attributed to merging of outflows from pulsating or separate downdrafts.

3.4.3 Wind-Shear Indicators

The aircraft hazards presented by gust fronts (or similar gravity currents) arise from three sources:

1. Vertical change of the horizontal wind, causing rapid change of airspeed for an aircraft, ascending or descending through the shear layer.

2. Horizontal change of the horizontal wind, causing airspeed to change along a horizontal flight path.

3. Horizontal change of the vertical wind, or turbulent fluctuation, causing vertical displacement of an aircraft flying along a nearly horizontal path.

Each of the above is related to the overall intensity of the gust front, and we will discuss the associated hazard in terms of just the vertical shear of wind in the direction of frontal motion (the normal component), du_n/dz. Full description of the total (vector) vertical wind shear also requires du_p/dz, the shear of the parallel component, but we have assumed that maximum shear can be represented by the former.

Recall that for the NSSL cases we have represented wind shear by the vertical gradient of wind speed, regardless of direction. Comparing the u_n fields with corresponding u_p fields for the Haswell events shows that maximum shears are usually associated with regions of strong directional changes in the wind. It is not surprising, therefore, that maximum shears at Haswell exceed those at NSSL by a large factor. If we consider that an aircraft moving in a straight line experiences air speed changes which depend on just

one component of wind shear, we see that it is appropriate to consider individual wind-shear components in assessing flight hazards. Furthermore, it is important to consider the method of "shear" computation when comparing the Haswell results to others for which wind speed gradient is used (e.g., Hall et al., 1976).

3.4.4 Relationships Between Shear and Surface Measurements

To assess the probable wind-shear intensity in gust-front currents we can turn to a simple conceptual model proposed by Hall, et al. (1976), in which it is assumed that maximum shear, S, depends only on the core wind speed, U, and a boundary layer thickness, δ; i.e., $S = U/\delta$. If we further assume that δ does not vary from one case to another, and that U is directly related to propagation speed, C_p, we find that shear is proportional to C_p:

$$S = U/\delta = aC_p$$

where a is a constant. We have plotted vertical shear versus C_p in Figure 3.20 for the Haswell data, and observe that linear relationships are indicated for both maximum and sustained shears. We also find that Goff's (1975) observations tend to support such a relation, but the shear estimates from his plotted data are not accurate enough to be included here. Because gravity current structure need not be invoked to obtain this relation, it should be valid even near downdraft bases.

This result indicates that an array of pressure-change detectors (which we will refer to as a "ΔP array") may serve as a good indicator of gust-front intensity, and would at the same time define the motion of the front. Propagation speed is determined with a ΔP array by simply comparing arrival times of the front at various locations.

If the Froude number, F, is constant for atmospheric currents as it seems to be for laboratory flows, we can relate C_p to the product ($\Delta T\ D_h$) as follows

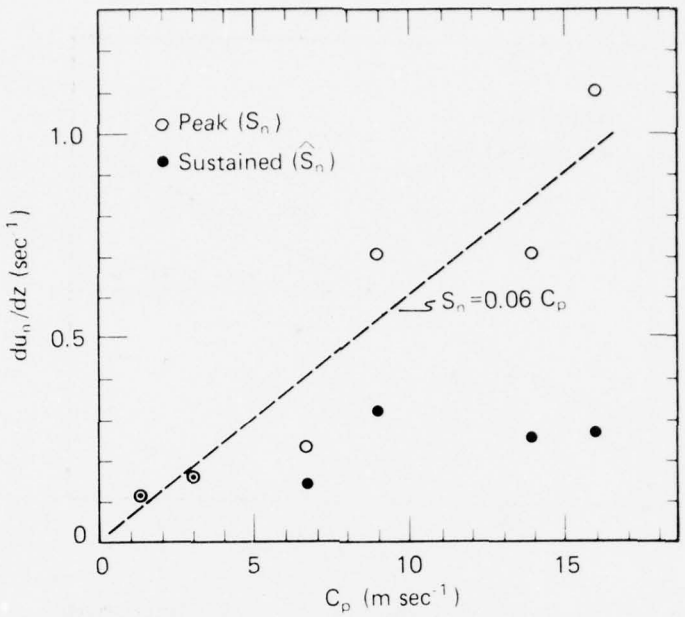

Figure 3.20 Maximum wind shear vs. C_p for Haswell events.

$$C_p = b\ (\Delta T\ D_h)^{\frac{1}{2}}$$

where the Froude number, gravity, and representative ambient temperature are included in the constant b. Figure 3.21 shows that the above relation is valid for the Haswell results. However, its practical use is limited by the difficulty in measuring D_h. We could consider replacing ($\Delta T\ D_h$) by the total pressure rise under a hydrostatic assumption but, particularly in the region of downdrafts, this assumption is not likely to be valid. Therefore the relation seems to be of little practical value.

Next we consider surface temperature which is easily measured and can be important in determining gravity current intensity. Figure 3.22 shows that shear and maximum temperature difference, ΔT_{max}, are approximately linearly related. Hall et al. (1976) present a similar empirical relation. They also point out that if the current depth could be assumed to be constant from one case to the next, we should expect C_p (and related shear) to be proportional

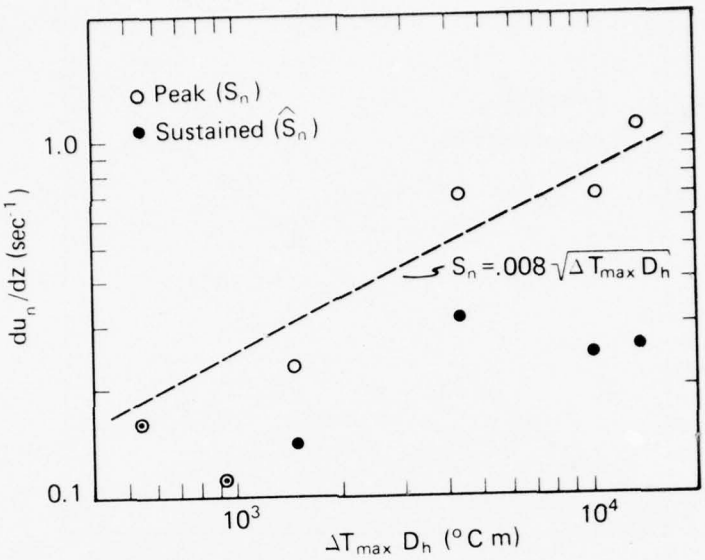

Figure 3.21 Maximum wind shear vs. $\Delta T_{max} D_h$ for Haswell events.

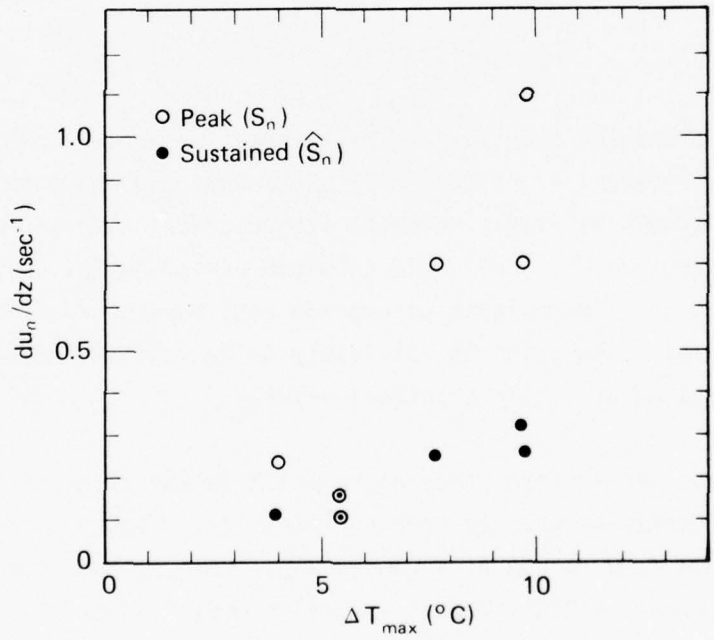

Figure 3.22 Maximum wind shear vs. ΔT_{max} for Haswell events.

to the square-root of ΔT. Our results make it clear that substantial shear is to be expected in currents of widely different depths, explaining why the square-root relation is not observed.

Unfortunately, the temperature drop, ΔT, measured near the ground is not likely to be representative of ΔT_{max}. Referring to our temperature fields in Figures 3.3, 3.6, 3.10, and 3.14 through 3.19, one can see that ΔT at low levels is not always indicative of higher level values, especially when stable inversion layers are present as commonly occurs during night-time hours. In his model Mitchell (1975) considered the effect of ambient stability on several gust-front parameters and found that high stability results in a far smaller frontal temperature drop than does a neutral atmosphere. Figure 3.23 shows the effect in terms of the Brunt-Vaisala frequency, $\omega = (g/\Theta(z) \cdot d\Theta(z)/dz)^{\frac{1}{2}}$, where Θ is the potential temperature. As discussed earlier, our case studies tend to substantiate this as do the case studies presented by Goff (1975). From his 10 min 450 m time-height plots, we estimated both the drop in potential temperature near the surface (<50 m) and the

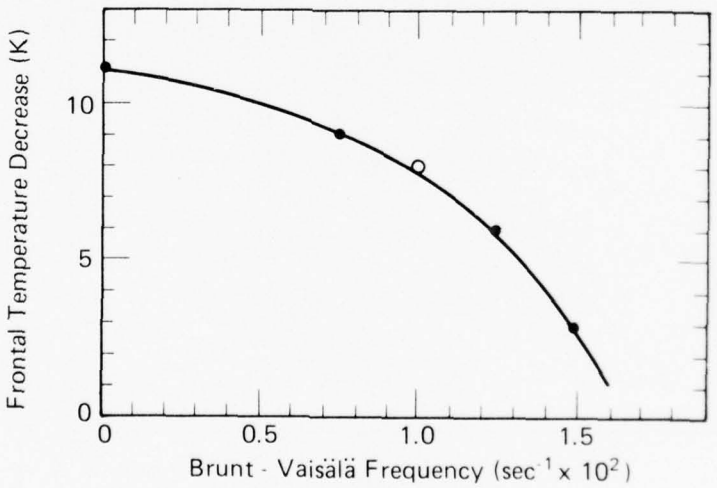

Figure 3.23 Gust-frontal temperature decrease as a function of ambient stability.

maximum change in horizontal wind speed normal to the gust front, Δu_n. We also estimated ω for these events based on the potential temperature change between the surface and 450 m from his isotherms. Figure 3.24 is a plot of $\Delta\theta$ vs. Δu_n in which the x's represent events with neutral or near neutral stability ($\omega < 10^{-2}$) and the circles represent the stable cases. Mitchell's model indicates that stable conditions also decrease the horizontal wind field but not nearly so much as the temperature drop. Because the high-stability cases show mostly a small surface $\Delta\theta$ but higher level wind changes (comparable to the neutral cases) the results presented in Figure 3.24 are in agreement with the model.

Direct measurements of the surface winds, like temperature, are also expected to be important. However, our cases studies show that wind measurements near the ground often do not represent true gust-front intensity or movement. In several cases (notably 1, 3, 4 and 5) there is a large discrepancy between the maximum low-level wind and that at the elevated wind core. Although Mitchell's (1975) results suggest that peak surface wind is approx-

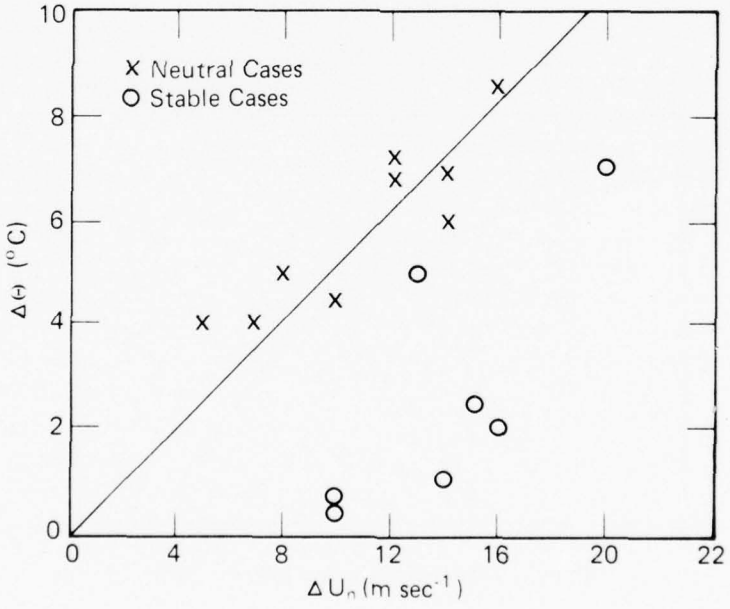

Figure 3.24 Surface temperature decrease vs. horizontal wind change for neutral and stable cases.

imately equal to front propagation speed, the model does not simulate the three-dimensional nature of the gust front, nor does it adequately treat the surface boundary layer. Our case studies suggest that there are several limitations to estimating actual maximum wind and gust-front motion from low-level wind measurements:

1. Strong winds may be isolated from the surface layer depending on low-level stability (inversion layers, as in case 1) and on the height of the wind core.

2. Maximum low-level winds are sometimes delayed by 30 minutes or more (see cases 4, 5, and 7) after strong winds are observed at higher levels.

3. Strong cross-components and highly variable wind directions (see the Haswell cases) show that gust-front propagation direction often is not represented by local wind.

Based on the present case studies we conclude that surface wind measurements would probably not provide reliable gust-front warnings in many instances, although we do not have enough actual surface wind data to quantify this conclusion (Colmer, 1971).

3.5 Analysis of Surface Winds During the August 1975 Denver Accident

The case studies discussed in the previous sections represent a cross section of events which produced shear conditions ranging from minor to severe. Aside from damaging some instruments, however, they were case studies only of scientific interest toward a more practical goal. The goal is the prevention of aircraft accidents and incidents caused by low-level wind shear. In this section we summarize an analysis of wind-shear conditions responsible for just such an occurrence.

On 7 August 1975, Continental Flight 426 crashed at Stapleton International Airport in Denver, Colorado while attempting to take-off. Caracena

(1976) performed a detailed streamline analysis of the wind field at the time of the crash from an array of 12 surface anemometers. Using a technique called isogon analysis, Caracena derived a more accurate representation of the surface streamlines than is usually obtained by merely sketching them.

The passage of a storm with strong outflow cells resulted in the streamline pattern over the airport, shown in Figure 3.25, at the time the Continental flight began to roll. A smaller scale analysis, based on the same technique, resulted in the probable streamlines of surface winds at the runway illustrated in Figure 3.26. Using the available flight recorder data, Caracena was also able to derive the probable corresponding isotach field at the time (Figure 3.27). From the last two figures, it is apparent that the aircraft began its take-off with a slight tail wind which became a headwind about a third way along the runway. Significantly, the aircraft encountered very strong tail winds again along the last third of the runway. In fact, the situation was even worse than depicted due to the advection of the storm toward the east. This motion may have subjected the aircraft to the maximum horizontal shear, as shown to the west of the runway in Figure 3.26.

An estimate of the downdraft velocities that the aircraft may have encountered suggests that the downdraft alone could not have been responsible for the crash but may have contributed to it. An analysis of the horizontal wind shear as a function of height reveals that at the aircraft's maximum altitude of 37 m, the shear was 0.1 sec^{-1} or more than twice the value at the 5 m anemometer level.

A qualitative picture of the outflow wind velocities is shown in Figure 3.28 and illustrates the conditions under which Continental Flight 426 crashed. The kind of quantitative analysis performed by Caracena demonstrates the potential for deriving conditions hazardous to aircraft but also points out the deficiencies of relying solely on ground-based anemometers.

3.6 Summary

Through the use of instrumented towers and acoustic sounders we have been able to make detailed observations of wind and temperature structure,

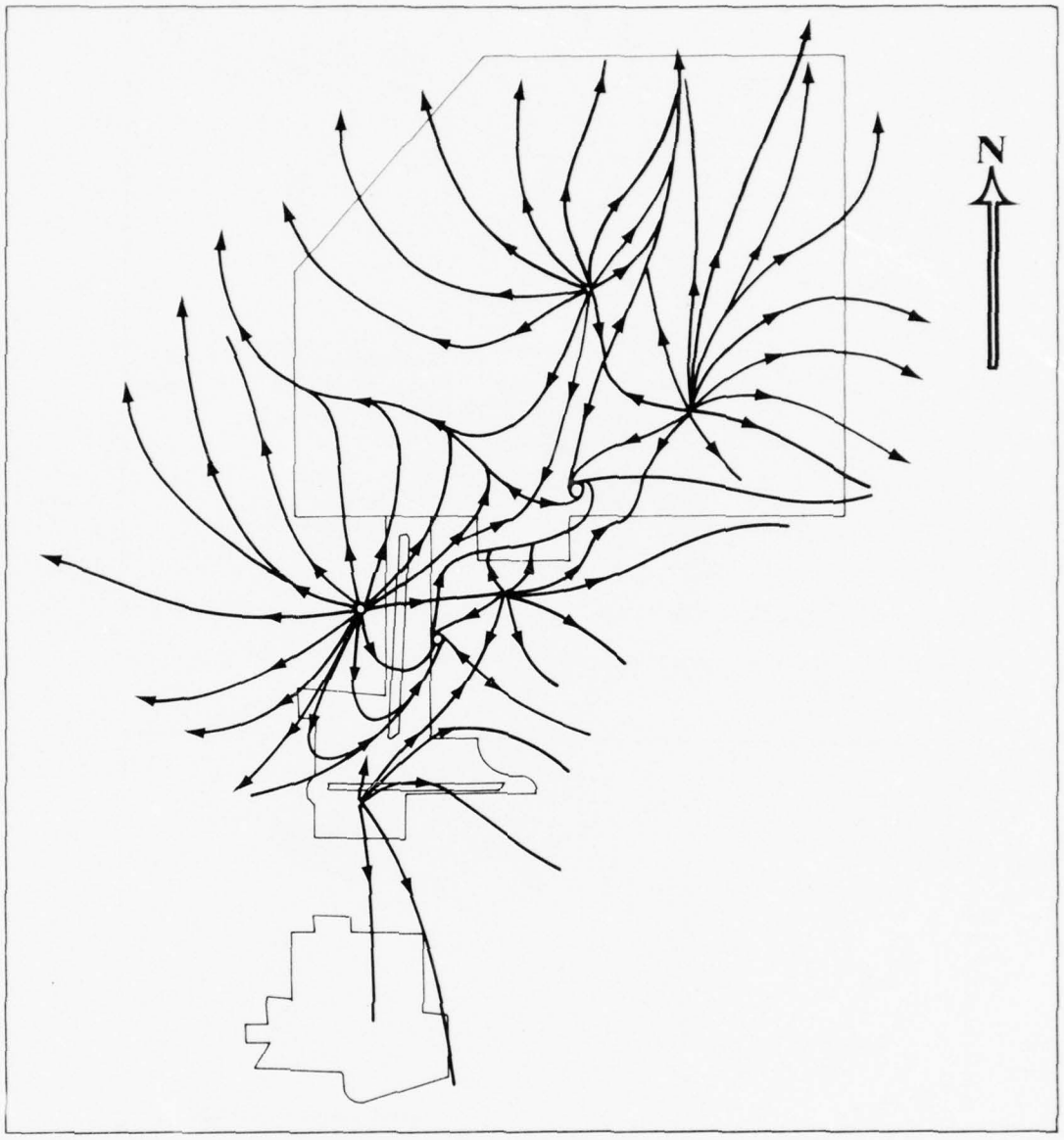

Figure 3.25 Streamlines drawn from time-space conversion and isogon analysis over Stapleton Airport between 1600-1620 MDT on August 7, 1975.

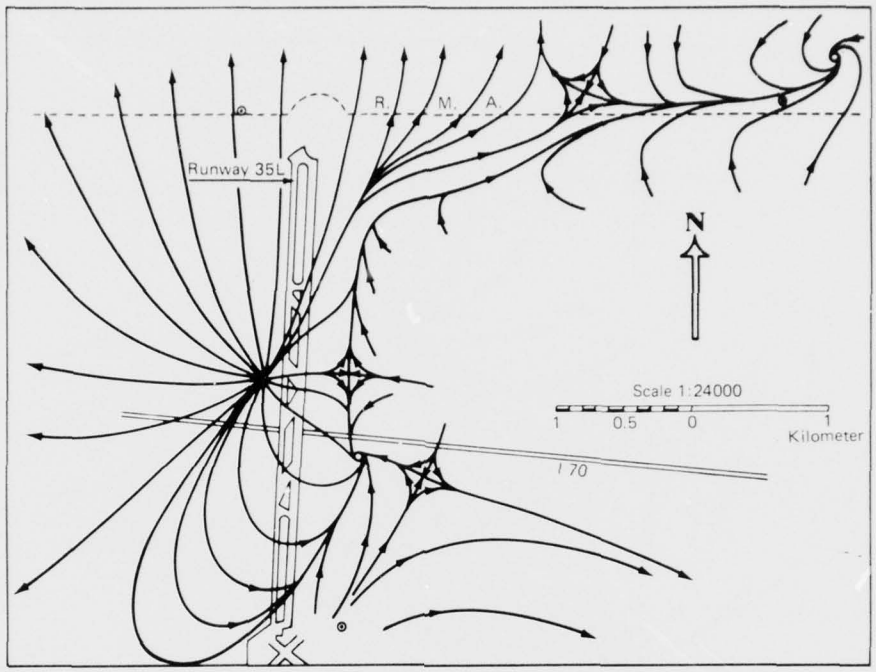

Figure 3.26 Surface airflow pattern in the vicinity of Runway 35L at 1610 MDT on August 7, 1975.

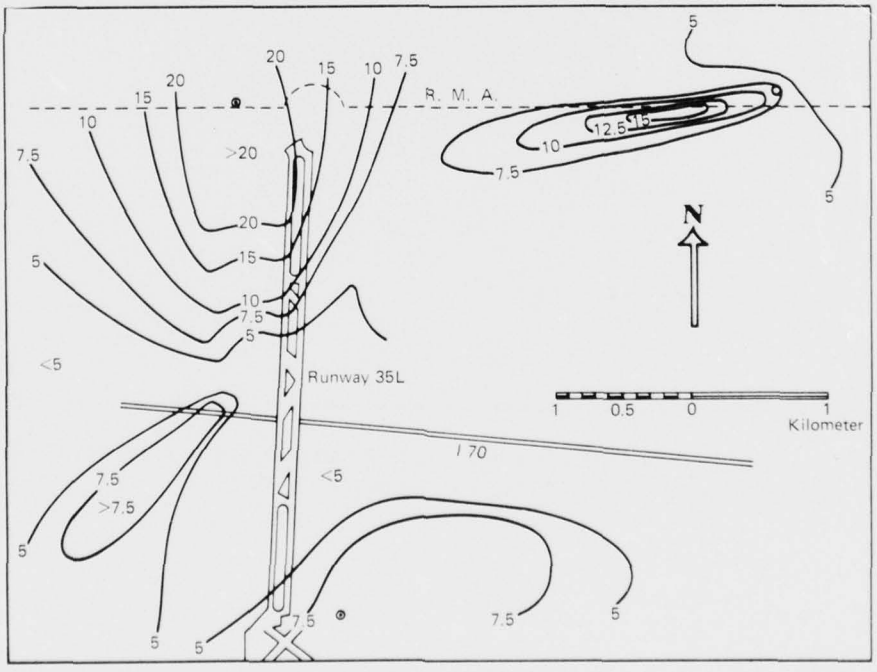

Figure 3.27 Isotachs of wind field (m sec $^{-1}$) at Runway 35L at 1610 MDT on August 7, 1975.

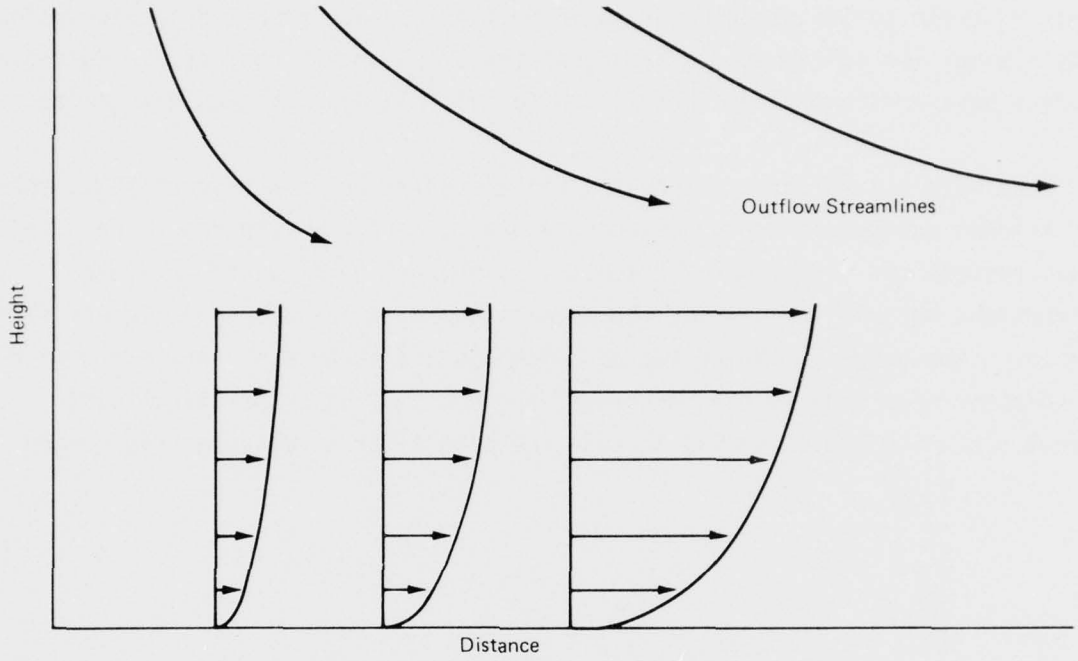

Figure 3.28 Horizontal and vertical dependence of outflow wind velocities.

and wind-shear intensity within a number of atmospheric gravity currents (gust fronts). The results have been discussed with reference to existing models and the findings of other investigators, in an effort to improve our general understanding of the phenomenon.

We have found that observed atmospheric gust fronts compare quite well with laboratory and model counterparts, but several essential differences are noted. The atmospheric currents are relatively longer and shallower, and in several cases frontal slopes are observed to be less than the miniumum slope achieved in the laboratory by eliminating surface friction. On the other hand, the more intense gust fronts have nearly vertical slopes near the ground (i.e., in the tower interval) regardless of stable surface layers that should minimize friction, indicating that the frontal slope at low levels is insensitive to surface friction. Elevated projecting noses are observed in several gust-front temperature profiles, even though model and laboratory results indicate that such a feature is not to be expected. Mixing is found to be much greater in the atmosphere than in laboratory flows, suggesting

that multiple surges often observed in gust fronts may result from disruption (by mixing) and subsequent reforming of the front and current head. Multiple surges have previously been attributed to multiple or pulsating downdrafts.

We have attempted to assess the relationships between several measurable gust-front parameters and wind-shear severity. Surface temperature and wind measurements can be reliable indicators except during times of low-level inversions which often prevent the more severe dynamics at higher levels from reaching the ground. The parameter which appears to be most consistent with wind-shear magnitude is the gust-front speed of motion; a practical gust-front detection system should include the capability to measure this motion.

4. STATISTICAL ANALYSES

4.1 Introduction

The detailed case studies of the previous section show considerable variations in the parameters from one gust front to another and we discussed several reasons for these differences. Until we improve our knowledge of the more detailed shear dynamics, however, it is also helpful to consider some of the broader characteristics of wind-shear occurrence and relationships.

In this section we have developed statistics for a five-year period at the Chicago O'Hare Airport area by comparing barograph data with corresponding meteorological information in order to help evaluate the concept of gust-front detection by pressure jump detector arrays. We also present statistics on the frequency of occurrence of significant vertical shear as measured by the NSSL meteorological tower during the spring of 1976 data collection period and compare the results with gust-front detection by other methods.

4.2 A Statistical Study of Atmospheric Pressure Jumps

4.2.1 Introduction

Atmospheric pressure changes accompany virtually every meteorological event. On the synoptic scale, pressure variations occur with amplitudes measured in tens of millibars over time periods of hours or days. On smaller spatial scales, pressure fluctuations with amplitudes of several millibars and time scales of minutes also can occur. Their sources include gravity waves, gravity-shear waves, hydraulic jumps and thunderstorm gust fronts. The impetus for the study described here results from a need to know more about the statistical properties of gust-front events and the dangers they present.

Accordingly, a concept has evolved for using sensitive pressure jump detectors to detect and track thunderstorm gust fronts. A proper evaluation of the effectiveness of such techniques also requires the development of a statistical data base. The design of pressure-jump detectors requires a knowledge of rise-time and pressure-amplitude statistics for gust-front pressure jumps. In addition, pressure changes due to other sources may cause false alarms. The operational usefulness of any detection system must be gauged by a realistic evaluation of false-alarm and miss-rates.

For these reasons, we studied the statistics of pressure jumps for the Chicago O'Hare Airport area for the period 1968 through 1972. After reviewing causes of atmospheric pressure disturbances, we outline the sources of data used in our study and describe our criteria for distinguishing between the various causes of pressure disturbances, as well as our definition of threshold values for detection. Finally, we present the statistics for these pressure data on yearly bases and summaries of the five years covering the distribution of source mechanisms, the time-of-year occurrences, and the pressure-amplitude and rise-time statistics.

4.2.2 Causes of Atmospheric Pressure Disturbances

The Gust Front

A sudden rise in surface pressure accompanies the passage of the cold-air outflow from thunderstorms and such pressure increases can occur more than 20 km from the storm center (Figure 4.1a). Pressure rise times shorter than 10 min and pressure amplitudes above 1 mb frequently occur. Bedard and Beran (1977) review past measurements of such gust fronts and the works of Charba (1974) and Goff (1975) present detailed measurements on the characteristics of these systems. One goal of our studies is to develop empirical relations between the gust-front pressure field, its rise time and amplitude, and maximum surface wind gust, temperature difference, speed of motion and peak magnitudes of the wind shears. The goal of the statistical study described here is the documentation of pressure-amplitude, rise-

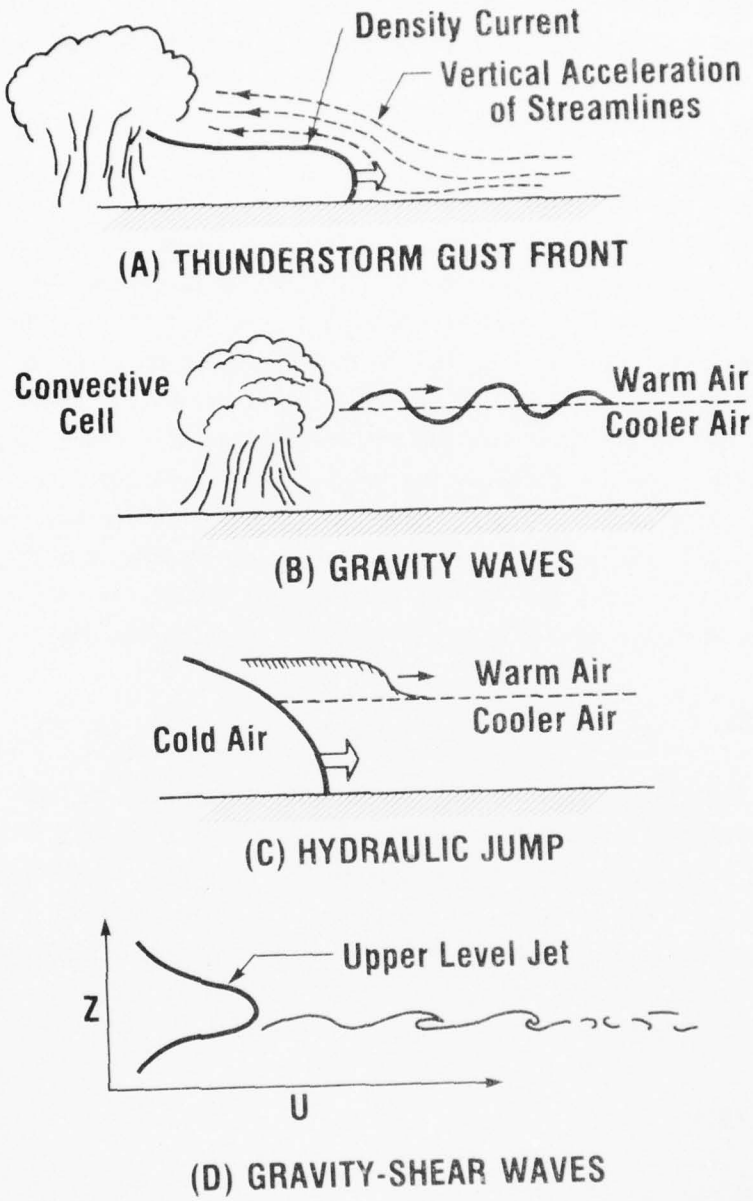

Figure 4.1 Causes of atmospheric pressure disturbances.

time, time-of-year and frequency-of-occurrence statistics and, if possible, identification of the sources and their fraction related to thunderstorms.

Dynamic Effects

Although density increases in an air column are the dominant mechanism for many of the measured pressure jumps, vertical accelerations of air parcels are an additional cause of sudden pressure changes associated with gust fronts. Convective flow interacting with a mean wind field (Figure 4.1b) is another example of a situation capable of producing large vertical accelerations and hence pressure variations. Such accelerating fields could explain some of the pressure fluctuations we list as unknown. Perry (1976) attributes dynamic effects as the origin of pressure jumps he could not otherwise relate to meteorology. Moreover, intense thunderstorm downflows (Figure 4.1a), similar to a jet impinging on a boundary, can produce significant pressure increases. Fujita and Caracena (1977) indicate that *such downbursts may have been a factor in several aircraft accidents.*

Frontal Passages

Williams (1953) and Clarke (1961) review statistics that include pressure data related to frontal passages. Clarke finds that most frontal pressure jumps with amplitudes greater than 0.5 mb occur in the months of August through April but exhibit no strong peak. Williams reviews statistics comparing the various types of weather systems related to pressure jumps measured in the central midwest of the United States and shows that pressure jumps frequently occur with cold fronts.

Gravity-Shear Waves

Just as hydraulic jumps can propagate on surfaces of density discontinuities aloft, more complex propagating wave fields can occur (e.g., when a convective system perturbs such an interface). Curry and Murty (1974) present an example of pressure disturbances that they attribute to gravity waves from a thunderstorm (Figure 4.1b).

On the other hand, when wind shears occur aloft as in an upper-level jet stream (Figure 4.1d), large-amplitude pressure perturbations can appear at the surface of the earth. Flauraud, et al. (1954) and Keliher (1975) present details of the measurement of these waves. They tend to occur during the winter months in the northern hemisphere and last for many hours while tracking the speed and direction of high-altitude tropospheric winds. Several studies relate the presence of these waves to aircraft turbulence reports (e.g., Kirk, 1963; Hooke and Hardy, 1975).

Because the speeds of propagation of long-period gravity-shear waves tend to be higher than gust-front speeds and because the two phenomena tend to occur at different times of the year, we expect that a gust-front detection system based on sensing pressure perturbations would not have many "false alarms" caused by gravity-shear waves.

Hydraulic Jumps

Tepper (1950) developed a hydraulic jump model as an explanation of prefrontal squall lines. A hydraulic jump driven by a frontal system (Figure 4.1c) can propagate on a density interface and produce pressure jumps at the earth's surface. Tepper (1954) tracked such pressure disturbances for many kilometers across the midwestern United States. He hypothesized that such a jump can trigger convective activity because of the upward forcing of parcels of air, and tracking such jumps offers the possibility of predicting the location of pre-frontal squall lines prior to their development.

Combination of Causes

A single gust-front system can provide examples of several of these sources of pressure perturbations. The presence of a low-level inversion could permit a hydraulic jump to propagate from the edge of the density current, disturbing the inversion surface. Charba (1974) advances this mechanism as an explanation of the early arrival of pressure disturbances in front of the leading edge of the density current. Accelerations of the

ambient air in advance of such systems also perturb the pressure field, and gravity-shear waves can propagate on the interfacial surfaces between the density current and the surrounding air. Thus, many factors can act simultaneously to make the interpretation of pressure data difficult; although more detailed analyses might distinguish between various source mechanisms even if they are present simultaneously (e.g., the form and magnitude of the pressure disturbance can differ greatly for gravity-shear wave and gust-front events). Also, future studies might provide indices for determining which gust-front events are most dangerous (e.g., Blecker and Andre, (1950) found a linear relation between peak pressure and total rainfall from thunderstorms) and combinations of observables may provide reliable detection criteria (e.g., peak pressure and speed of motion of the discontinuity).

4.2.3 Application to Aircraft Operations

Thunderstorm gust fronts and the wind shears related to them constitute hazards to aircraft, particularly during take-offs and landings. This section of the report, although oriented specifically towards evaluating pressure sensors as detectors of such gust-front systems, also provides estimates of the frequency of occurrence of large gravity-shear-wave events and frontal passages. A number of workers (e.g., Hardy, 1971) related gravity-shear waves to aircraft turbulence encounters. Perry (1976) related reports of severe low-level turbulence to the existence of pressure jumps which he ascribes to a variety of weather situations.

Thus, in addition to gust front detection, other useful information can be derived from surface measurements of pressure perturbations. This is our reason for putting the words "false alarm" in quotes when we speak of detection of events not related to thunderstorm gust fronts. At the same time, we must emphasize that, at present, we do not have a method for distinguishing clearly between all the possible sources using only surface pressure data without additional external information (such as knowledge of

the presence of thunderstorm echoes, upper-level jets or approaching fronts). This limitation also applies to anemometers and thermometers.

4.2.4 Data and Analysis

Sources of Data

We used standard National Weather Service (NWS) twenty-four-hour barogram traces in the analysis of the statistics of pressure disturbances from Chicago's O'Hare International Airport (1968-1972). A rise in pressure greater than 0.005 inches of mercury (0.17 millibars) per minute with a total rise greater than 0.02 inches of mercury (0.667 millibars) is the NWS definition of a pressure jump. Events meeting these criteria provided information on the time of occurrence, rise times, and magnitudes of positive changes in pressure. To determine the meteorological conditions that caused the pressure disturbances we used many sources. These included daily surface weather maps and station weather for 0700, EST, Storm Data and severe weather phenomena (which included location, date, time, and character of the storm), and radar summaries for the United States, to determine the type of local weather phenomena occurring at the time of the event.

Definition of Pressure Events

In analyzing the twenty-four-hour barograms, we singled out pressure jumps that produced a pressure rise of at least 0.667 millibars in a period of fifteen minutes (900 sec). This criterion suppressed some long-period changes meeting the NWS definition. Also, our minimum criterion is lower than the one millibar rise per ten minutes (600 sec) which is the threshold for a type of sensitive pressure jump detector designed for possible use as part of a future shear warning system.

Examples of typical pressure jumps appear in Figures 4.2 and 4.3. We use three categories for identifying the meteorological source; the first one we relate to local thunderstorms. Two examples (May 12, 1970, and

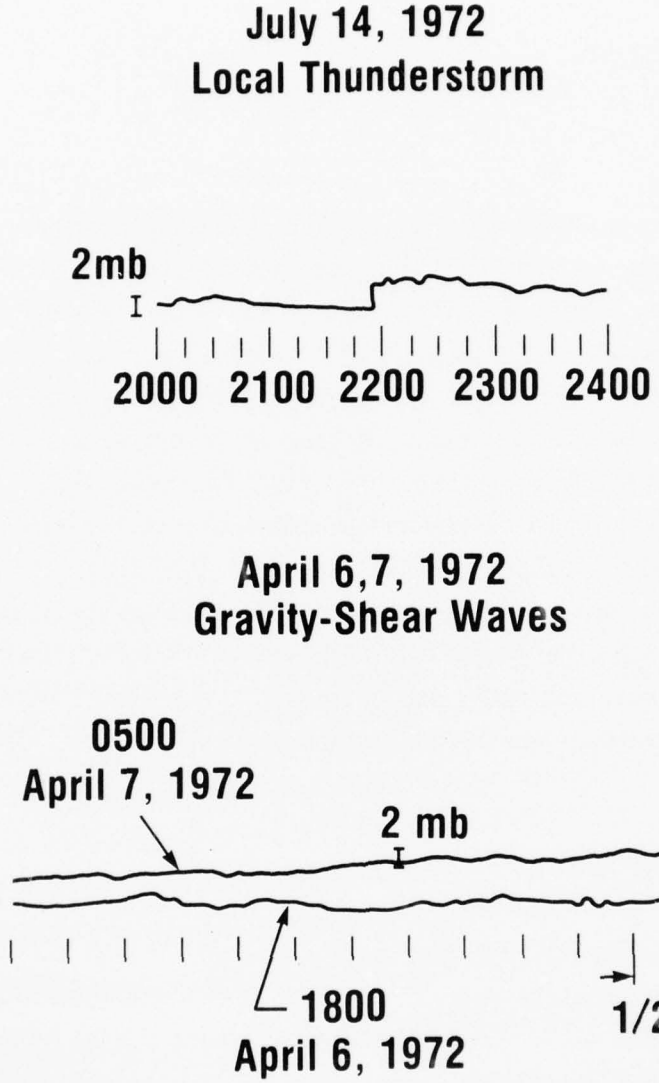

Figure 4.2 Examples of typical pressure jumps.

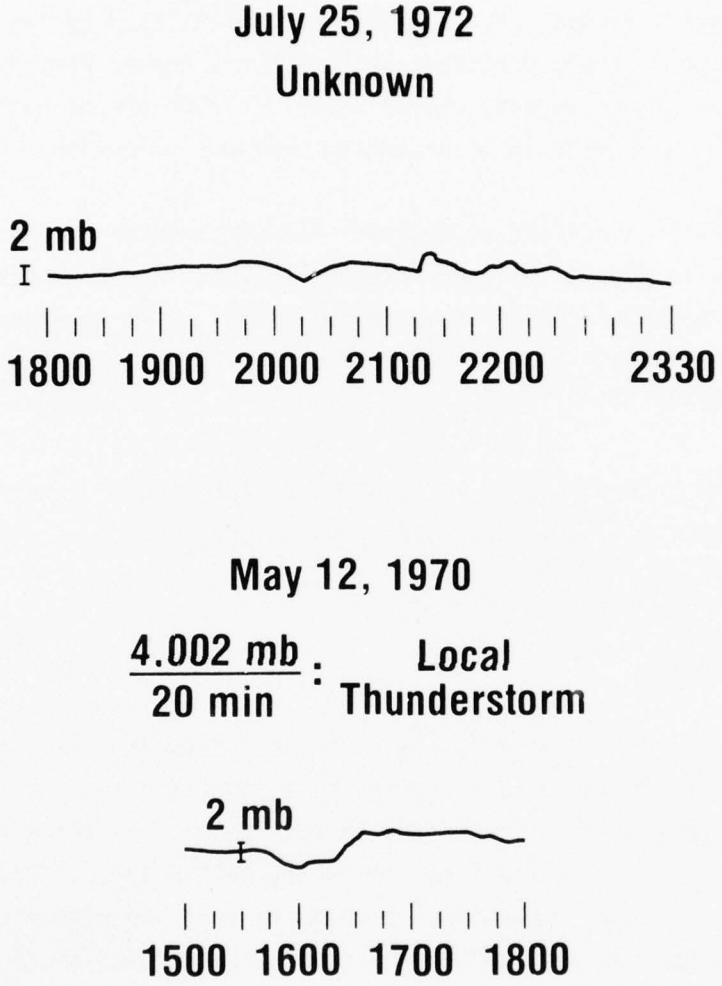

Figure 4.3 Examples of typical pressure jumps.

July 14, 1972) are shown in Figures 4.2 and 4.3. Each shows a pressure rise of two millibars or more in a period of less than fifteen minutes.

A second record of pressure perturbations, shown in Figure 4.2 (April 6, 7, 1972), depicts gravity-shear waves. These were identified by the presence of wave-like pressure perturbations over an extended period of time on the barogram traces usually occurring in the presence of high winds aloft. Some of the waves were large enough to meet our criterion.

The third category consisted of pressure changes related to frontal systems. As we saw in Figure 4.1, such pressure changes could be caused by the propagation of a sudden change in inversion height, with an example being the pre-frontal squall line with the cold front providing the initial piston-like impetus.

The rest of the pressure jumps meeting the criteria were categorized as unknown (see Figure 4.3, July 25, 1972) due to the absence of recorded weather phenomena.

Limitations and Problems

One limitation on distinguishing pressure jumps from the available pressure data is that the standard barograms have poor time and amplitude resolution. The barograph pen traces are, in many cases, too thick to discern the exact change in pressure for an event, with a typical uncertainty of ± 0.1 mb. Another operational problem is that the pens occasionally get hit or bumped, causing small marks on the traces similar to pressure jumps, and pen-chart friction can reduce the short-period response. Thus, the main problem in studying the barogram traces is the correct identification of the origin of the different types of pressure jumps. Gravity-shear waves with a pressure jump at the beginning or end of the event or a pressure jump followed by a long rise in pressure that is gradual but meets the criteria are examples of cases that are difficult to categorize.

Another limitation was the lack of sufficient data on weather phenomena corresponding to the pressure jump. Also radar summaries from June 1 through June 15, 1969 and daily surface weather maps from January 1 through April 15, 1968 were not available.

Results

A study of the causes of pressure disturbances shows that thunderstorm-related gust fronts as well as other surface discontinuities such as frontal passages produce pressure jumps. We studied five years of data from 1968 through 1972 recorded at Chicago's O'Hare International Airport and present the results below.

We use three kinds of comparisons to present these data. The first type (e.g., Figure 4.4) compares the percentages of events correlated with thunderstorms, gravity-shear waves, frontal passages and unknowns. A second type consists of a graph of the maximum change in pressure in millibars versus the rise time of the disturbance in minutes, recorded for each event related to thunderstorms (e.g., Figure 4.7). The third type of comparison is the number of events as a function of month of the year for the thunderstorm, gravity-shear wave or frontal sources that would trigger pressure-jump detectors (e.g., Figure 4.8).

Table 4.1 shows the sources of pressure disturbances by percentage of occurrence of the total number of events (298) for each of the five years. This comparison used our most sensitive criterion of a change in pressure of 0.667 mb in fifteen minutes. Thunderstorms were usually the single greatest source of pressure disturbances, with the percentages varying from a high of 44% in 1968 to a low of 27% in 1972. The percentages for gravity-shear waves varied from year to year from 5% to 25% and unknown sources from 4% to 24%. Frontal passages represented between 30% and 43% of the sources during the five-year interval. Figure 4.4 shows a summary of the data for the entire period with thunderstorms and frontal passages accounting for about equal portions of almost 3/4 of all the cases. Gravity-shear wave events and unknowns in almost equal numbers accounted for the remaining events.

Table 4.1. Sources of Pressure Disturbances at Chicago's O'Hare International Airport by Percent of Occurrence (Detection Criterion = .667 mb/15 min)

	% of Occurrence				# Total Cases
	Thunder-storms	Fron. Pass.	Gravity-Waves	Unknowns	
1968	44	30	5	21	66
1969	35	35	23	7	58
1970	43	43	10	4	51
1971	36	32	8	24	71
1972	27	38	25	10	52
1968-1972	37	36	13	14	298

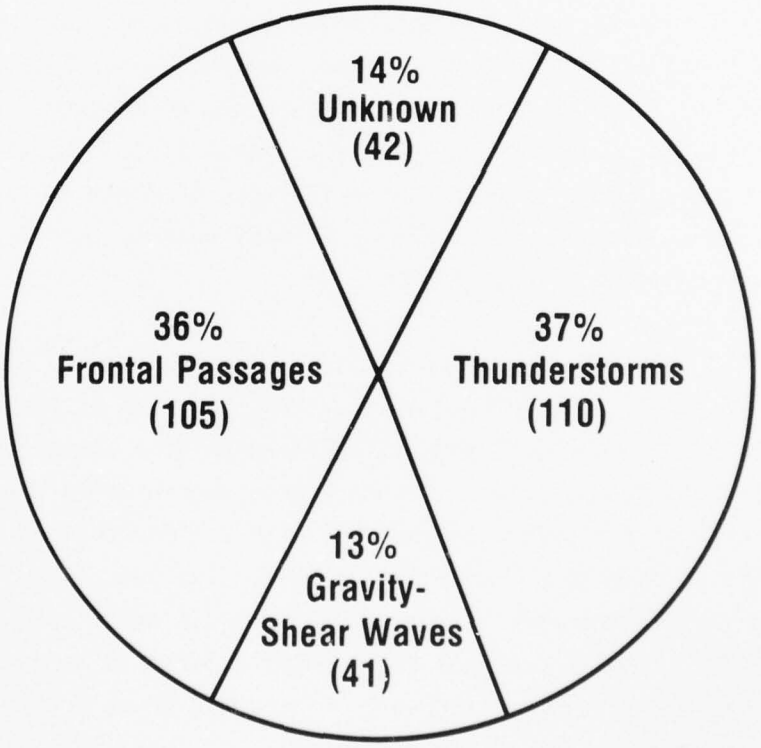

Figure 4.4 1968-1972 sources of pressure disturbances at Chicago's O'Hare International Airport by percentage of occurrence.

Table 4.2 shows sources by percentage of occurrence capable of triggering a particular pressure jump detector design. The percentage of thunderstorms as the source of pressure disturbances becomes larger (e.g., compare Tables 4.1 and 4.2 which show an increase from 44% to 60% for the 1968 data set) merely by the change in our threshold. A pressure change of 1 mb in 10 minutes is the criterion used to define events capable of triggering the detectors. The total number of thunderstorms on a yearly basis varied from as few as 6 in 1971 to 21 in 1968. For the 1971 cases, we eliminated all the gravity-shear wave events by applying this new criterion. Comparison between summary Figures 4.4 and 4.5 shows that the percentages of cases due to gravity-shear waves and unknown causes were reduced while the percentage related to thunderstorms increased.

Table 4.2. Sources of Pressure Disturbances at Chicago's O'Hare International Airport by Percent of Occurrence Capable of Triggering Detectors (Detection Criterion = 1 mb/10 min)

	% of Occurrence				# Total Cases
	Thunder-storms	Fron. Pass.	Gravity-Waves	Unknowns	
1968	60	26	3	11	35
1969	40	40	9	11	35
1970	50	40	7	3	30
1971	39	38	-	23	13
1972	37	34	16	13	32
1968-1972	47	35	8	10	145

Using the detection criterion of 1 mb in 10 minutes, we analyzed the data on a time-of-year basis and present the source breakdown statistics considering only the months of May through September (the months when thunderstorm activity reaches a maximum). These data appear in Table 4.3. Comparisons between the summary Figures 4.4, 4.5, and 4.6 show that the sources accounted for by thunderstorms increase to 60% while the number of cases related to frontal passages and gravity-shear waves decreases.

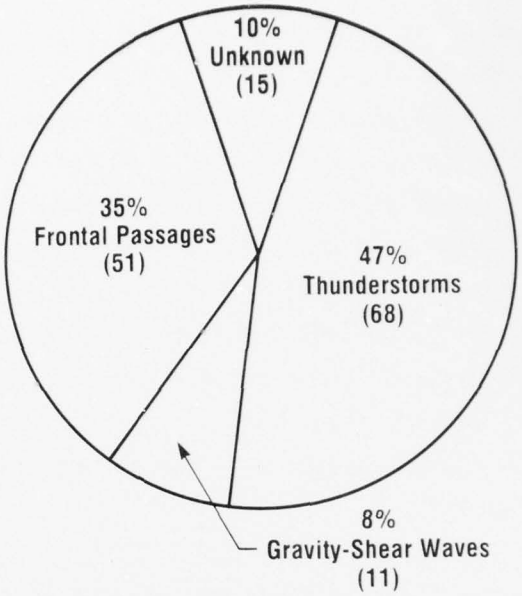

Figure 4.5 1968-1972 sources of pressure disturbances at Chicago's O'Hare International Airport by percentage of occurrence capable of triggering detectors.

Table 4.3. May-September Sources of Pressure Disturbances at Chicago's O'Hare International Airport by Percent of Occurrence Capable of Triggering Detectors (Detection Criterion = 1mb/10 min)

	% of Occurrence				# Total Cases
	Thunder-storms	Fron. Pass.	Gravity-Waves	Unknowns	
1968	69	21	-	10	29
1969	53	29	6	12	17
1970	69	25	-	6	16
1971	43	14	-	43	7
1972	50	20	10	20	20
1968-1972	60	22	4	14	89

A second type of comparison shows the relation between the pressure amplitude and rise-time statistics for thunderstorm-related cases meeting the 1 mb rise in 10 minutes criterion, triggering our pressure-jump-detector design (see Figure 4.7). It is clear from Figure 4.7 that the majority of

AD-A043 391 NATIONAL OCEANIC AND ATMOSPHERIC ADMINISTRATION BOUL--ETC F/G 4/2
WIND SHEAR CHARACTERIZATION.(U)
FEB 77 G E GREENE, H W FRANK, A J BEDARD DOT-FA76WAI-622
FAA-RD-77-33 NL

UNCLASSIFIED

2 OF 2
AD
A043 391

END
DATE
FILMED
9-77
DDC

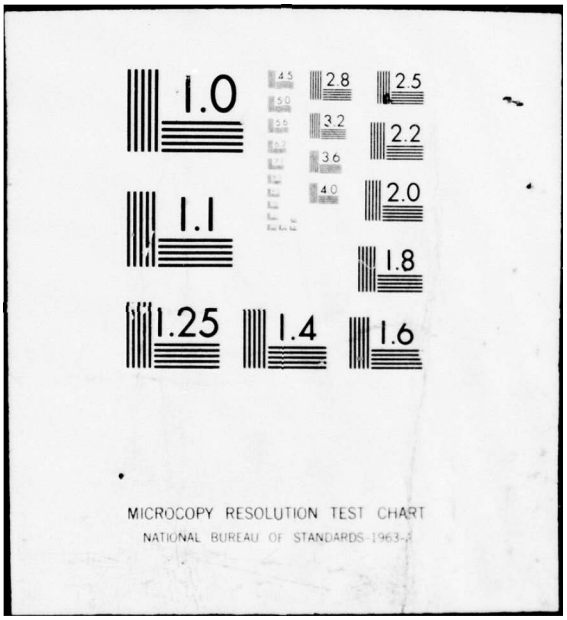
1.0
1.1
1.25
1.4
1.6
1.8
2.0
2.2
2.5
2.8
3.2
3.6
4.0
4.5
5.0
5.6
6.3
MICROCOPY RESOLUTION TEST CHART
NATIONAL BUREAU OF STANDARDS-1963-A

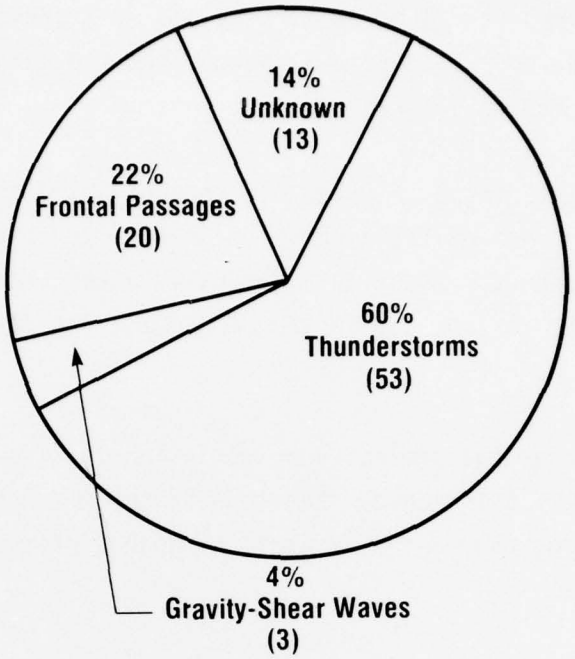

Figure 4.6 May-September 1968-1972 sources of pressure disturbances at Chicago's O'Hare International Airport by percentage of occurrence capable of triggering detectors.

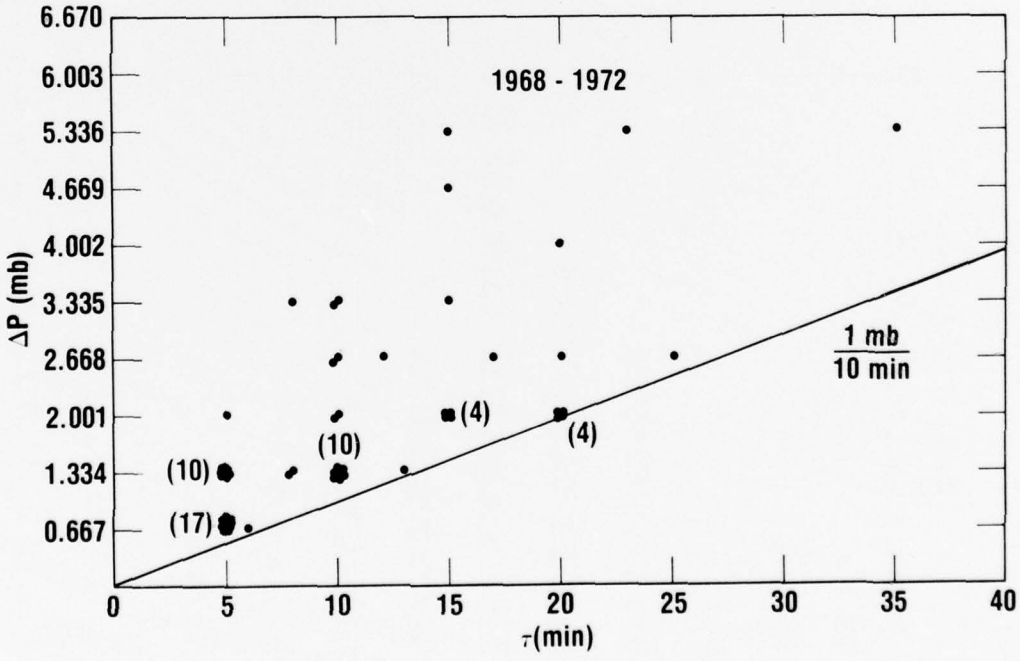

Figure 4.7 Pressure amplitude vs. rise time statistics for thunderstorm-related cases.

events had rise times from 5 to 10 minutes and most pressure amplitudes exceeded 1 mb. There is also some evidence that the larger rise times occur with the largest changes in pressure.

The last set of graphs (Figures 4.8 through 4.10) shows the month-of-year variation for each of the identified sources capable of triggering pressure-jump detectors. These data generally agree with past observations of the time-of-year variability of thunderstorms, gravity-shear waves and frontal passages.

Figure 4.8 shows the time-of-year variation of thunderstorm-related source mechanisms. It indicates that thunderstorms cause pressure disturbances mainly during the months of April through September, the peak months being May and June.

The summary figure for gravity-shear wave time-of-year variation (Figure 4.9) shows peaks in March, April and November with few events in the summer. December and January have no events in contrast to the winter maximum observed

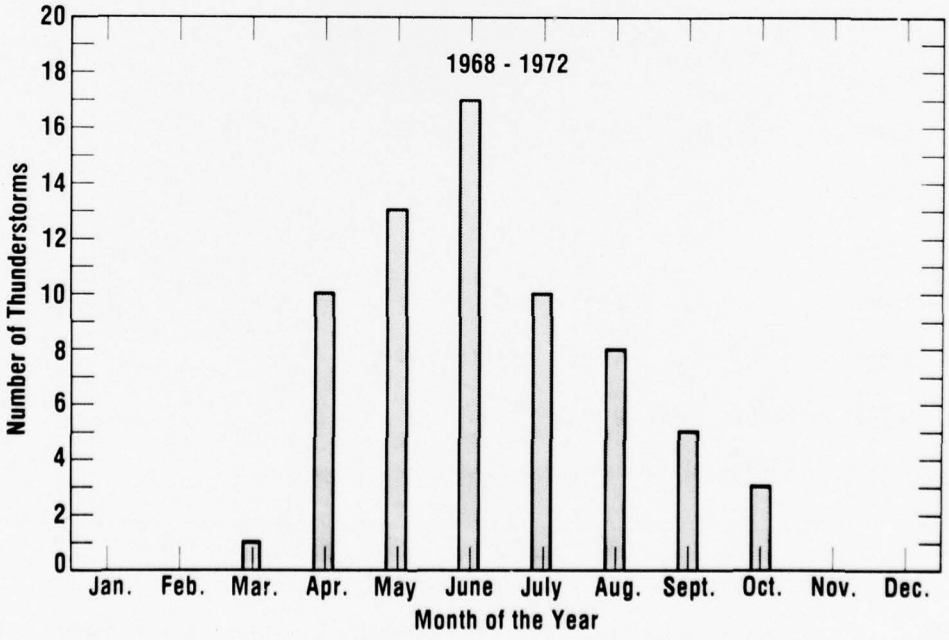

Figure 4.8 Month of year variation for thunderstorm-related sources capable of triggering pressure detectors.

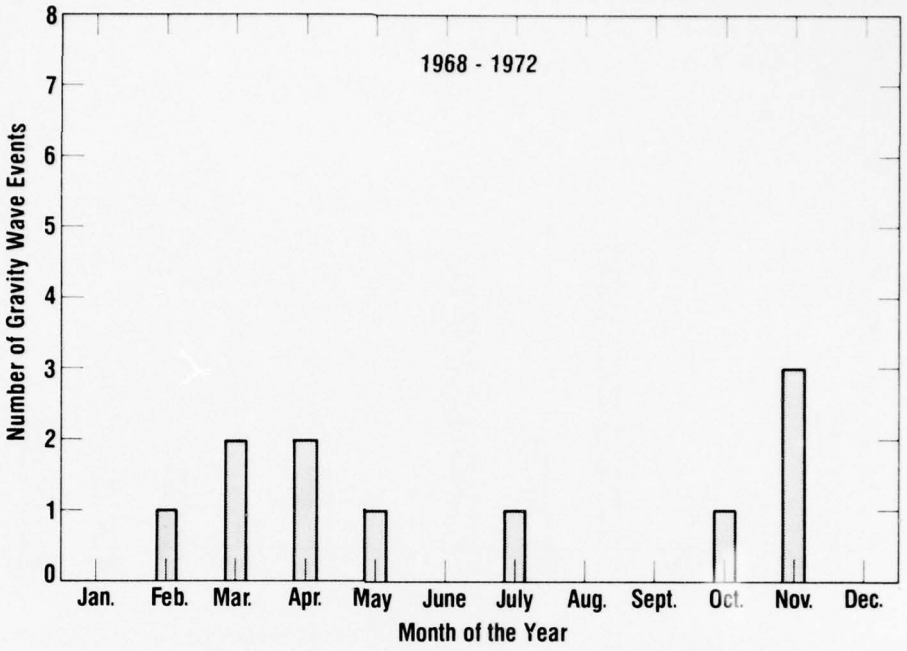

Figure 4.9 Month of year variation for gravity-shear waves capable of triggering pressure detectors.

by Flauraud et al. (1954). This may reflect the movement of the upper level jet to lower latitudes.

Figure 4.10 presents data on the time-of-year occurrence of disturbances related to frontal passages. We found no clear peak in the yearly statistics for these events.

4.2.5 Pressure Jump vs. Gust-Front Speed Change

We analyzed surface anemometer recordings for O'Hare Airport for the five-year period during the months of May through September and noted the maximum change in speed (Δu) for all cases where a sudden gust surge appeared (an increase greater than 4.5 m sec^{-1} (10 mph) usually occurring within 5 minutes). The Δu values constitute minimum changes, not taking into account changes in wind direction often associated with gust fronts. Thirty out of 30 cases with a Δu value greater than 9 m sec^{-1} (20 mph) had pressure jumps associated with them. We measured the pressure maximum and rise time, τ, for each of the events and present these data in two ways. Figure 4.11 is a plot

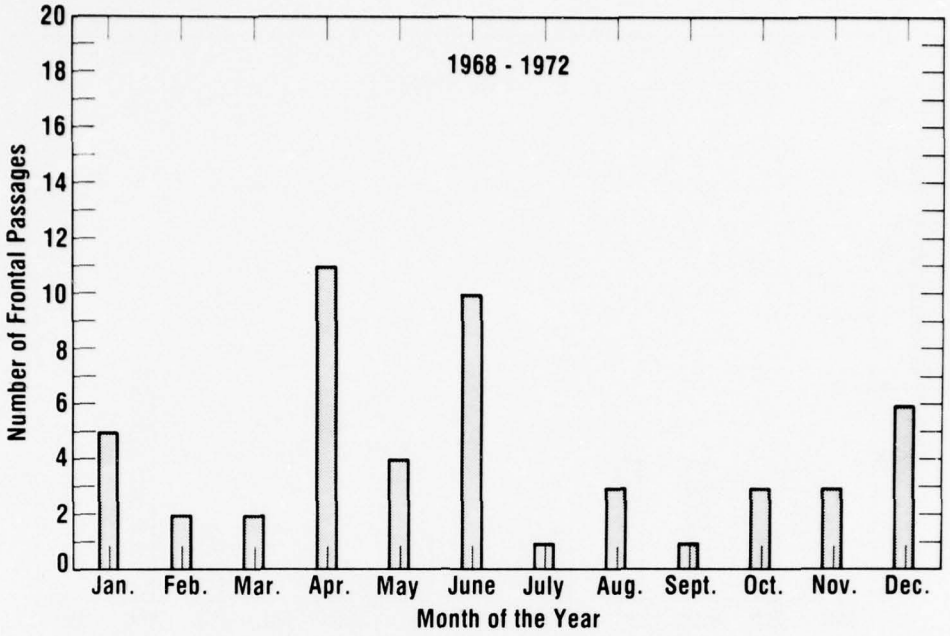

Figure 4.10 Month of year variation for frontal sources capable of triggering pressure detectors.

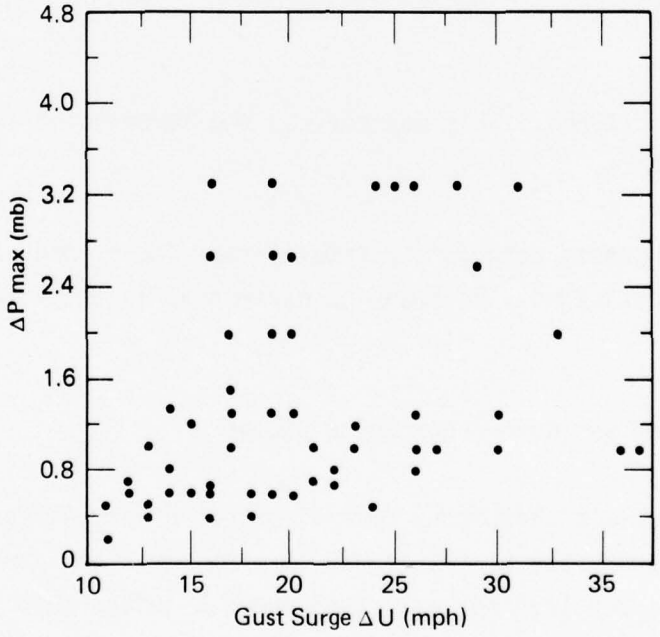

Figure 4.11 Plot of maximum pressure change vs. gust surge

of ΔP_{max} as a function of Δu and appears as a scatter plot with no evidence of the $(\Delta P)^{\frac{1}{2}}$ law frequently assumed for density currents. On the other hand if we plot $\Delta P_{max}/\tau$ as a function of Δu, a better fit becomes evident (Figure 4.12). We interpret these results as evidence that atmospheric gust-front systems move primarily due to driving forces in the central outflow region, as opposed to being driven by pressure gradients across the density discontinuity at the nose of the current. These data imply that statistically some value of gust-front severity can be chosen as a warning threshold for operational systems. We need to know more about the statistics of these relations however.

4.3 Frequency of Occurrence of Significant Vertical Shear

In order to better understand the effect of a gust-front passage on the generation of significant vertical wind shear, we need some knowledge of the frequency of occurrence of shears during undisturbed periods. The wind data at the various levels on the NSSL tower were recorded on magnetic tape

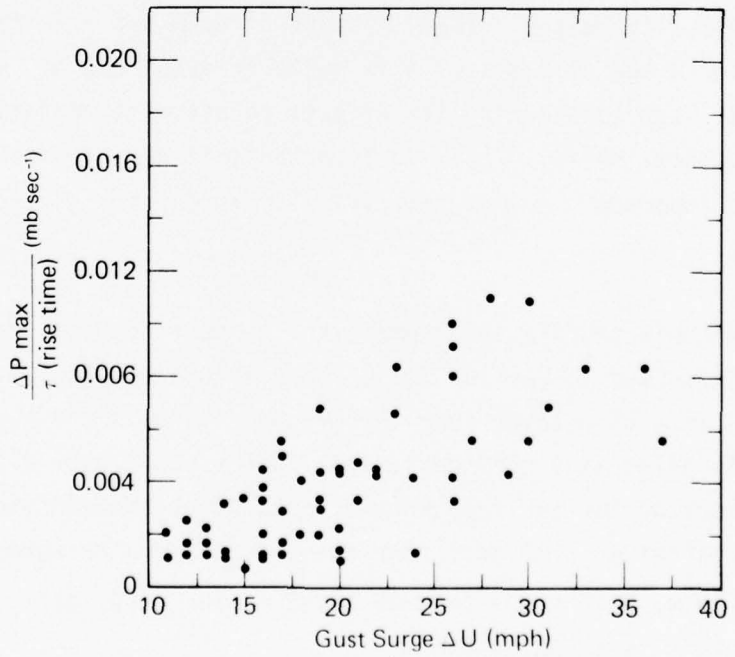

Figure 4.12 Plot of maximum pressure change divided by rise time vs. gust surge.

essentially continuously from 15 April to 24 June 1976 and provided an opportunity to examine this question more closely. Since time did not permit us to analyze the complete data set over this period, we chose five intervals, ranging from four to twelve days to look for the frequency of occurrence of "significant" shear.

Initially, based on Sowa's (1974) operational definition of gradual shear, we used the value of 0.08 sec^{-1} as our significant shear cutoff. This number is based on an 8.4 m sec^{-1} wind change through a 100 m height level. The thickness of the layers for which shear could be determined from the tower data were, from the surface up, 25, 20, 45, 87, 89, and 178 m. It soon became evident that the frequency with which 0.08 sec^{-1} shear occurred within the lower two layers (surface to 25 m and 25 to 45 m) was so high at all times as to be essentially meaningless. The reason for this lies in the need to consider significant shear not only in terms of $\Delta u/\Delta z$ but also the magnitude of Δz itself. For instance, the occurrence of 0.08 sec^{-1} shear between the surface and 90 m (roughly the 100 m used by Sowa) is due to much higher values within the lower layers rather than a near constant shear throughout the entire 90 m. This is hardly surprising given that the wind profile tends to be logarithmic with height. Thus, a shear of 0.08 sec^{-1} in the first 25 m (a change in wind speed of 2 m sec^{-1}) is quite frequent and not very significant, especially when considering its effects on aircraft operations. It should be noted that, while $\Delta u/(\Delta z)$ is important, it can be shown that $\Delta u/(\Delta x)$ is more important, or more specifically $\Delta u/(\Delta x/\cos \alpha)$ where α is the approach angle.

If a logarithmic profile is assumed, and a shear of 0.08 sec^{-1} over 90 m is used (as discussed in Section 1.1), shear values of about 0.12 sec^{-1} can be expected in a 25 m layer near the ground. This is the same as the value frequently given as significant; i.e., 3.5 m sec^{-1} over a 30 m layer. Therefore, in looking for the frequency of occurrence of significant shear, we used cutoff values of 0.12 sec^{-1} for the layers from the surface to 25 m and from 25 to 45 m, 0.10 sec^{-1} from 45 to 90 m, and 0.08 sec^{-1} from 90 to 177 m, 177 to 266 m, and 266 to 444 m.

The program used to find the frequency of occurrence of significant shear simply divided wind magnitude differences by height differences over a 30 sec averaging time. Wind direction was not taken into account so the values derived are always on the conservative side. Most of the time the wind direction with height was constant enough to have little bearing on the shear value. Wind direction changes can become important during the passage of gust fronts and some of these have been covered in a separate analysis but it does not markedly affect the general statistics.

The method used to display the frequency of occurrence of significant shear, Figure 4.13, was simply to count the number of times (using 30 sec averaging) the significant value was exceeded within each layer during 30 minute intervals. The height of the black portion within each block is a measure of that number. Although the maximum number of occurrences within each 30 minute interval is 60, very few cases exceeded 40; therefore, we used 40 as the maximum number within a block. Thus, a half filled block, for example, indicates that the significant shear value was exceeded 20 times in that half-hour interval. Tower height levels are given at the left. Time in CST is given at the top and each column is 30 min long. Intervals of data that were unreliable (obvious malfunctions or unacceptably erratic readings) are indicated by an X. Periods for which no data was recorded are marked by wavy horizontal lines through the missing interval. As an example, on 13 June, the significant shear criterion given earlier was exceeded in the first two layers a total of 8 times (over a 30 sec averaging interval) from 1800 to 1930. In the next half hour, the criterion was exceeded six times in the 25-45 m layer and four times in the 45-90 m layer. Then 7, 19, and 4 times within the first three layers followed by frequent occurrences through the fourth level. During this time a gust front passed over the tower as indicated by the notation below the display. For each period shown, any indication of a disturbance by the acoustic sounder (marked with an A) or the pressure trigger sensors (marked with a P) are annotated at the appropriate time and are accompanied by brief comments on the meteorological conditions observed at the tower.

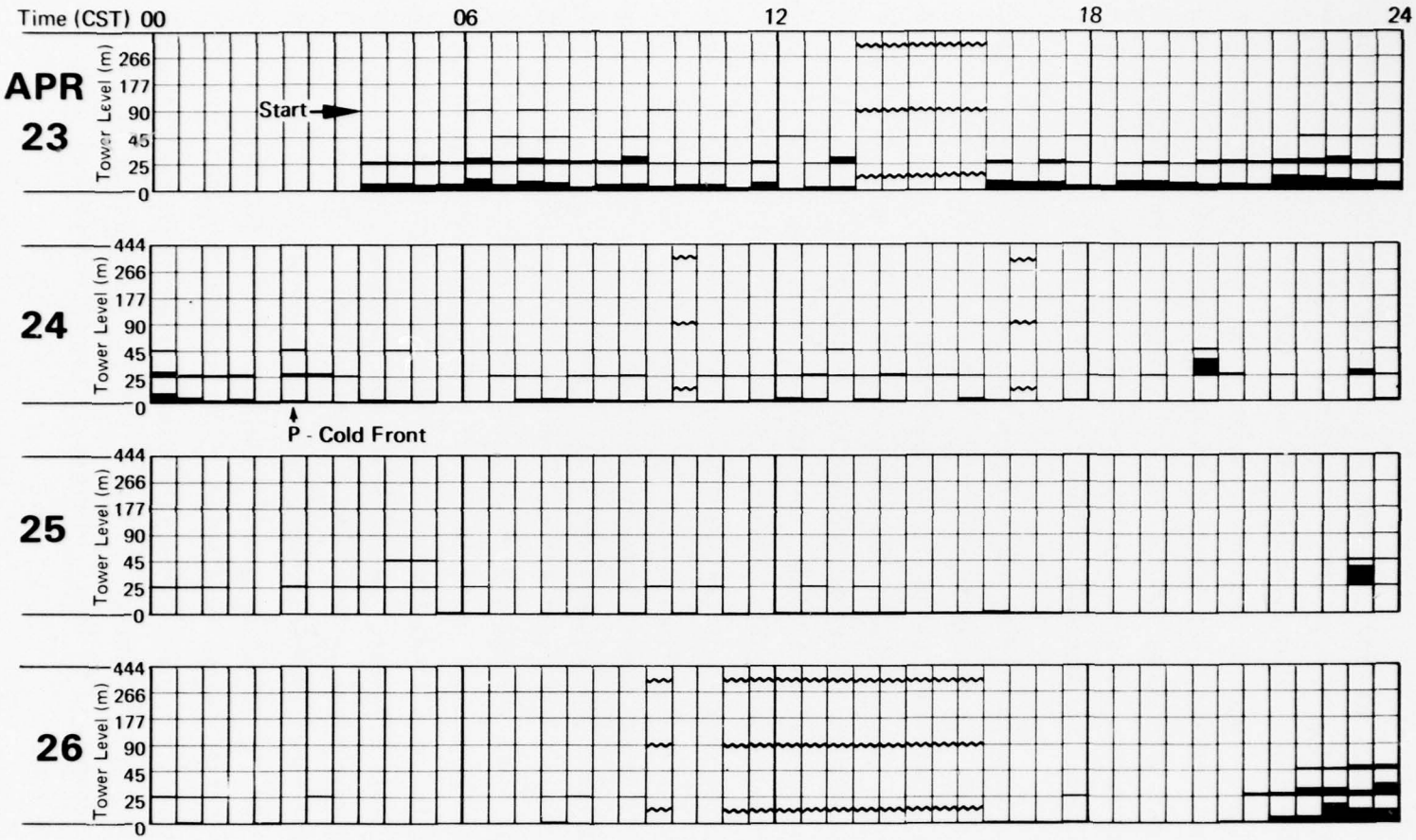

Figure 4.13a Frequency of occurrence of significant vertical shear at NSSL.

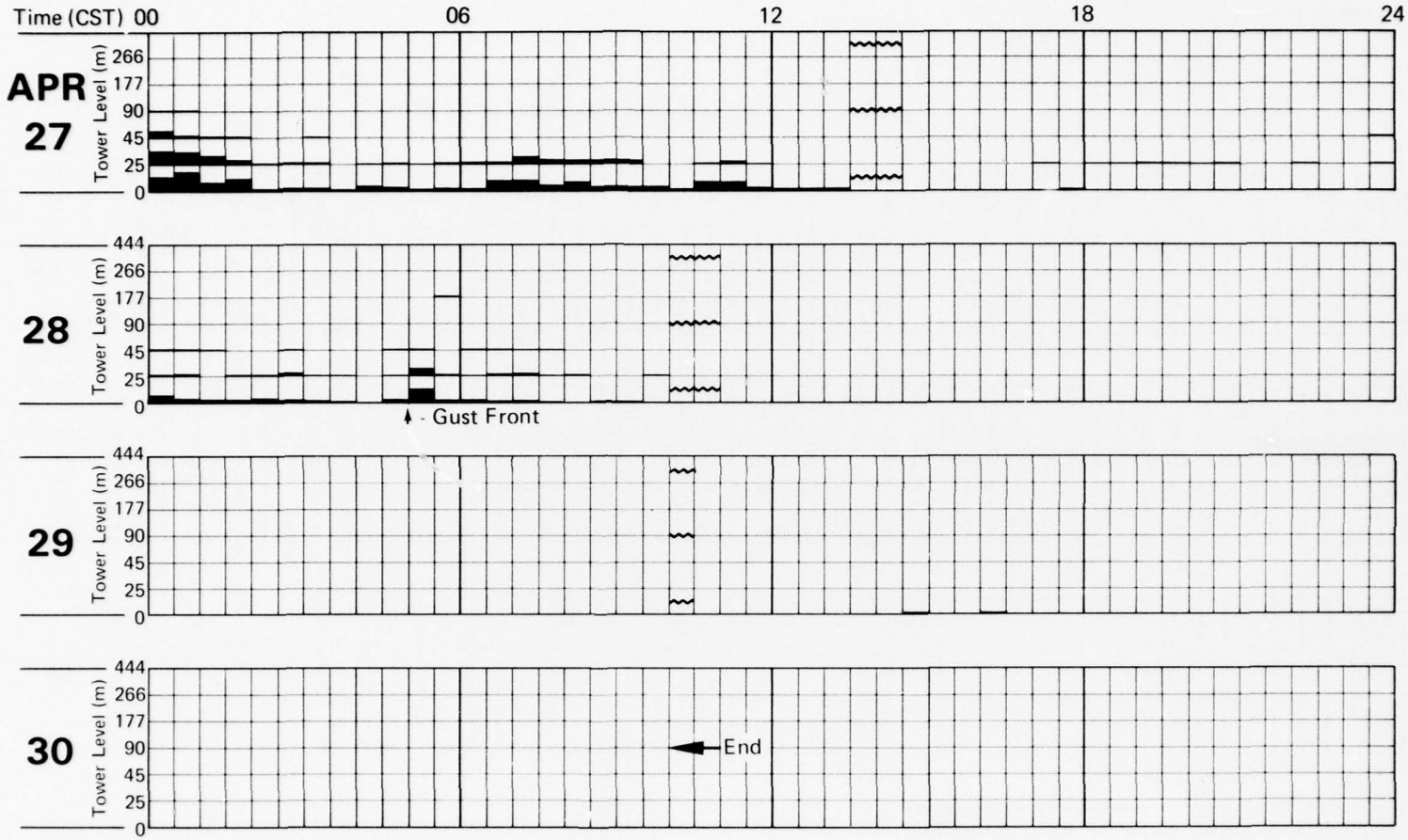

Figure 4.13b Frequency of occurrence of significant vertical shear at NSSL.

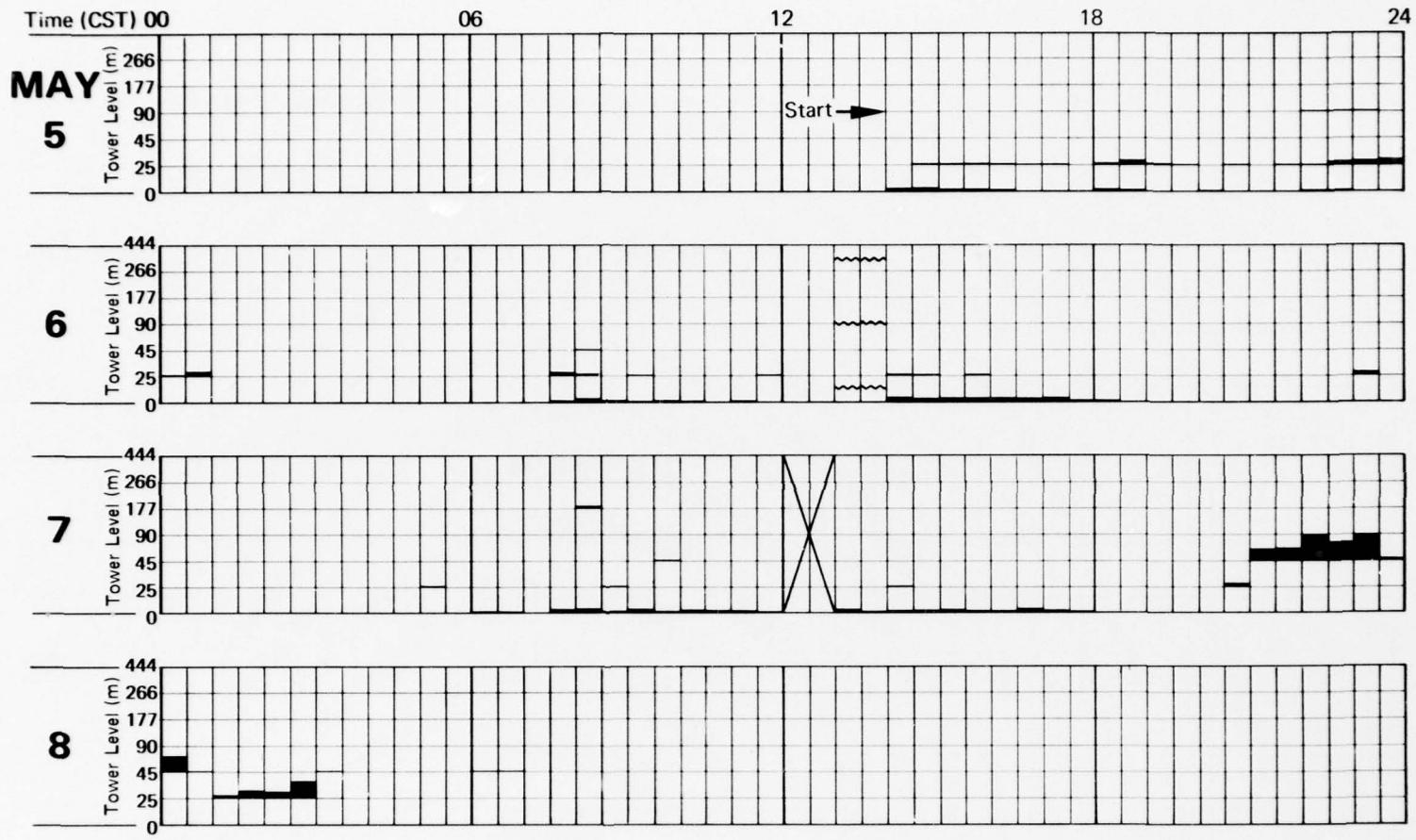

Figure 4.13c Frequency of occurrence of significant vertical shear at NSSL.

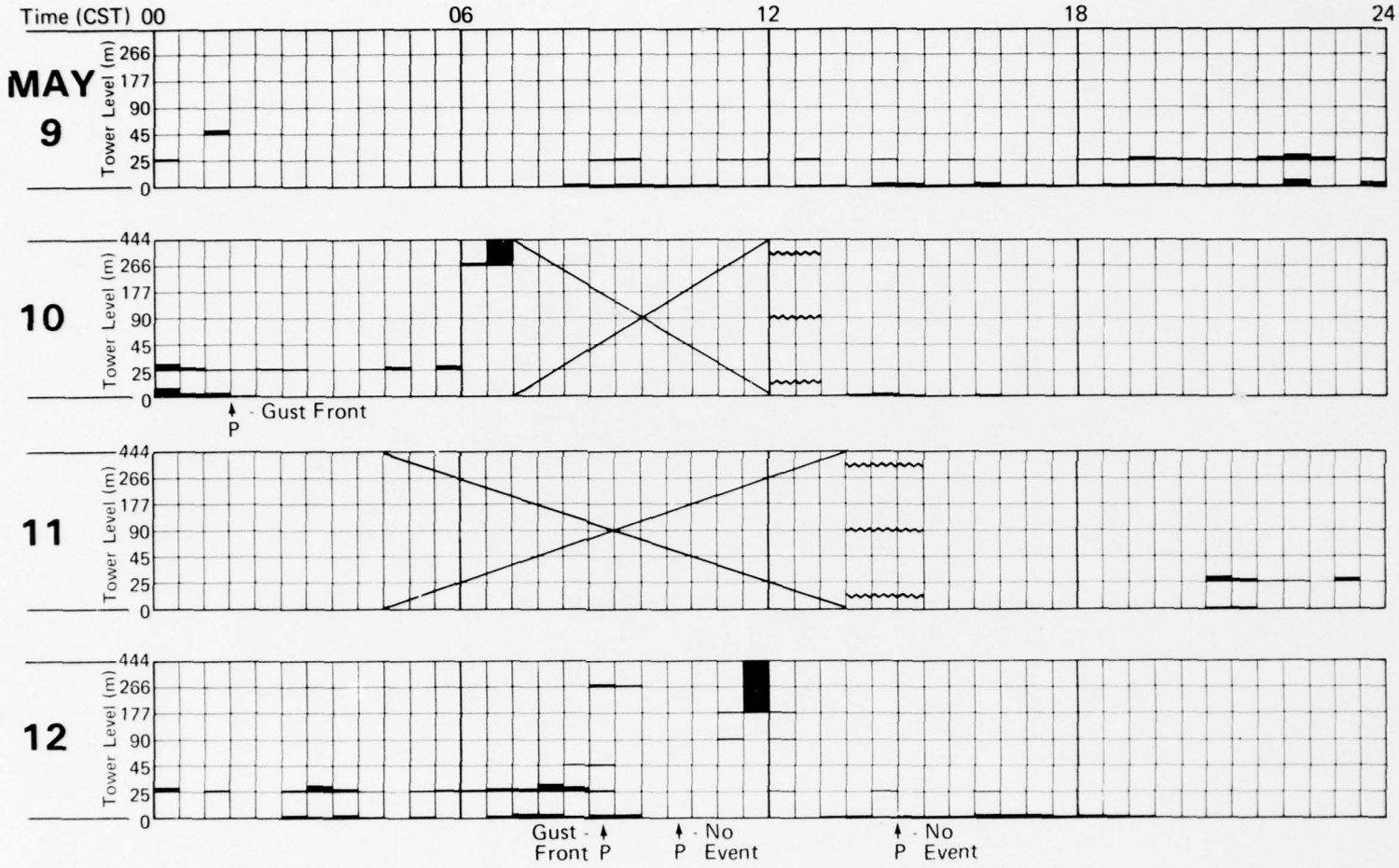

Figure 4.13d Frequency of occurrence of significant vertical shear at NSSL.

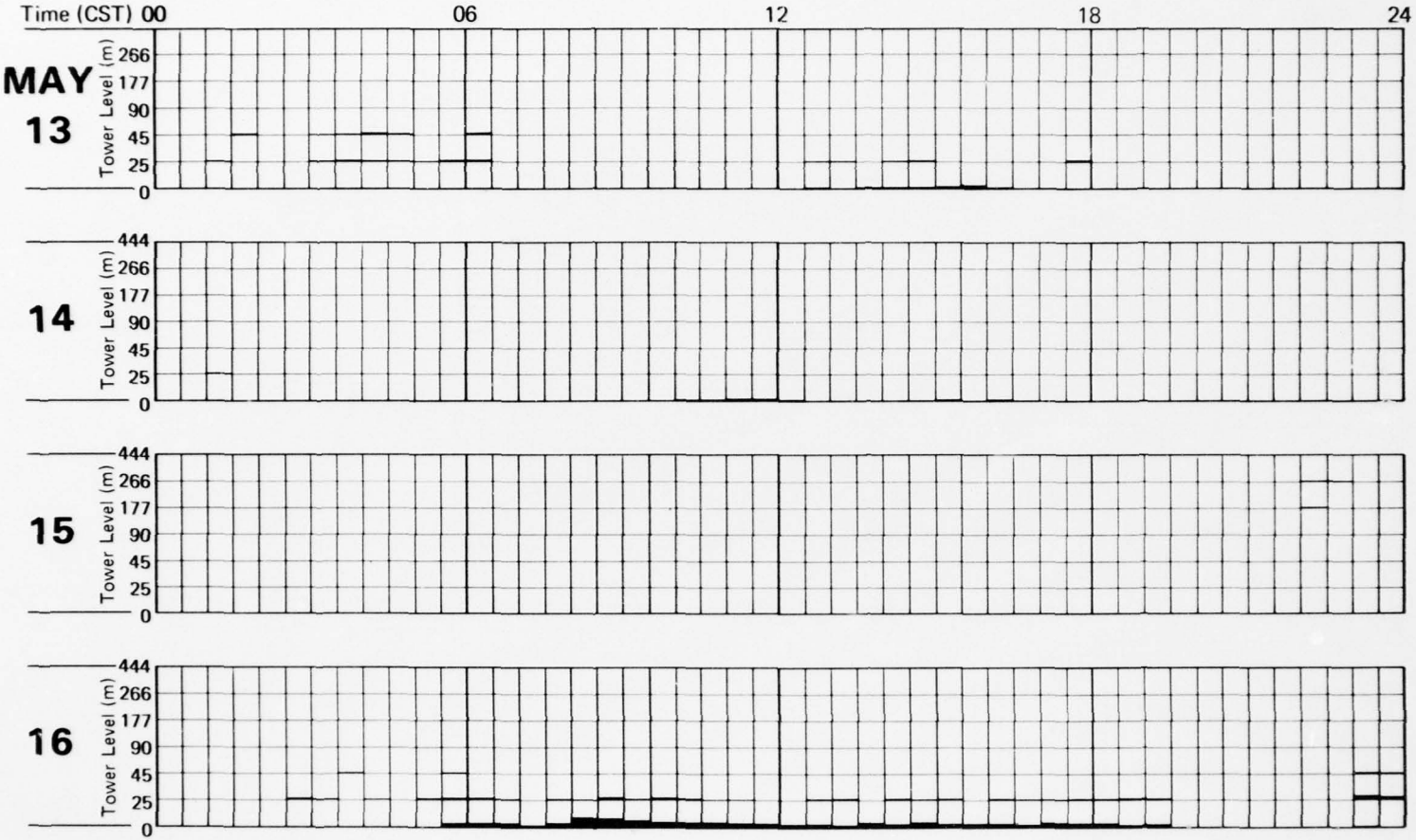

Figure 4.13e Frequency of occurrence of significant vertical shear at NSSL.

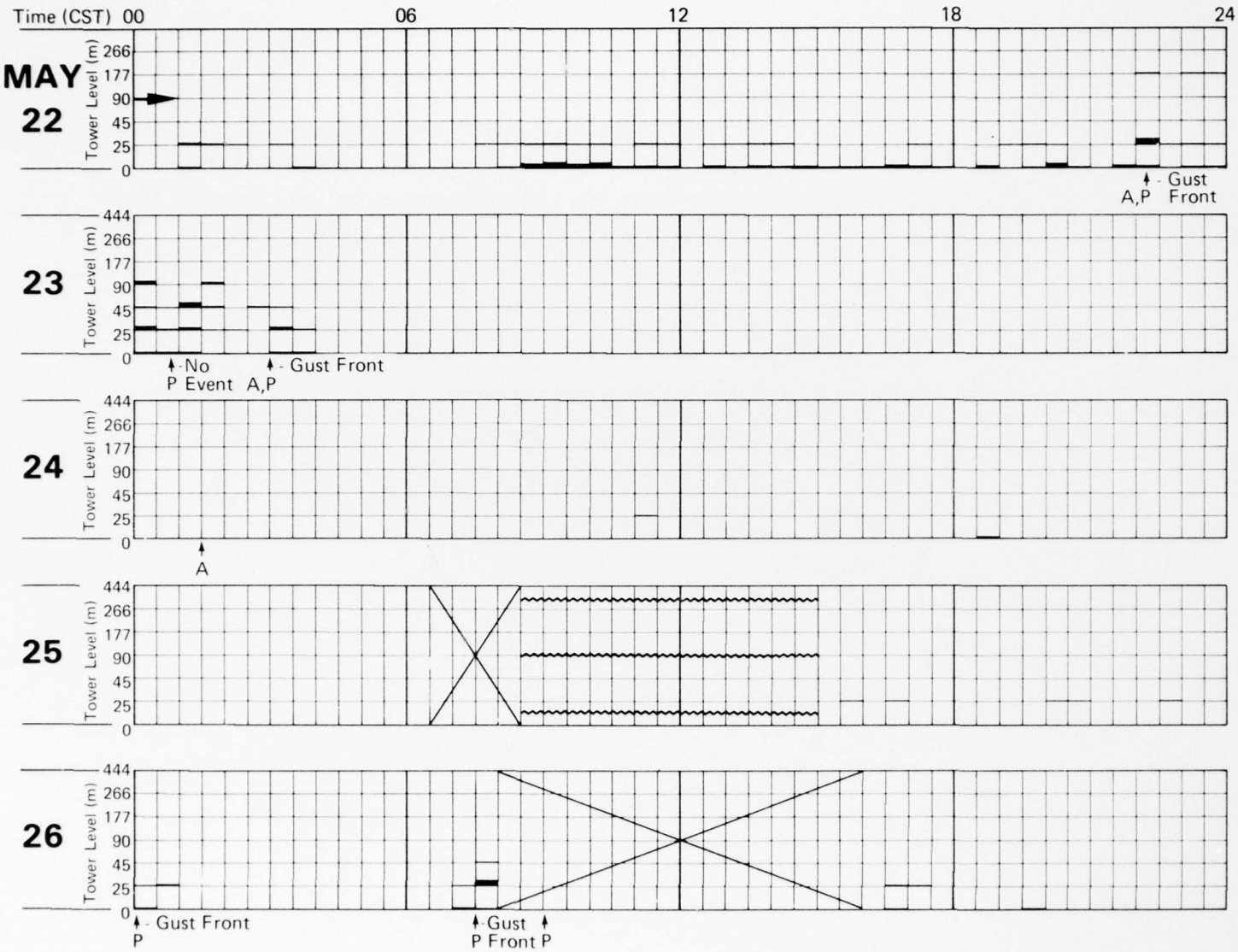

Figure 4.13f Frequency of occurrence of significant vertical shear at NSSL.

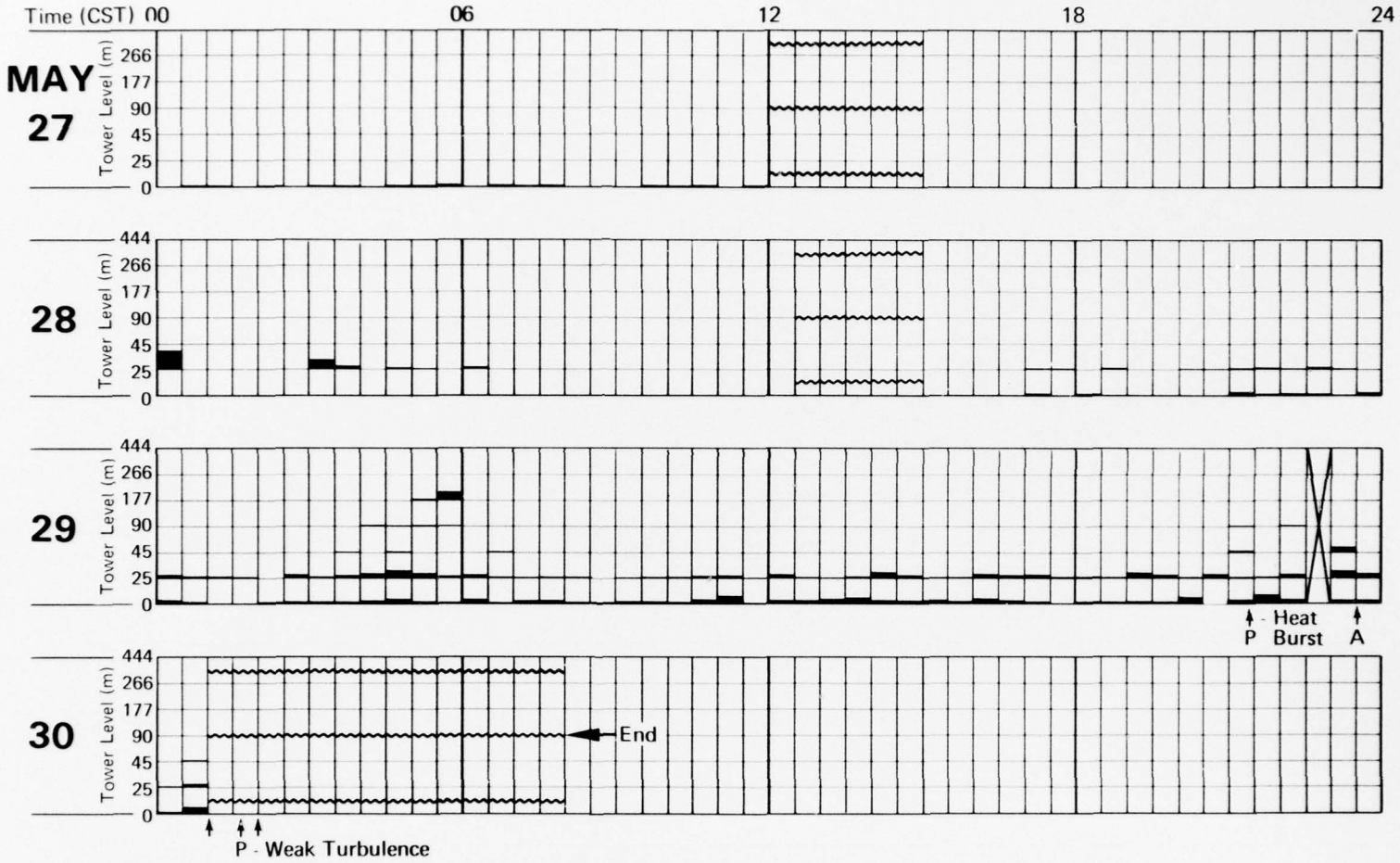

Figure 4.13g Frequency of occurrence of significant vertical shear at NSSL.

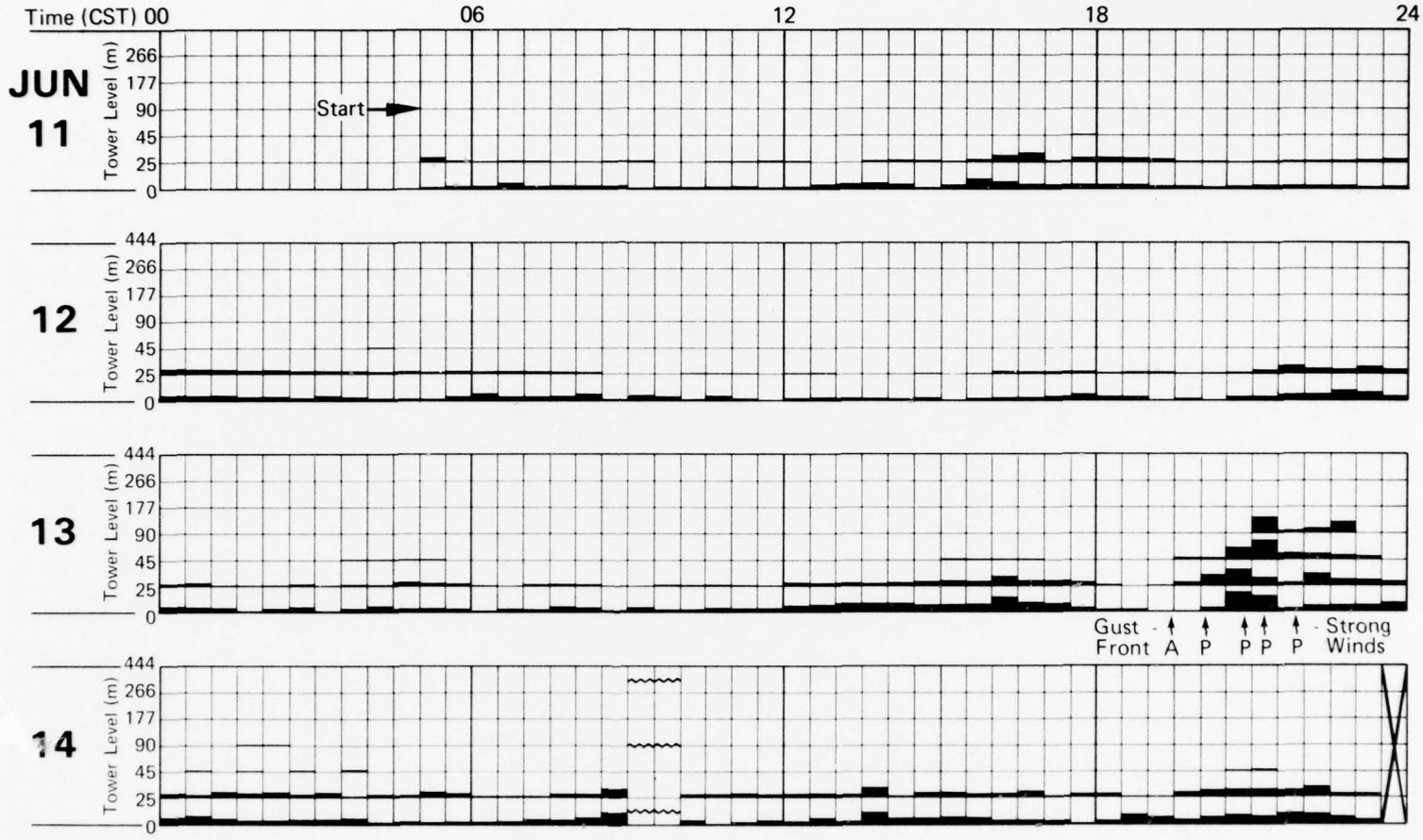

Figure 4.13h Frequency of occurrence of significant vertical shear at NSSL.

In general, shears occurred most frequently during the night-time hours and may be due to the low-level, or nocturnal jets (See Section 1.2). However, there were also several periods of shear during the day for which neither the acoustic sounder nor the pressure detectors indicated a cause. We did not have sufficient time to investigate the possible sources of all the shear occurrences but a full analysis could be performed later to help to determine the frequency of shear by various causes.

The pressure-jump detectors were triggered a total of 20 times. Some of these were multiple triggers during a single event and a total of 16 events were associated with the detectors. Of these, 11 were accompanied by, or shortly followed by, an increase in vertical shear over that which preceded the trigger. Two others coincided with gust fronts which did not generate much shear in the vicinity of the tower, one was associated with a cold front, and the cause of the other two is unknown. The acoustic sounder began operation on 20 May, 1976, after the first eight events identified above. During two other events (26 May), it was out of operation due to a malfunction. Four of the remaining five events were correctly identified as gust fronts from the sounder record. The fifth one (22 May at 0100) occurred while the record was showing extreme wind noise, probably as a result of a gust front which passed by less than three hours earlier. In addition, the sounder identified one event (24 May) which did not trigger the pressure jump detector. This gust front, discussed in Section 3.2, was very shallow and weak, however.

It is important to note that these shear data represent a point measurement in horizontal space. Consequently, a disturbance might have passed near enough to the tower to produce some peripheral shear that was recorded on the tower anemometers, but not sufficiently near to be detected by the sounder or pressure detectors. We want to emphasize that these statistics are meant only to give an indication of the frequency of occurrence of vertical wind shear and are not an adequate data base for serious comparison with other detection methods. A future study will analyze in detail the events which caused the pressure sensors at NSSL to trigger, including the possible presence of significant horizontal shear which is not included here.

4.4 Summary

A study of pressure disturbances at the Chicago O'Hare Airport vicinity over a five year period shows that nearly 75% of them were related to frontal passages or thunderstorms. When we apply the threshold of a pressure jump detector designed to respond to such disturbances (the threshold value is still considered experimental), the number of gravity-shear and unknown events decreases while that associated with thunderstorms increases. For the summer months, the thunderstorm category makes up 60% of all events. Work is continuing to make detection systems based upon pressure jump detectors more reliable. For example, by applying additional criteria for estimating storm severity and type based upon $\Delta P/\tau$, one should be able to distinguish among gravity-shear waves, synoptic-scale fronts, and thunderstorm gust fronts as well as between dangerous and nondangerous gust fronts.

An analysis of anemometer data at Chicago O'Hare Airport allowed us to compare gust surges with the accompanying pressure rise characteristics. We find that the maximum change in surface wind speed is related to the time rate of increase of pressure with implications that could lead to a warning threshold for operational systems.

Statistics for several time intervals at the NSSL tower during the spring of 1976 show considerable variation in the frequency of occurrence of significant vertical wind shear. The majority of these shears occurred during the night and may be due to the low-level, or nocturnal jet. Eleven of the 17 events identified by the acoustic sounder and/or pressure trigger sensors were accompanied by some increase in the amount of significant vertical shear within the tower height. Three others occurred during the passage of gust fronts which did not generate a significant amount of shear at the tower.

5. A SOURCE-DRIVEN DENSITY CURRENT MODEL AND ITS APPLICABILITY TO ATMOSPHERIC GUST FRONTS

5.1 Introduction

The cold air outflow from the base of a thunderstorm can last for many minutes in the source region and could dominate the dynamics of such storms for a significant portion of their lifetime. For example, assuming downflow lifetimes between 10 and 30 minutes and a constant speed of motion of 10 m sec^{-1} for the leading edge of the density current, the gust front can travel distances between 6 and 18 km. Moreover the source-driven systems can represent the most dangerous segments of the most intense density currents, since these tend to be related to the greatest downdrafts and be most severe during the first 20 km of their paths.

Although many past gust-front studies compare measurements with simple density current flows, little attention has been given to source-driven models and their application to thunderstorm gust fronts. The numerical work of Mitchell (1975) is one exception. Thus, while sea breeze fronts and cold fronts could fit a simple density current model quite well, it would seem that analyses of thunderstorm gust fronts, particularly those near the source region require more attention to source effects.

5.2 Assumptions

The simple source-driven density current model presented here (see Figure 5.1) is based upon the following assumptions:

1. The density difference, $\Delta\rho$, between the surrounding air, ρ_2, and the density current and source region, ρ_1, is constant.

2. The influences of vertical components of the velocity within the source region are neglected.

3. The source region height, H, extends from the surface to the freezing level. In calculations, H is assumed to be 3 km.

4. The speed of motion of the discontinuity remains constant over a significant portion of its path.

5. The initial rise time, τ, of the pressure jump is caused by accelerations of air preceding the discontinuity. This leads to a further assumption.

6. The height of the current at the leading edge, h, is equal to the product τc, where c is the speed of motion of the front relative to the earth's surface. This is true if the distance scale over which the acceleration of air occurs is equal to the height of the system and implies that density currents act as bluff bodies.

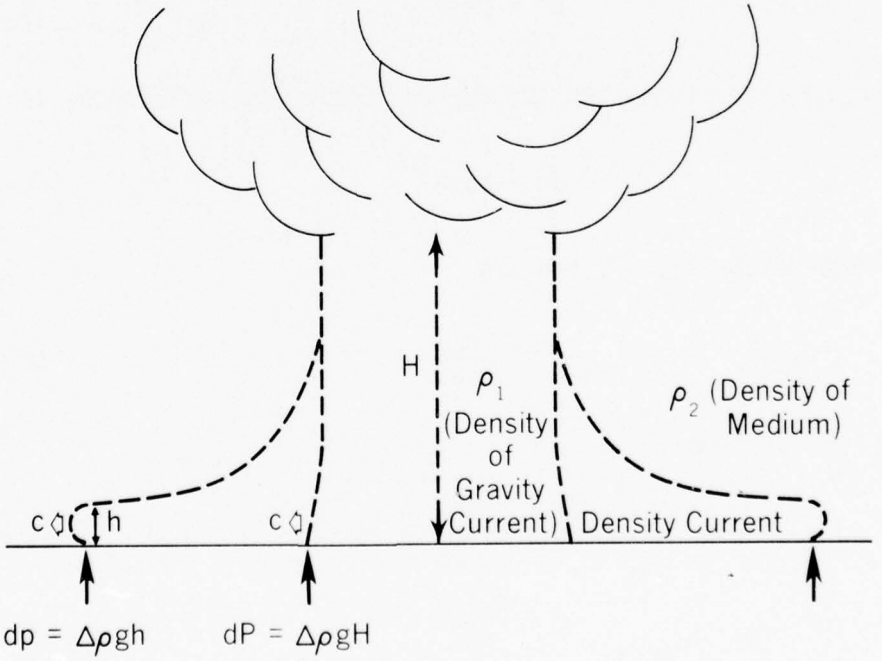

Figure 5.1 Source-driven density current model.

This last assumption is made so that the model may be expressed in terms of observables which consist frequently of pressure measurements sensitive to the leading edge of the discontinuity.

5.3 A Source Driven Model

At the source region we see from the hydrostatic equation that:

$$\Delta P = \Delta\rho g\, H, \tag{5.1}$$

where ΔP is the pressure increase beneath the column of air and g is the local acceleration due to gravity. From Bernoulli's equation

$$\Delta P = 1/2\rho c^2 \tag{5.2}$$

where ρ is the average density of the medium and c is the frontal speed of motion. Thus

$$c^2 = \frac{2\Delta P}{\rho} \quad . \tag{5.3}$$

At the leading edge of the density current the pressure increase is

$$dp = \Delta\rho g h. \tag{5.4}$$

Thus from Equations 5.1, 5.3 and 5.4

$$c^2 = \frac{2dpH}{\rho h} \quad . \tag{5.5}$$

Letting $h = \tau c$ we find

$$c^3 = \frac{2dpH}{\rho\tau} \quad . \tag{5.6}$$

or

$$c = \left(\frac{2dpH}{\rho\tau}\right)^{1/3} \tag{5.7}$$

A comparison of the source-driven and simple density current models show several forms:

Source driven model:

$$c = \left(\frac{2\Delta\rho gH}{\rho}\right)^{1/2} = \left(\frac{2\Delta TgH}{T}\right)^{1/2} = \left(\frac{2\Delta pH}{\rho h}\right)^{1/2} = \left(\frac{2\Delta pH}{\rho\tau}\right)^{1/3} \qquad (5.8)$$

Simple density current:

$$c = \left(\frac{2\Delta\rho gh}{\rho}\right)^{1/2} = \left(\frac{2\Delta Tgh}{T}\right)^{1/2} = \left(\frac{2\Delta p}{\rho}\right)^{1/2} . \qquad (5.9)$$

The above assumes that the medium is not in motion. Where u, a component of medium motion along the direction of motion of the gust front exists, another expression for c results, namely

$$c = \left[\frac{2\Delta pH}{\rho\tau\left(1-2\,\frac{u}{c}+\frac{u^2}{c^2}\right)}\right]^{1/3} . \qquad (5.10)$$

Comparing the above relations, it becomes evident that pressure measurements should provide a sensitive indicator of the relative importance of the two models. The data appearing in Figures 4.11 and 4.12 of Section 4.2 indicate that $\Delta p/\tau$ is correlated with surface gust data whereas Δp shows little correlation. These data are plotted on a log-log plot in Figure 5.2 and show evidence for a $(\Delta p/\tau)^{1/3}$ relation. The solid line is a least-square fit to these data. In addition, recent results from experiments at both O'Hare airport and the National Severe Storms Laboratory (NSSL) provide evidence for a source-driven model. There is a wide range of h values observed for density currents depending on the life time and measurement position of a given gust front. Thus, one would expect to have to include h estimates in plotting such data. The fact that Simpson (1972) found a good fit for a c proportional to $(\Delta T)^{\frac{1}{2}}$ plot argues that variations in h values were not important for his data or that H was approximately constant. We expect that the relative variations in h will

exceed those in H. Moreover, since H appears to the 1/3 power in Equation 5.10, the dependence of c upon H will be weak.

Middleton (1966) tested the expression for the initial velocity of saline surges found by Keulegan (1957) namely

$$c = 0.46 \left(\frac{\Delta\rho g H}{\rho}\right)^{\frac{1}{2}}$$

which has the same form as Equation 5.8. Middleton observed using water tank data that the speed of motion remained constant for a distance of about 10 scale heights of the source region. This indicates that source-driven effects extend for significant distances from the source region.

Thus, it seems wise to look at data sets for atmospheric gust fronts from both viewpoints. It is probable that measurements made close to evolving or mature systems will follow source-driven models while measurements made of dissipating systems at larger distances from the source will

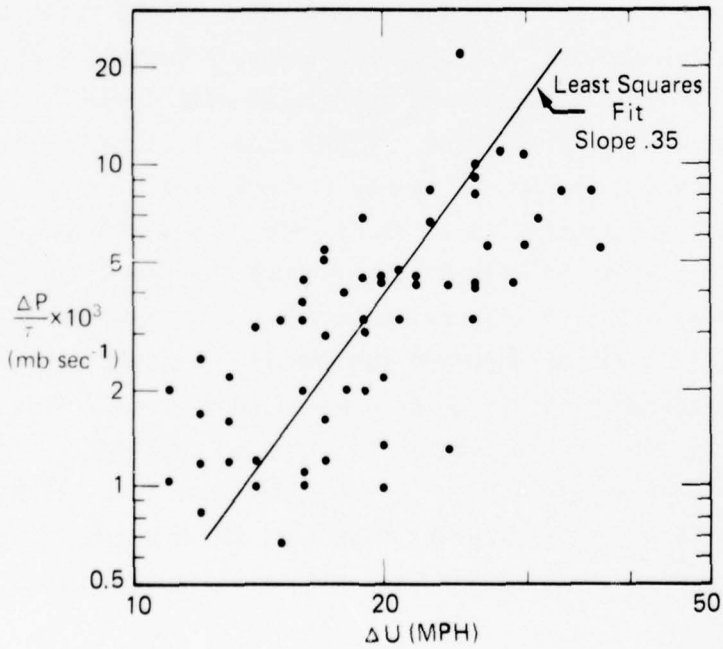

Figure 5.2 Plot of time rate of pressure change vs. gust surge.

follow a simple density current model. We suggest the addition of recording rain gauges to sensing arrays as one means of estimating source functions for those systems. Future scale model and field experiments should study source effects. Also, extension of the work of Mitchell (1975) could yield guidance concerning the possibility of providing warning information based upon radar studies of the source region.

6. SUMMARY AND CONCLUSIONS

This report is concerned with the study of one of the hazards affecting aircraft operation in the airport environment: wind shear. Three mechanisms capable of producing hazardous wind shear have been identified: (a) Synoptic-scale fronts, (b) Low-level jets, and (c) Thunderstorm-generated gust fronts. Our main emphasis has been placed on analyzing the gust front, using both case studies and statistical techniques.

We have analyzed in detail nine gust-front events at NSSL, Oklahoma and Haswell, Colorado, which were initially believed to be gust fronts associated with nearby thunderstorms. One of these was later determined to have been caused by a cold front which produced significant shear and was included in the study. Instrumented towers, acoustic sounders, Doppler radar, and pressure sensors provided the information necessary for comparing gust-front parameters and for investigating relationships among them. A wide range of parameter values as well as some significant similarities and differences have been observed. One of the more important differences is due to the state of atmospheric stability at the time of arrival of the gust front. Because low-level surface inversions inhibit mixing, none, or only part of the dynamics within the density current reach the surface. As a result, ground-based anemometers and thermometers may measure changes in wind and temperature which do not adequately reflect the extent of wind-shear severity at higher levels. We have found a linear relation between vertical wind shear and the maximum temperature decrease across the front; however, the maximum temperature change occurred well above the surface, especially when an inversion was present.

One of the measurable parameters which appears to be independent of stability with respect to shear severity, is the speed of motion of the density outflow. We have found a reasonably linear relation between the gust-front speed and maximum vertical shear which leads us to conclude that a warning system should have the capability to measure the gust-front motion directly. Studies currently being conducted with arrays of pressure sensors at Chicago, O'Hare airport are investigating the potential of these

sensors for the detection and tracking of gust fronts. A larger installation at Dulles International, Washington, D.C., should test the concept of providing operational warnings. A five-year statistical study on the causes of significant pressure jumps in the vicinity of Chicago's O'Hare Airport revealed a high correlation with nearby thunderstorm activity. By applying a criterion of at least one millibar pressure rise within 10 minutes, we have found that 60% of the summer-time pressure increases were related to thunderstorms, the remainder being caused by frontal activity, gravity shear waves and unknown sources. Moreover, from statistics comparing pressure and anemometer records, we have found that the time rate of change of the pressure disturbance caused by a cold-air density-current passage was related to the gust surge, or change in horizontal wind speed produced by the event. Additional data on the effect of ambient stability on this relationship is needed to help to substantiate it, but the preliminary results suggest that pressure measurements may provide some indication of wind-shear severity.

Microwave Doppler radars are recognized as powerful tools which can detect gust fronts and measure wind shear at distances of 10 km or more. Their cost and manpower requirements prohibit widespread use as warning devices, so at the present time they must be viewed as research devices only. However, Doppler radar techniques at both microwave and acoustic frequencies are currently being tested by WPL for wind shear detection in the immediate vicinities of airports.

Temperature and wind profiles were compared to acoustic sounder facsimile records and showed that the sounder displayed the internal structure of the gust-front dynamics in detail, making it a valuable tool for wind-shear studies. The sounder's sensitivity to ambient noise, such as wind and rain, was a frequent limitation during our case studies. Because by burying the acoustic antenna it is possible to alleviate most of the noise problem, the sounder may still find use as part of an overall detection system.

We have compared gust-front features determined from our case studies with theoretical models, laboratory experiments, and previous case studies. Our major results and conclusions are summarized below.

1. Laboratory flows and sea-breeze observations indicate that the ratio of front propagation speed to that of the steady upstream flow increased with distance travelled. Our results show no such trend and are consistent with previous gust-front observations.

2. Some gust-front models suggest that the circulation within the head would either prevent the formation of an elevated nose at the leading edge of the density current or cause it to collapse very quickly once it formed. Extrapolation of laboratory flows to the atmosphere predicts nose heights of only a few meters. We find that, while elevated noses were not generally apparent in the temperature profiles, they were observed in at least seven of the nine wind profiles. Furthermore, the ratio of wind maximum height to head depth showed good consistency among the events.

3. The Haswell density currents were considerably longer and shallower than their laboratory counterparts. The current head depth-to-length ratios (D_h/L_h) of laboratory flows are about 0.4, but all of the Haswell currents had smaller ratios, averaging about 0.12.

4. Frontal slopes of laboratory flows have been found to decrease with diminishing surface drag, reaching a minimum of $\pi/8$ or 0.39. Three of the Haswell currents had slopes of 0.2 or less. The other three had very steep slopes within the tower height even in the presence of surface temperature inversions which tended to minimize surface friction. These latter three were the most intense events, indicating that the slope is more sensitive to the age and intensity of the outflow than to surface drag.

5. Our observations show that greater mixing occurs in atmospheric gravity currents than was indicated by laboratory experiments, which suggests another possible cause for the multiple surges often observed. These surges are usually attributed to the merging of outflows from pulsating or separate downdrafts. However, if the outflow source continues to supply cold air, a surge may be produced by the formation of a new current head in place of the previous one disrupted by intense mixing.

6. The relationship we have found between the gust surge and the time rate of change of the pressure disturbance caused by a gust-front passage has led to a model which suggests that the dynamics of thunderstorm gust fronts are more dependent on the influence of the source than previously thought. Some observed results are not consistent with the behavior of a simple density current flow, but can be explained by a source driven model.

From anemometer measurements made at six levels on the NSSL tower, we have determined the frequency of occurrence of significant vertical wind shear for several time intervals during the spring of 1976. A large percentage of this shear occurred during the night and was probably caused by the low-level, or nocturnal jet. Eleven of the 16 events which triggered the pressure detectors showed some increase in the frequency of occurrence of shear, but several other instances of frequent shear were not detected by either the pressure sensors or acoustic sounder. The causes of these events will require further study.

The production of significant shear by synoptic cold and warm fronts has been reviewed. We have described briefly an operational method for forecasting shear severity from frontal characteristics. Similar forecasting methods for gust-front shear production appear to be much more complex, if at all possible.

7. RECOMMENDATIONS FOR FUTURE WORK

This report contains the analysis and interpretation of data collected at Haswell, Colorado, NSSL, Oklahoma, and Chicago, Illinois. Because of the limited number of locations represented, the climatological significance of these data is somewhat restricted. To develop and design an optimum wind-shear detector, one needs to know considerably more about the climatology and detailed dynamics of wind shear. The above objectives can be met only by collecting and analyzing long-term data at a large number of locations that are affected by wind shear.

The FAA has a major effort in meteorological data management and is obtaining data from several locations and facilities, including some of those we discuss in Section 7.1. These data are to be made available to interested scientists for further analysis.

Because of the large number and diverse nature of the sensors involved, the costs of wind-shear data gathering can become large. This means that most of the data will have to be collected at existing facilities, not necessarily designed for wind-shear work. Not only will the sensor types, their speed of response, and separation be inappropriate in many cases, but the essential characteristics and data format of the various installations will also vary greatly. Nevertheless, we feel that valuable data for understanding the causes, dynamics, internal structure, and climatology of wind shear could be collected at a number of locations around the country. Some of these facilities could be used in their present condition while others should be upgraded or augmented. A substantial effort would have to be expended on making the resultant data sets compatible and performing the required analyses.

7.1. Facilities for Wind-Shear Data Collection

In the following we describe briefly some of the facilities that would be suitable for data gathering and discuss their capabilities.

7.1.1 Boulder Atmospheric Observatory (BAO)

The Boulder Atmospheric Observatory, a joint venture of NOAA and the National Center for Atmospheric Research (NCAR), will be a unique facility for studying the boundary layer. It will consist of a 300-m tall tower (with the option of extending it to 500 m) instrumented with high-quality, fast-response anemometers, thermometers, and humidity and pressure sensors at eight levels. In addition, a fully-instrumented moveable carriage will be able to provide detailed profile information over the entire length of the tower. A number of remote sensors using laser, radio, and acoustic wave propagation will be operated at the tower, in effect increasing the depth of the atmosphere sampled well above the maximum height of the tower. Extensive data collection facilities will insure the archival of all these data continuously (for several years, if necessary). The BAO facility is expected to become operational during the latter part of 1977.

Although BAO is not located in a region with frequent gust-front occurrences, the facility will still be most valuable for collecting data to investigate the detailed dynamics of wind shear and to contribute to wind-shear climatology.

7.1.2 KTVY-TV Instrumented Meteorological Tower, Oklahoma

For a number of years the National Severe Storms Laboratory (NSSL) of NOAA has been operating a 481 m tall meteorological tower near Oklahoma City, Oklahoma. The tower is instrumented at six levels with wind, temperature, and humidity sensors. During the past storm season, the tower instrumentation has been augmented with a pressure-jump detector array and an acoustic echo sounder. The data collected by NSSL have been particularly valuable for characterizing thunderstorm gust fronts.

7.1.3 Dulles Wind-Shear Detection System

A facility, not duplicated anywhere else, to detect hazardous wind shear has been set up at Dulles International Airport in Washington, D.C. It

consists of a dual, acoustic/EM radar wind-measuring system capable of obtaining wind profiles up to 510 m and an array of 125 pressure-jump detectors (60 of which are now installed and operating). The wind profiling system was designed to detect wind shear associated with synoptic-scale fronts while the pressure-jump sensors indicate the location and speed of an approaching gust front. The continued operation of this facility will provide much needed long-term data on wind-shear occurrences, attendant meteorological conditions, and the performance of the remote sensors installed at the site.

7.1.4 Other Facilities

In addition to the facilities listed above, there are a number of other locations suitable for gathering wind-shear data. For example, arrays of pressure-jump detectors and absolute pressure sensors in conjunction with six towers instrumented with anemometers and temperature sensors have been installed and are operating at O'Hare International Airport in Chicago. Tall instrumented meteorological towers have been in operation near Philadelphia, Pennsylvania (Drexel University Tower), Aiken, South Carolina (Savannah River Laboratory Tower), Las Vegas, Nevada (AEC BREN Tower), and Kennedy Space Center, Florida (NASA Tower). All of these could provide potentially useful data for future wind-shear studies.

7.2 Recommendations for Data Collection and Analysis

Our study has shown that low-level wind shear falls within the mesoscale range of meteorological phenomena. The present, coarse synoptic-scale observations provide only a meager amount of information on the structure and climatology of any mesoscale feature; consequently, no adequate wind-shear data base exists today. To rectify the mesoscale-forecasting situation, WPL has embarked on an initiative to develop a Prototype Regional Observing and Forecasting Service (PROFS). Basically, PROFS would provide an essentially real-time, detailed meteorological data set suitable for preparing "nowcasts" and short-term local forecasts for an area corresponding to the 350 km grid spacing of the present radiosonde network. The objectives of PROFS will be achieved by the maximum use of ground-based and satellite-borne remote

sensors. The soon-to-be-operational Boulder Atmospheric Observatory (Section 7.1.1) will be a key element in the development of PROFS. Clearly, data collected by PROFS would be eminently suited for both studying and forecasting wind shear.

Until PROFS becomes a reality, data gathered at the facilities discussed in Section 7.1 should be used to better our understanding of wind shear. Only an organized program of long-term data collection at a sufficient number of locations around the country can establish the sorely needed wind-shear climatology. These data would then be analyzed to answer the many outstanding questions regarding the frequency of occurrence, generating mechanisms, location and spatial extent, internal structure, severity, and time duration of wind shear. To obtain the maximum benefit of data collected at a given site, the existing instrumentation in some cases will have to be augmented. For example, to study the relationship between the cold-air outflow and its source, radar tracking of the parent thunderstorm will have to supplement the data gathered by an instrumented tower.

Because pressure sensors have demonstrated great promise for detecting and tracking thunderstorm gust fronts (Sections 4 and 5) and perhaps for eventually predicting the resultant wind shear, we feel that pressure data should play a prominent role in future data gathering and analysis efforts. Pressure data already are being collected at Dulles, Chicago, and NSSL. The data base could be significantly expanded and the analysis be made much more meaningful by augmenting the anemometers to be installed at Houston, Atlanta, and Denver airports with collocated pressure sensors. The potential worth of already existing data sets should not be overlooked either. For example, barograms and pressure array records taken at Washington, D.C. would allow the further investigation of the relationship between the rate of change of pressure discontinuities caused by a cold-air density outflow and the speed of motion of the current. Our study strongly suggests that gust-front motion is related to wind-shear severity, however, additional data analysis is needed to help to substantiate this conclusion.

With respect to the ultimate aim of all the wind-shear studies, the authors would like to suggest the collection of a data base that we feel addresses the problem of aircraft safety most directly. Specifically, we recommend that, after landing, pilots be encouraged to document the conditions, during wind-shear events, under which they landed and departed (and especially when the events occur at airports that already have some type of wind-shear warning devices installed such as Dulles and O'Hare). The compilation of "real life" flight conditions would allow comparisons to be made with other available information such as routine weather data. For example, a comparison of pilot comments over a six-month period with standard NWS barograms may reveal that when pilots were encountering difficulties, a certain type of pressure characteristic was frequently present. We feel that a data set based on pilot reports will have a direct bearing on solving the wind-shear problem. For no matter what we have learned about the dynamics of the atmosphere, if pilots encounter difficulties when theory predicts none, or vice versa, it means that we have not yet solved the problem.

The ultimate success of our efforts will largely depend on how well we will be able to coordinate and combine the work of many individuals and organizations.

REFERENCES

Bedard, A. J. Jr. and D. W. Beran (1977). "Detection of gust fronts using surface sensors." NOAA Tech. Memo. ERL WPL-20.

Benjamin, T. B. (1968). "Gravity currents and related phenomena." J. Fluid Mech., 31, Part 2, 209-248.

Blackadar, A. K. (1957). "Boundary layer wind maxima and their significance for growth of nocturnal inversions." Bull. Amer. Meteor. Soc., 38, 283-290.

Blackadar, A. K. and G. C. Reiter (1958). "Objective forecasting of low-level wind shear." AFCRC TN #58-437, prepared for Air Force Cambridge Research Center under contract No. AF19(604)-2059.

Blecker, W. and M. J. Andre (1950). "Convective phenomena in the atmosphere." J. Meteor., 7, 195-209.

Bonner, W. D. (1968). "Climatology of the low-level jet." Mon. Wea. Rev., 96, 833-850.

Byers, H. R. (1974). General Meteorology (Fourth edition). McGraw Hill, Inc.

Caracena, F. (1976). Weather Analysis. NTSB Exhibit No. 5E-1 of Stapleton accident.

Charba, J. (1972). "Gravity current model applied to analysis of squall-line gust front." NOAA Tech. Memo. ERL NSSL-61.

Charba, J. (1974). "Application of gravity current model to analysis of squall-line gust front." Mon. Wea. Rev., 102, 140-156.

Clarke, R. H. (1961). "Mesostructure of dry cold fronts over featureless terrain." J. Meteor., 18, 715-735.

Colmer, M. J. (1971). "On the character of thunderstorm gust fronts." Royal Aircraft Est., Tech. Memo. Aero 1316, Bedford, Eng.

Curry, M. J. and R. C. Murty (1974). "Thunderstorm-generated gravity waves." J. Atmos. Sci., 31, 1402-1408.

Flauraud, E. A., A. H. Mears, F. A. Crowley, Jr., and A. P. Carey (1954). "Investigations of microbarometric oscillations in eastern Massachusetts." Tech. Rept. 54-11 Geophys. Res. Paper 27, Air Force Cambridge Res. Lab., Mass.

Fujita, T. T. and F. Caracena (1977). "An Analysis of three weather related aircraft accidents." (to be published in Bull. Amer. Meteor. Soc.).

Glossary of Meteorology (1959). American Meteorological Society, Bost., Mass.

Goff, R. C. and W. D. Zittel (1974). "The NSSL (WKY-TV) tower data collection program: April-July 1972." NOAA Tech. Memo. ERL TM-NSSL No. 68.

Goff, R. C. (1975). "Thunderstorm-outflow kinematics and dynamics." NOAA Tech. Memo. ERL NSSL-75.

Goldman, J. L. and P. W. Sloss (1969). "Structure of the leading edge of thunderstorm cold-air outflow." Proc. Sixth Conf. on Severe Local Storms, Amer. Meteor. Soc., Boston, Mass., 71-79.

Grossman, R. L. and D. W. Beran (1975). "An investigation of extreme low-level wind shear at selected stations in the conterminous United States." J. Appl. Meteor., 14, No. 4, 506-512.

Hall, F. F., W. D. Neff, and T. V. Frazier (1976). "Wind shear observations in thunderstorm density currents." Nature, 264, 408-411.

Hardy, R. N. (1971). "Gravity wave severe turbulence near Cyprus." Meteor. Magazine, 100, 209-220.

Hill, C. D. (1976). "Other kinds of wind shear." NOAA Tech. Memo. NWS WR-108.

Hooke, W. H. and K. R. Hardy (1975). "Further study of atmospheric gravity waves over the eastern seaboard on 18 March 1969." J. Appl. Meteor. 14, 31-38.

Idso, S. B., R. S. Ingram, and J. M. Pritchard (1972). "An American haboob." Bull. Amer. Meteor. Soc., 53, 930-935.

Keliher, T. E. (1975). "The occurrence of microbaragraph-detected gravity waves compared with the existence of dynamically unstable wind shear layers." J. Geophys. Res., 80, No. 21, 2967-2976.

Keulegan, G. H. (1957). "An experimental study of the motion of saline water from locks into fresh water channels." Natl. Bur. Standards, Rept. No. 5168.

Keulegan, G. H. (1958). "Twelfth progress report on model laws for density currents; the motion of saline fronts in still water." Natl. Bur. Standards, Rept. No. 5831.

Kirk, T. H. (1963). "Some synoptic features of an occurrence of low-level turbulence." Meteor. Magazine, 92, 147-154.

Lhermitte, R. M. (1966). "Probing air motion by Doppler analysis of radar clear air returns." J. Atmos. Sci., 23, No. 5, 575-591.

Midleton, G. V. (1966). "Experiments on the density and turbidity currents. I. Motion of the head." Can. Journ. Earth Sci., 3, 523-546.

Mitchell, K. E. (1975). "A numerical investigation of severe thunderstorm gust fronts." NASA CR-2635.

Neff, W. D. (1975). "Quantitative evaluation of acoustic echoes from the planetary boundary layer." NOAA Tech. Rept. ERL 322-WPL 38.

Perry, J. D. (1976). "An analysis of pressure jumps at Luqa, Malta, in the years 1968-1972." Meteor. Magazine, 105, 166-184.

Peterssen, S. (1956). Weather Analysis and Forecasting, Vol. 1. McGraw Hill Book Co., Inc., 196-198.

Simpson, J. E. (1964). "Sea-breeze fronts in Hampshire." Weather, 19, No. 7, 208-219.

Simpson, J. E. (1969). "A comparison between laboratory and atmospheric density currents." Quart. J. Roy. Meteor. Soc., 95, 758-765.

Simpson, J. E. (1972). "Effects of the lower boundary on the head of a gravity current." J. Fluid Mech., 53, Part 4, 759-768.

Snyder, C. T. (1968). "Analogue study of longitudinal response to wind shear and sustained gusts during landing approach." NASA TN D-4477, Ames Res. Center, Moffett Field, Calif.

Sowa, D. (1974). "Low-level wind shear effects on approach and climbout." D. C. Flight Approach. No. 20, McDonald Douglas Corporation, 10-17.

Tepper M. (1950). "A proposed mechanism of squall lines: the pressure jump line." J. Meteor., 7, 21-29.

Tepper, M. (1954). "Pressure jump lines in midwestern United States, January-August 1951." U.S. Dept. of Commerce Weather Bureau Research Paper No. 37.

Williams, D. T. (1953). "Pressure wave observations in the central Midwest." Mon. Wea. Rev., 81, 278-289.